Coordinated Frequency and Active Power Control of Hybrid Power Plants

An Approach to Fast Frequency Response

AALBORG UNIVERSITY

DENMARK

Master Thesis by

Daniel Vázquez Pombo

Aalborg University
Energy Technology

Energy Technology
Aalborg University
http://www.aau.dk

AALBORG UNIVERSITY
STUDENT REPORT

Title:
Coordinated Frequency and Active Power Control of Hybrid Power Plants

Theme:
Electric Power Systems

Project Period:
Spring Semester 2018

Project Group:
EPSH4-1035

Participant(s):
Daniel Vázquez Pombo

Supervisor(s):
Florin Iov

Copies: 1

Page Numbers: 80

Date of Completion:
May 31, 2018

Abstract:

The dramatic reduction of inertia suffered by worldwide grids due to the transition towards renewable and power electronic based generation, rises the risk of disturbances and blackouts due to frequency related issues. Therefore, in this thesis, state of the art techniques aiming to minimise such challenges are reviewed and analysed. Also power and frequency control strategies are presented along with a deep analysis of the issues caused by large integration rates of renewable energy sources. Additionally, past and future relevant scenarios of the European grids are analysed. Subsequently, after presenting the topology of the Hybrid power plant (compound by a Wind Farm, a Photovoltaic Plant and a Battery Energy Storage System), a control strategy aiming to mimic the inertial response of synchronous generators is proposed and tested in a relevant simulation environment.

The obtained results show how, by mimicking inertial response, renewable plants are capable of responding to critical events, protecting the frequency stability of the grid without suffering undesired stresses, in a similar way as for the traditional synchronous generators.

In the last chapter, the findings and contributions of this work are summarised while also outlining directions for future research.

Acknowledgement

The document placed in front of you is nothing but the product of seven years of university studies and the final requirement of a two years long Master of Science in Electric Power Systems. Four semesters that I spent exploring different topics, from Minimisation of Distributed Generation Integration Issues to Techno-Economical Optimisation of Demand Response in Time-Dependent Billing Systems, and finally, Frequency and Active Power Control in Renewable Hybrid Power Plants. What a journey.

First of all, I would like to express my most sincere gratitude towards all the members of the Smart Energy Systems Laboratory at Aalborg University for their help, advice, and support during these past months, but especially to my supervisor, Ph.D. Florin Iov for his guidance and encouragement.

Sadly, when I look back to my bachelor period I can only remember being sat in front of a screen, books... feeling that I was studying pointless stuff all the time. Even if it sounds strange, in Spain I was taught how to be a cold, efficient, hardworking robot, while here in Denmark I learned to enjoy life in all its facets. When I think about my time in Aalborg, interesting discussions with either colleagues or professors, a feeling of accomplishment (and yes, the occasional party) come to mind, but also the pride of having taken part in an institution that values ideas, creativity, and self-exploration over curriculum.

In 2016, by this time of the year, I was finishing up my bachelor thesis in a German start-up. In the acknowledgement section of such document I left a note for present me: *Try to be part of the solution in the biggest challenge of the XXI century, the Energy Transition*. I think he would be pleased with what I'd achieved, but most importantly, with what's about to come.

Two years latter, I have different hopes, expectations and priorities than the ones I brought to this country; I'd grown but I feel younger. Finally, and above all, I would like to thank past me for choosing Electrical Engineering in the first place while Power Systems and Aalborg University in second; even though Denmark resulted to be an acquired taste. Also, I don't want to miss the opportunity of reminding future me not to let his job get in the way of his happiness. Make sure not to disappoint me.

Preface

This report was written from February to June of 2018 during the 4th semester of the Electrical Power Systems and High Voltage Engineering MSc. programme at Aalborg University.

The individual chapters in the report are introduced and concluded with a section written in the *italic* font. Throughout the report there will be stated references all listed by the end of the paper in the Bibliography. The references are denounced with the typical IEEE simplified format, number of apparition throughout the text. This reference refers to the bibliography where books are referred by author, title, ISBN-number, publisher, edition and year while websites are referred by author, title, year, URL and time of last visit. Technical papers are referred by author, title and year. It should be noted how, if the source is added before a full stop it implies that it belongs to the contents of that sentence. However, if the source is added after a full stop, it covers the contents of the entire previous paragraph. A CD containing all Data, models, downloaded web pages and PDF references, might be attached to the physical copy of the report. While figures, tables and equations are numbered according to the particular chapter they're placed in. The first figure in chapter three will, therefore, be assigned with figure number 3.1 and the second 3.2 etc. Descriptive captions for tables and figures are found under relevant tables and figures.

Aalborg University, May 31, 2018

Daniel Vázquez Pombo
<daniel.vazquez.pombo@gmail.com>

Contents

Nomenclature

Abbreviations

BESS	Battery Energy Storage System
DFIG	Doubly Fed Induction Generator
DG	Distributed Generation
DSO	Distribution System Operator
FCR	Frequency Containment Reserve
FFR	Fast Frequency Response
FRR	Frequency Restoration Reserve
GM	Gain Margin
ICT	Information and Communication Technologies
IES	Integrated Energy System
IR	Inertial Response
MPPT	Maximum Power Point Tracking
PCC	Point of Common Coupling
PFR	Primary Frequency Response
PM	Phase Margin
PMSG	Permanent Magnet Synchronous Generator
POC	Point Of Connection
PV	Photovoltaic Panel
PVP	Photovoltaic Plant
RE	Renewable Energy
RES	Renewable Energy Sources
ROCOF	Rate Of Change Of Frequency
SC	Super Capacitor
SCR	Short Circuit Ratio
SFR	Secondary Frequency Response
SO	System Operator
TSO	Transmission System Operator
WF	Wind Farm
WT	Wind Turbine
X/R	Impedance Resistance Ratio

List of Symbols

C	Capacity	F
E	Energy	J
f	Frequency	Hz
G_x	Transfer Function of x	
H_x	Transfer Function of x	
H	Inertia	s
I	Current	A
j	Complex Number Operator	$\sqrt{-1}$
k	Gain	
log	Decimal Logaritmic	
P	Active Power	W
p_{ij}	Polynomial Coefficient	W
Q	Reactive Power	VAr
R	Droop constant	
R	Resistance	Ω/km
$ROCOF$	Rate Of Change Of Frequency	Hz/s
S	Aparent Power	VA
s	Laplace Operator	
t	Time	s
T_a	Time Constant	s
U_0	Intermediate Voltage	V
U_c	Capacitor Voltage	V
V_g	Grid Voltage at the PCC	V
X	Reactance	Ω/km
Z	Discrete Operator	
$_C$	Capacitance	Ω/km
$_c$	Controller	
$_{cl}$	Closed loop	
$_G$	Generation	
$_L$	Load	
$_L$	Inductance	Ω/km
$_{loss}$	Losses	
$_{ol}$	Open loop	
$_p$	Plant	
$_n$	Nominal	
Δ	Variation	
φ	Angle	DEG
Ω	Resistance	Ohm
ω	Angular Velocity	rad/s
0	Initial	

List of Figures

List of Tables

Chapter 1

Introduction

This chapter contextualises the scope of the thesis and its importance. A short review introduces the current situation of the energy transition, but also discusses the challenges to overcome in the near future. The scope of this report is focused on ancillary services provided by renewable power plants. Subsequently, the project's motivation, objectives and limitations are presented.

1.1 Background

During the past few decades environmental and energy security concerns had steadily increased, causing national and international agreements to be signed. From an European perspective the most important of those alliances is the Renewable Energy Directive [1], since it establishes particular targets and a roadmap for the European Union as well as for each of its members. In such roadmap a shift towards the use of Renewable Energy Sources (RES) is stated, e.g., 20 % of energy production based on RES by 2020. Particularly, Denmark self-established more strict requirements; as its Renewable Energy (RE) production must reach 50 % by 2020, while the goal for 2050 is to become 100 % fossil fuel free [2]. It should be noted how becoming 100 % renewable implies not only meeting the electrical demand but also heat and transport needs are to be satisfied.

The aforementioned measures, and the subsequent economical investments, have allowed Wind Turbine (WT) technology to improve and mature to the point where its cumulative cost of energy has become competitive with conventional generation technologies. As a consequence, the capacity of wind energy has increased significantly, i.e., reaching nearly 60 % of the country's installed power in Denmark and supplying 43,4 % of the consumed energy during 2017 [3].

Furthermore, the willingness to include higher rates of RE in the power systems, has caused to substitute conventional centralised power plants, equipped with large synchronous generators, with numerous smaller units referred as Distributed Generation (DG). By itself, such transition poses several challenges like power quality, congestions and bottlenecks since the conventional grid was not designed for such large penetration of variable generation in lower levels of the distribution grid. However, it also possesses advantages such us emissions reduction, market liberalisation or versatility since some DG units are capable of generating other forms of energy like heat. [4]

In addition, most of the DG units consist of power electronic converter interfaced generation, i.e. solar photovoltaic (PV). Therefore, causing a decrease in power system

inertia, making it time variant, increasing frequency stability issues which escalates the need for load shedding and increments the blackout risk. [5]

On the other hand, recent literature like [6, 7] have introduced the idea of combining different energy sectors like transport, electricity, heat and gas; resulting in the so called Integrated Energy System (IES), whose aim is to incorporate the synergies among those and other areas in order to satisfy the global energy needs. However, meeting the control and coordination requirements of an IES demands the use of Information and Communication Technologies (ICTs); since complex measuring systems, and data analysis are to be combined with the traditional power grid, resulting in the concept known as Smart Energy System [8].

1.2 Problem Formulation

As aforementioned, stability is an important concern for the power system operators which starts by maintaining the equilibrium between generation and consumption. In fact, the electrical frequency in a power system can be seen as a measure of the balance between generation and load of electric power. In general, the frequency of a system is determined by the electrical speed of the synchronous generators (50 Hz in Europe). As long as the generators produce exactly the amount of power demanded by the load, this value remains constant. However, even if we could consider that generation and demand remain matched for a period of time, unexpected eventualities like tripping of a power plant due to a short circuit or any other fault will cause an immediate unbalance. In such a case the frequency will fall below its nominal variation until the generation and load are matched again. The next equation explains how changes in the supply and demand affect the system's frequency.

$$P_G - P_L = \frac{2\,H\,S}{f_n}\,\frac{\Delta f}{\Delta t} \tag{1.1}$$

Where H, S, f_n and $\frac{\Delta f}{\Delta t}$ stand for equivalent rotational inertia [sec], apparent power [VA], nominal frequency [Hz] and frequency variation [Hz/s]. From the equation can be extracted how, a variation in generation vs load balance will cause higher variations in the frequency of a system with a smaller inertia. As rule of thumb, the higher the inertia, the smaller the rate of change. High inertia values in a power system can thus reduce the impact of sudden load imbalances and contribute to the frequency stability. Traditional system reached values of inertia close to 7, however, as the RE penetration increases, H falls, currently reaching values of 2 or 3 in countries like Denmark [9].

Provided the importance of the inertia in any power system, the potential issues that arise as inverter-based generation increasingly replaces conventional generators in modern power systems, poses a major problem for Transmission System Operators (TSO), who are responsible of keeping the system stability. The synchronous inertia is reduced more and more as PV and modern wind-based generators are not synchronously coupled to the grid. Their electrical design is instead based on partial or full converters, which are effectively decoupling the electrical generator from the grid. As a consequence, the risk of high values of the Rate Of Change Of Frequency (ROCOF) following a loss of generation or demand is increasing with decreasing number of conventional generators remaining connected to the system. This, in turn, increases the risk of instabilities in the system or even disconnection of generation in distribution systems due to

activation of ROCOF-relays, which perform load shedding strategies and isolate parts of the grid. Due to this, European TSOs have joined forces in order to design a set of common regulations that forces all the generation plants to support the grid, i.e., control of active power and frequency [10].

Large frequency disturbances had historically lead to emergency events and even blackouts. The incidence of such events will increase in the future due to the lost of inertia unless corrective measures are taken in advance. In order to highlight the importance of this research work, here are presented some of those events.

- Italy blackout 2003: It was a serious event caused by a sudden load increase. The subsequent cascading effect produced the tripping of a 400 kV line connecting to France. Which reduced the system's frequency to 47,5 Hz during 2,5 minutes, causing the loss of 7,5 GW of DGs. [11]
- Austria 2003: Krsko Nuclear Power Plant in Slovenia, tripped during tests. Fortunately, huge load shedding avoided the total blackout, the system took 2 hours to be fully restored. [12]
- Denmark-Sweden 2003: A short circuit in Southern Sweden caused a chain of events that led to a 1,850 MW lost in around 90 seconds, which caused a frequency drop that ultimately caused protection relays to trip; leaving nearly 2,5 million people without electricity. [13]
- India blackout 2012: This was the biggest blackout in history by number of affected people, 620 million, 9 % of global population. The unnecessary tripping of a relay caused several GW of power to be lost within seconds, the automatic load shedding was not enough to prevent the system from collapsing. [14]
- Australia blackout 2016: This event was caused by two causes; a line tripped due to grid faults, which happen simultaneously with losses of wind generation up to 315 MW, 3 different Wind Farms (WF), in less than 20 seconds. That lead a major interconnector to overload, finally tripping causing a major blackout. [15]

Recently, several industry member have been interested in developing a renewable power plant that combines different types of energy sources like wind and PV which are refereed to as Hybrid Power Plant (HyPP) [16, 17]. The idea is to combine the advantages of the different energy sources in order to reduce the disadvantages such as frequency and power fluctuations. However, as it will be thoroughly presented in Chapter 2, the available literature on the topic is poor or even nonexistent in topics related to the actual implementation of such system at a transmission level, and the necessary control strategies to be applied. This thesis is focused on how the provision of power and inertia from HyPPs [18, 19, 20], can be used in Fast Frequency Response (FFR). It should be stated that such plant is compound by a WF a Photovoltaic Plant (PVP) and a Battery Storage System (BESS). Also, the so called emulated or synthetic inertia is also investigated in this thesis due to its relevance when developing a frequency controller with RES.

1.3 Objectives

Provided the ability of HyPPs of supporting the grid with ancillary services, the objectives of this thesis are:

- Develop a FFR control strategy for a HyPP in the context of a large power system considering its overall actuation and performance in the Point of Common Coupling (PCC).
- Define individual actions at component level in order to meet the PCC's requirements.
- Take into account industrial standardised perspective approaches for the controllers and plant's responses.

1.4 Assumptions and Limitations

Despite of the thoroughness of the developed work, several assumptions restricting the scope of the project were taken, thereafter a list of such limitations is presented.

- Frequency controller uses local measured frequency and acts accordingly. Thus, the whole power system is assumed to have the same frequency.
- The only power plant providing frequency support to the considered system is the Hybrid one.
- The inertial response from synchronous generators is not considered, therefore the expected frequency drops are more dramatic than they would be in the real system; worst case scenario.
- As it is presented in Chapter 2, frequency restoration strategies have three stages, however, in this thesis only the first stage controller, FFR, is designed.
- Meteorological data (wind speed, irradiance, etc) is considered static trough out the entire simulation and no differences are assumed between assets.

1.5 Outline of the project

The outline of the project is as follows:

Chapter 2 - State of the Art: This chapter consist of a review of the most relevant topics related to this thesis' scope. The covered subjects are: RE Generation, HyPP Concept, Virtual Inertia Provision, Frequency in Power Systems, Control Strategies, Power Plant Coordination and, finally, the influence of ICTs in the Smart Energy System.

Chapter 3 - System Characterisation: In this chapter, the system's operational essence, the topology of the HyPP as well as the power grid in which is connected are presented. Also, grid requirements, functional descriptions, and evaluation criteria are covered.

Chapter 4 - Control System Design: In this chapter, the methodology used to derive the plants' transfer function is presented, along with the estimation and impact of

the electrical losses. Also, several controllers are designed to regulate the normal operation of the HyPP. Subsequently, the approach of the implemented Dispatch function is explained. Finally, the FFR controller is designed and included in the model.

Chapter 5 - Tests and Evaluation: In this chapter, the developed model is tested along with the different control systems. Such tests are undertaken first in continuous time and then, after converting the the model from the S-domain to the Z-domain, in discrete time. In the particular case of the discrete model, several scenarios are defined and, then, evaluated. Lastly, conclusions are dragged from the analysed scenarios.

Chapter 6 - Conclusion and Future Work: This final chapter summarises the report, discusses its findings and contributions, points out limitations of the current work, and also outlines directions for future research.

Chapter 2

State of the Art

In this chapter, a literature review of the most relevant topics of the project is presented. Technologies, theories and strategies related to frequency support from non-traditional generation units are presented. Finally, to conclude, the research path is defined.

2.1 Renewable Generation Technologies

WTs represent the fastest growing renewable energy industry and also the biggest part of the installed renewable power; therefore, they are the most important energy source of the industry [21]. Even though a comparison between the different types of turbines is out of the scope of this project, it is important to acknowledge few similarities and differences between the two most widely extended technologies in variable speed wind turbines; Doubly Fed Induction Generators (DFIG) and Permanent Magnet Synchronous Generator (PMSG) [22].

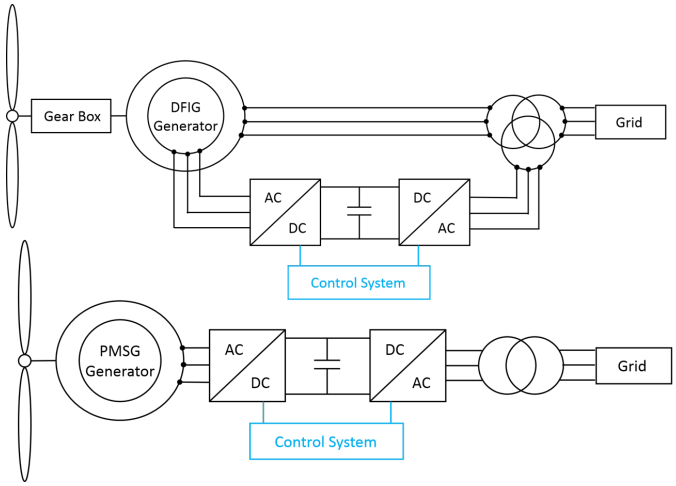

Figure 2.1: Simplified schematic of DFIG (top) and PMSG (bottom) technologies.

Such technologies are presented in Figure 2.1, where it can be seen how both are decoupled from the grid due to their power converter-based interface, therefore the mechanical energy stored in the rotating shaft remains isolated from the power grid. From the point of view of the inertia response, the main difference is the size of the converter, since for the PMSG is the nominal power of the wind turbine, while for the DFIG is only about 30 % of the generator's rated power. Finally, it should be stated how a more formal comparison of the DFIG and the PMSG can be found in [23, 24, 25].

Finally, it is worth mentioning how disregarding of the type of PV or BESS technology the connection to the grid is as presented in Figure 2.2 with a converter rated power equal to the plant's. [19]

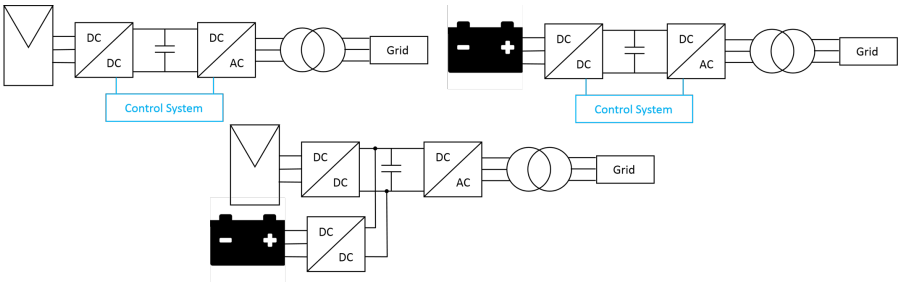

Figure 2.2: Simplified grid connection of PV (left), BESS (right) and combined system (bottom).

2.2 Hybrid Power Plant

This section justifies the interest in combining WF, PVP and BESS in the same generation plant, the HyPP. In recent years, the interest in increasing the full load hours of WF is been growing. Typical values for the full load hours are 30 to 40 % for onshore and from 35 to 45 % for offshore [26]. The idea is that, the full size of the plant connections are underutilised approximately 60 % of the time, thus, if additional generation units are included, the full production hours increase.

Following such idea, some manufacturers are considering the inclusion of additional WTs and/or PV fields [16, 17]. As it has been already stated, in this thesis, the addition of a PVP and BESS unit is considered in order to obtain a full production curve similar to the one presented in Figure 2.3. It should be noted that a 100 % utilisation is not expected, however the idea is to rise it as much as possible. The BESS results a key element capable of providing extra generation during particular periods of shortcoming, but also avoiding curtailing the power of the plants during over-generation ones.

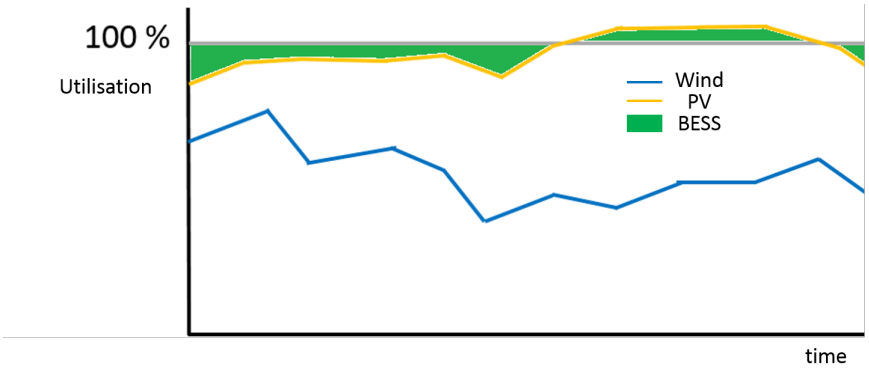

Figure 2.3: Full hour production concept for Hybrid Plants.

2.3 Virtual Inertia

As aforementioned, power system stability is threaten by inertia loss. However, modern literature has proven how to extract the so called virtual or synthetic inertia from

power converters [27]. Nevertheless, the author disagrees with such terminology, since it points out to the nonexistence of such inertia. Although, it is true that special control approaches must be implemented in order to exploit it, such inertia is real. Therefore, a different terminology is proposed in this thesis for the new inertia sources attending to their origin: mechanical and electrical.

2.3.1 Mechanical Inertia

There are two mechanical sources suitable to provide inertia support in WT: Blade Pitch and Spinning Shaft. Pitching can be used to create an energy reservoir capable of providing frequency support. However, this strategy forces the WT to deviate from the Maximum Power Point Tracking (MPPT), sacrificing a percentage of the captured energy for system support during normal operation; except in extremely high wind speed conditions where no deviation from the MPPT is necessary. Additionally, the response is slow (2 to 5 seconds) due to the regulation of pitch angle and it causes mechanical stress and fatigue in the WT, which will lead to reduced life-span. [28, 29]

On the other hand, the rotating kinetic energy stored in the spinning shaft can be used in frequency regulation with a controlled inertia response system [28]. Briefly, after detecting a frequency deviation, the active power control modifies the power set-point of the WT, either releasing stored rotational energy in order to obtain a generation peak or absorbing it, thus reducing the instantaneous power delivered to the grid. However, it must be noted how the generation peak has a limited time length and the WT will suffer a comparably long recovery time before reaching pre-event generation and efficiency levels. Also, a similar phenomenon is found in the complementary actuation. [29]

In conclusion, a significant production loss is almost inevitable when providing frequency support with both methods. However, the overall efficiency is considerably higher in the second method, since it only affects in the case of applying support and during a relatively short period of time.

2.3.2 Electrical Inertia

The last available source capable of providing inertia support has its origin in power converters, due to the lack of a better name in recent literature, the term electrical inertia is proposed in this thesis. Such source is easily demonstrated by the following set of equations [30]. Figure 2.4 presents a conceptual schematic of the phenomenon; it should be noted how the current source represents a generator and the generator-side converter.

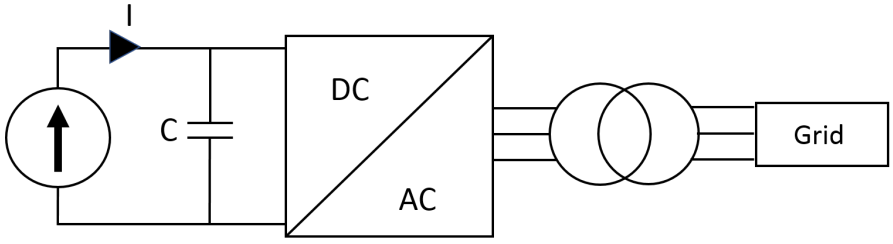

Figure 2.4: Electrical Inertia's Conceptual Schematic.

First, the time constant Ta is defined as:

$$\frac{\Delta P}{P_0} = T_a \frac{d}{dt} \frac{\Delta f}{f} \tag{2.1}$$

where P_0, f, ΔP and Δf and stand for active power in the grid, nominal frequency and their respective variations correspondingly. It should be noted how if ΔP is positive, the converter feeds additional power into the grid and vice versa. Subsequently, the power stored into the DC-link (capacitor C in Figure 2.4) is defined as:

$$\Delta P = \Delta I \, U_0 \tag{2.2}$$

where U_0 and ΔI represent the intermediate voltage and the variation of current inside the capacitor respectively. Thereafter, assuming a fairly constant capacitor voltage the definition of the voltage-current is:

$$\Delta Uc\,(t) = \frac{1}{C} \int \Delta I\,(t)\, dt \tag{2.3}$$

where ΔU_c and C stand for the Voltage variation at the capacitor and the capacity respectively. Now, by combining equations 2.1, 2.2 and 2.3 the expression of the intermediate solution is obtained as:

$$\Delta Uc\,(t) = \frac{1}{C} \int \frac{P_0\, T_a}{U_0} \frac{d}{dt} \frac{\Delta f}{f_0} dt \tag{2.4}$$

Now, the maximum energy content of a capacitor is expressed as:

$$E_0 = \frac{1}{2} C \, {U_0}^2 \tag{2.5}$$

Finally, by combining equations 2.4 and 2.5 the relationship between the DC-link voltage and the frequency is found as presented in equation 2.6, or rearranged as in 2.7.

$$\frac{\Delta U_c\,(t)}{U_0} = T_a \frac{1}{2} \frac{P_0}{E_0} \frac{\Delta f}{f} \tag{2.6}$$

$$\frac{\Delta U_c\,(t)}{U_0} \propto \frac{\Delta f}{f} \tag{2.7}$$

Therefore, it is possible to alter a system's frequency by modifying the voltage level of the DC-link, since it is proportional to the frequency variation. However, in order to be able to provide such support it is necessary, in general, to have some kind of fast energy storage system. When an over-frequency event appear, the voltage level of the DC-link ought to be reduced, therefore curtailing the generation or reducing supply by storing energy. On the other hand, when an under-frequency event appear, the voltage level of the DC-link has to be increased, thus supplying more power. Therefore, it can be easily understood how, in the case were no storage is present, the PV unit must keep a reservoir at all times in order to provide support if necessary, thus reducing its overall efficiency. Additionally, the support capacity is reduced if no storage is present. [30]

According to [29, 31] DFIG technology has issues providing electric inertia due to mechanical stress and the reduced size of its converter, thus the capacitor; whereas such problems are not found in PMSG due to its full size converter [32]. Also, current literature considers unfeasible for a standalone PV unit to provide frequency support [33]

even if combined with a BESS, being the reason, the reduced energy density of a BESS [29, 34]. That is why in recent literature frequency support strategies are presented using Super-Capacitors (SC) and DFIG [35], SC and PV [36], or even PV and a combined storage of BESS and SC [34]. However, most of this studies have been theorised in micro-grids and isolated systems. In fact, to the best of the author's knowledge, a combination of WF, PV and BESS in the same system implementing frequency support has never been studied as it is done in the present document.

2.4 Frequency in Power Systems

In Figure 2.5 the typical frequency response of any power system after a major power imbalance is presented. A represents the event starting point, B is the Nadir, or lowest value reached by the frequency, C represents the end of one of the control stages, and point D sets the steady state frequency. In the graph, three main actuation phases or stages can be distinguished: Fast Frequency Response (FFR), Frequency Containment Reserve (FCR), and Frequency Restoration Reserve (FRR) [37]. However, traditionally, the stages are called Inertial Response (IR), Primary Frequency Response (PFR) and Secondary Frequency Response (SFR) [38]; Table 2.1 presents a summary of control phases relating it to their actuation frame, impact and origin.

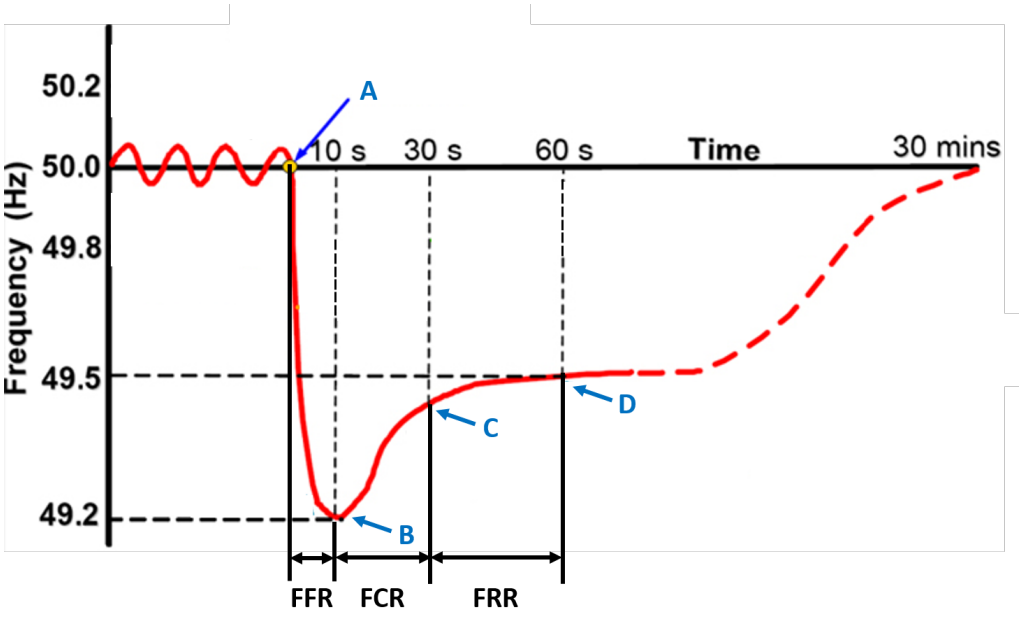

Figure 2.5: Frequency variation schematic (based on [39]).

Table 2.1: Control Phase Summary

Stage	FFR	FCR	FRR
Interval	A-B	B-C	C-D
Impact	Reduce ROCOF Increse response time	Bring Frequency to steady state	Restore nominal frequency
Origin	Inertia	Frequency containment reserve	PFR
Similar To	IR	PFR	SFR

It is worth mentioning the "second dip" concept, which is an additional frequency reduction occurred during the restoration process, typically between points B and D of Figure 2.5. The frequency reduction of the second dip is always of smaller amplitude than the Nadir, however it tends to cause even more damage to the power system stability, since frequency protections are usually triggered unnecessarily applying load shedding schemes. The main reason for the protections to get triggered is that they tend to detect the first and second dips as one single fault with a comparatively long duration. Currently, most of the research regarding frequency restoration does not acknowledge the importance the second dip as it will be further presented in Sections 2.5 and 2.6. Also, there is still no consensus about the actuation time frames of the new frequency control stages.

2.4.1 Fast Frequency Response

FFR, traditionally IR, is related to the inertial response of the synchronous generators in the system. However, as it has been already explained, due to the amount of converter-based generation units; it has been renamed to FFR. While IR was a natural uncontrollable response, FFR is a controllable non-spontaneous reaction of the generators in a grid. The capacity of this stage is limited by mechanical and electrical control boundaries, pre-event curtailed power, wind speed conditions, irradiance and other weather conditions in case of WF and PV units. In this thesis, it is considered to last up to five seconds.

2.4.2 Frequency Containment Reserve

FCR refers to a corrective measure activated automatically in a generation plant responsible for power balancing, which increases gradually over a period of few seconds. Typically, its full activation time is up to 30 seconds with a maximum allowed delay after the fault of 2 [18].

2.4.3 Frequency Restoration Reserve

FRR modifies the power set points and adjustments of the generation units in order to recover nominal frequency value. Traditionally, this measure is applied to thermal and hydro plants. Typically, its restoring action occurs over a period of 15 minutes.

2.4.4 Rate Of Change Of Frequency

ROCOF is defined as the time derivative of the system's frequency ($\frac{\delta f}{\delta t} \quad \left[\frac{Hz}{s}\right]$) and, its maximum theoretical value corresponds to the instantaneous gradient measured right after the dis-connection event, but before any controls become active [40]. However, measurement systems, most likely, won't detect the maximum theoretical ROCOF, but a smaller value; due to the inevitable delays involved in frequency assessment [41]. Lastly, all-island studies present that large $\frac{\delta f}{\delta t}$ variations between bus-bars for the first few cycles, which converge to one value; thus, implying the importance of fast calculation of $\frac{\delta f}{\delta t}$ [42].

Traditionally, ROCOF had minor relevance because the inertia of synchronous generators inherently counteract load imbalances, thus its values were small. However, it has been gaining relevance as the inertia reduces. Certainly, high ROCOF values endanger

safe operation of a power system due to the mechanical limitations of individual synchronous machines, protection devices that might be triggered by a particular threshold value or undesirable load shedding strategies activation. [40]

2.4.5 Frequency Detection

Provided the importance of knowing the exact value of a grid's frequency, it is important to understand the main issues of such measurement. In this section, a breve introduction to some of the key factors in frequency detection are presented, along with a recommendation from ENTSO-E.

There are several devices, algorithms and strategies used to measure the frequency of any grid as described in [43]. Some manufactures of measurement devices claim to have a very high frequency reporting rate, however, the shorter the calculation time, the noisier is the result. In fact, frequency measurement is affected by harmonics which hinders the $\frac{\delta f}{\delta t}$ acquisition. Therefore, if the reporting rate is too fast, the deviations that will arise between two time steps will lead to either a very high or low ROCOF value; finally resulting in an improper system response.

It should also be considered that, the main assumption when performing ROCOF calculation is that the frequency does not vary from bus to bus in a grid. Therefore, ROCOF is not calculated with the actual frequency of the grid, which varies from area to area, but with the so called "mean equivalent frequency". However, when a large power system is considered, the differences among local frequency measurements should be taken into consideration, nevertheless it is worth mentioning that there is no consensus related to the amplitude of such variations. [44]

Regarding local frequency, it should be stated how many phenomena that typically occurs in a grid disturbs its measurement, i.e. topology modifications, transformers' energization, short circuits, etc. In order to minimise the impact of such events, the measurement needs to be filtered in order to remove the noise from the actual signal. Such low-pass filter can be adjusted depending on the application; meaning that inertia support will need a fast measurement. [45]

ENTSO-E recommends that for ROCOF calculation is necessary to obtain the mean of five consecutive measurements in order to obtain a robust result. Usually, each of those measurement takes around 100 ms, resulting in a 0.5 seconds required period before a reliable ROCOF is obtained. Finally, regarding the accuracy, the typical range is $\pm$ 10 mHz on each individual measurement. [45]

2.5 Control Strategies

Control strategies for active power and frequency control aimed to support FFR have not been extensively covered in scientific literature. However, in this section, a brief review of several relevant publications is presented.

A extensive analysis of a FFR strategy for WT is presented in [46], where the main novelty is to distinguish between basic active power, governor and mechanical inertia control. Also, it follows a similar approach for the PVs, however it does not cover the

possibility of providing inertia with such units. The frequency response is promising, however, it considers the same frequency for the whole system (USA grid), performs the control in continuous time, and doesn't account for disturbance identification or communication delay. Another control procedure for FFR in WT is presented in [47], however, it only considers mechanical inertia, dismissing the possibility of also using electrical one. Despite of its promising results, the simulation has been performed in continuous time without delays for coordination, communications or event identification. Additionally, the renewable share is only of 30 % in the analysed system.

Regarding FFR control with PV plants, a frequency support strategy based on production curtailment is presented in [48]. The idea is to generate less than the actual possible maximum and then, after a down frequency event, returning the operation back to the MPPT. Therefore, electrical inertia is not considered in this support. Again, event identification and communications are not considered. Finally, [49] claims to support frequency with a mix of wind and PV, however only WF provide response after the event; remaining most of the stress in the conventional power plants. No attention is paid to fault identification, communications or coordination between plants.

2.6 Power Plant Coordination

While the provision of emulated inertia has been covered extensively in scientific literature, the response coordination of several renewable plants during diverse conditions has obtained fairly less attention. In fact, FFR strategies and inertia provision by wind farms have been covered extensively in technical literature, not so much for PV and electrical storage. However, most of the analysis are focus in the overall response of a plant in the Point of Common Coupling (PCC). To the knowledge of the author only few researches have considered to analyse what actions to perform at asset level (WT, PV, etc) in order to meet the needs in the PCC. Finally, it should be stated that no work has been developed in a HyPP with a WF, PV plant and BESS.

In [50], a coordinated strategy to control active power of WF to participate in the load frequency control of power systems is presented with a wind penetration rate of 70 %. This paper claims to be able to coordinate the operation on the PCCs of every WF. However, the analysis dismisses the different frequencies found all over the system, does not account for aspects such as event identification time, either reaction time of each element or the communications.

On the other hand, [51] presents a thorough coordination strategy for WF, where the power injection/curtailment is obtained at the PCC in the first place. Then, an optimisation trying to minimise the energy losses is performed in order to intelligently divide the necessary actuation among the individual WT of the plant. Again, the considered penetrations, 15 and 30 %, are smaller to the ones found as of now in the Danish grid. In this case, some delays are accounted for in the sense of communications, however as it is exposed in Section 2.7, the considered 20 ms are not high enough to represent an accurate approximation.

Prior work like [52], a coordination strategy, where the individual WTs inside a WF are classified according to the instantaneous wind speed, is presented. The power increments and reaction time of each group are balanced in order to support the grid's

frequency. However, it does not specify which type of WT is considering, it just assumes to be able to provide a certain amount of inertia. Also, it allows a second dip during the frequency recovery which is not accepted by most SO. Finally, it should be pointed out that the WF, in this case, only represents 10 % of the total installed capacity, it does not account for the time expended in event identification and communications.

Regarding WF and electrical storage, [53] proposes the inclusion of a flywheel, obtaining quite promising results. However, the wind penetration is only 21 %, being the flywheel 25 % of the installed wind power. In addition, the paper dismisses the importance of frequency analysis in favour of economical performance. A similar approach is found in [54], where a similar topology is studied, in this case focusing on frequency performance of the plant under different wind speed conditions. However, the analysed system is quite simplistic, two generators, one conventional and one WF, also it allows a second dip in the frequency recovery. Finally, [55] proposes an inertia control for FFR coordinating PMSG and a BESS. The battery overloading, the second dip and the recovery time are avoided by dragging energy at a low rate during more time. However, none of this papers address aspects such as storage sizing, fault detection, either communication.

Regarding PV and WF coordination for frequency support, [46] presents promising results in the frequency response of the USA' power grid. However, it does not define a grid topology, does not consider inter-area variations, or any kind of delay. Nevertheless, most of the published work is microgrid-based, comparable to [56], which proposes a coordination strategy for frequency control, however it does not consider imbalances, just regular operation. On the other hand, [57] analyses frequency response in a microgrid with PV, WF and diesel generator, although the results are promising, the PV plant remains inactive during the event and most of the corrective action is performed by the diesel generator in a similar way to coal power plants in large power systems.

As summary, there is a clear lack of research related to WF, PV and BESS coordination. The historical approach is first to find the overall necessary performance of the plant in the PCC and, then, address the individual actions to be performed by every element in the Point of Plant Coupling (PPC). However, in a complex HyPP, it is necessary to also address the actuation of each sub-plant. Figure 2.6 illustrates the followed analysis.

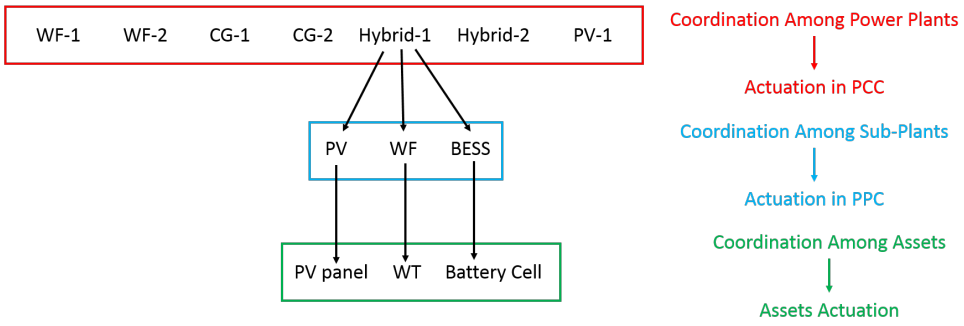

Figure 2.6: Simplified schematic of DFIG (left) and PMSG (right) technologies.

2.7 Information and Communication Technologies

As it can been inferred from this chapter, communications are a key factor in the Smart Energy System. Therefore, they have been reviewed in order to account for them in posterior analysis. Briefly, inside the scope of this project, two different communication layers can be defined: inter-plant and intra-plant. The first one, accounts for information exchange among power plants, critical in the coordination stage, while the second regards for the actuation inside a plant and its assets. Such topology is presented in Figure 2.7, where should be noted how every level can only communicate with those in direct contact.

The main characteristics to evaluate in an ICT are latency, reliability, data transmission rate, scalability, interoperability, flexibility and security. In fact, [58] uses such parameters when comparing different communication technologies, recommending 4G LTE, WiMAX and optical fiber for data transmission in inter-plant applications. Also in [59] different wireless communications technologies for the Smart Grid are compared reaching similar conclusions. However, the possibility of underestimate the necessary bandwidth for such applications is highlighted. Finally, [60] compares optical fibre and 5G for long distance transmission applied to control in power grids. The paper recommends 5G due to its simple installation, scalability, cost-effectiveness and security (both from natural interference and cyber attacks). However, it does not perform any experiment to validate such claims. On the other hand, [61] tests 5G at distribution level in fault management obtaining promising results. Nevertheless, it would be necessary to test it in long distance transmission scenarios. Finally, [62], Ethernet connection is presented as a good suitable option for intra-plant communication, specially for real-time control applications.

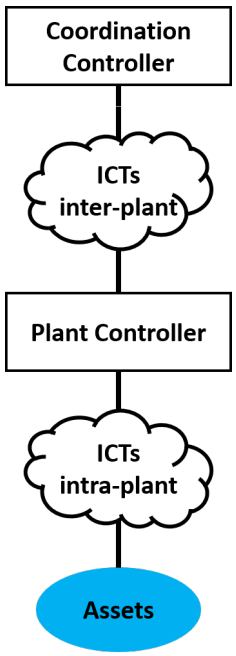

Figure 2.7: Conceptual ICT topology.

Despite all the apparent advantages of the 5G, such technology is not deployed. Instead, several authors [63, 64] suggest for intra-plant applications, wired technologies like fiber optic or Ethernet cable; while wireless technologies such as WiMAX or cellular

connections for longer distances than a few hundred meters. Publications like [65, 64] discuss and compare the performance of those technologies, reaching the conclusion that 3 ms delay is a good approximation for intra-plant communication.

It should be noted how, ICT's evaluation falls outside the scope of this project, however, due to the time-dependence of frequency control applications, it is necessary to consider the time expended in transmitting the information from one point to other of the grid or the plant. Therefore, in this project, the communications are accounted as delays in the actuation. Yet, the estimation of such delays is a complex procedure since it depends of characteristics not covered in this work like, topology, encryption, accessible bandwidth, etc.

2.8 Summary

Considering all the reviewed literature, what is been already covered and what is not, this thesis aims to fill some gaps in the current FFR research. Firstly, by considering a HyPP with WF, PVP and BESS. Secondly, accounting for the fault identification and the pertinent communications delays, since time is a critical factor. Finally, by considering a new approach for FFR.

To the knowledge of the author, it falls within reason to believe that FFR can be applied as follows. After a generation/load imbalance, i.e. a N-1 contingency; the frequency drops, ROCOF is then measured in all the power plants of the system. Such measurement along with an estimation of the available FFR capacity is then sent to a centralised controller of the area system; note how an area might be one individual country like Germany, a group like the Scandinavian countries or Spain and Portugal. This controller will then decide what actions should be performed by each and every power plant in order to clear the event and transmit such information back to the plants. Then, each plant will internally process how to provide that power to the PCC and perform the necessary operational adjustments. Therefore, this thesis is focused on estimating the FFR support capacity for a HyPP.

In a moment in history where the renewable-based generation is taking over the traditional plants, the particular characteristics of the HyPP, along with the synergies among the different involved sub-plants; results in a promising solution for the challenges posed by the renewables.

Chapter 3

System Characterisation

In this chapter, the model's topology of the HyPP as well as the power grid in which is connected are presented. Also, grid requirements, functional descriptions, and evaluation criteria are covered.

3.1 System's Operational Essence

Demand and supply are to be matched at every moment in order to keep the system in a stable state. However, after an N-1 contingency, a considerable amount of generation is lost in a fraction of a second, after which there are two options in order to return the system to balanced operation. On the one hand, applying load-shedding schemes, which will effectively reduce the overall demand of the system; however, this strategy is only used in order to avoid an imminent blackout. On the other hand, there are few power restoration procedures to be implemented, based on the individual action of one plant.

Traditional power systems relay in the synchronous inertia and load-shedding activation (only in extreme cases) in order to survive the N-1 contingency. After that, one power plant placed relatively close to the disconnected unit will gradually increase its production until the balance is regained. Such protocol is still in use nowadays, and it is usually lead by coal, gas or hydro plants. Contrarily, in future power systems dominated by renewable energy generation, the FFR substitutes IR and the restoration is to be coordinately performed by several plants at the same time due to its smaller installed power and operational set-point adaptability.

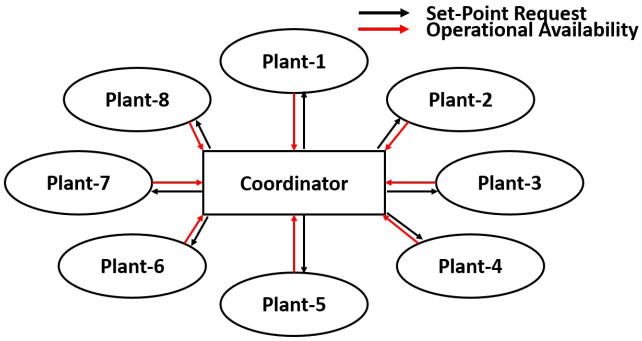

Figure 3.1: Schematic of the information flow in the system.

Consequently, one controller will supervise all the plants requesting them effective

set-point modifications (at the PCC). Then, every individual plant will internally decide and execute the necessary modifications in order to fulfil such requirements. Thus, the most critical part of such control and surveillance scheme, presented in Figure 3.1, is to effectively report, to the coordination controller, the present set-point, but also other possible states to be used in power system support. For example, as result of starting or stopping curtailing generation; note how such prediction may rely in uncontrollable factors like wind speed. In that way, the coordination controller will be able to request several modifications to different plants, improving the overall efficiency, reducing individual stresses, etc. Such idea is presented in Figure 3.2, where it should be noted that, the availability corresponds to the surface delimited by the red line. The time scale is considered in the range of 5 seconds, in order to be able to predict the generation within reasonable error, however it must be stated how each particular power profile (blue, yellow and green lines) are likely to vary, not remain flat and steady as shown.

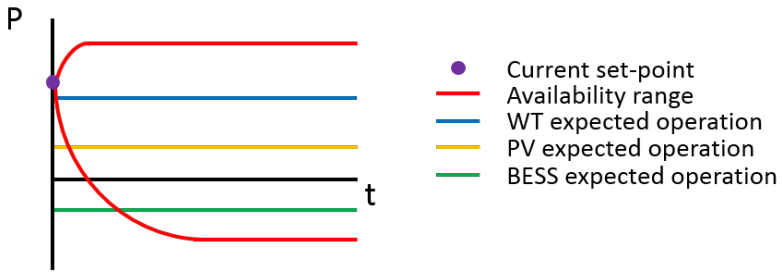

Figure 3.2: Conceptual representation of the Availability Concept.

Provided how critical results to know the range of possible set-points of a plant, not only for FFR, but also for FCR and FRR; this thesis focuses on obtaining such availability and then implementing it in FFR. In order to achieve that, a model of a transmission system has been chosen for testing in which a HyPP is been included; sections 3.2 and 3.3 cover, respectively, such topics.

3.2 Power Grid Topology - 12 bus System

The selected grid model is a generic 12-bus test system designed for wind power integration studies. Presented in [66], it is based on the actual topology of the UK grid. The system model, which will be referred to from now on as 12-bus, can be checked in Figure 3.3. Such 12-bus represents a power system with four different areas lead by thermal plants. The first area possess the biggest thermal power generation and a combination of residential and industrial loads. While hydro plants dominate the second one, where the loads are mostly rural. Subsequently, the third area constitutes a heavily industrial load centre with certain thermal generation. Finally, the fourth area is the one suitable for wind power installation, being placed mostly at bus-5.

The 12-bus is suitable for the purposes of this work due to its simplicity, since it represents an island, thus avoiding the complexity of continental interconnected systems, yet still capturing large frequency excursions. Lastly, it should be stated how the data suggested by the paper has been kept, except for the wind plant, which in this case is the HyPP as presented in the next section. Finally, it should be mentioned that, due to the lack of literature regarding local frequency estimation, the whole 12-bus has been

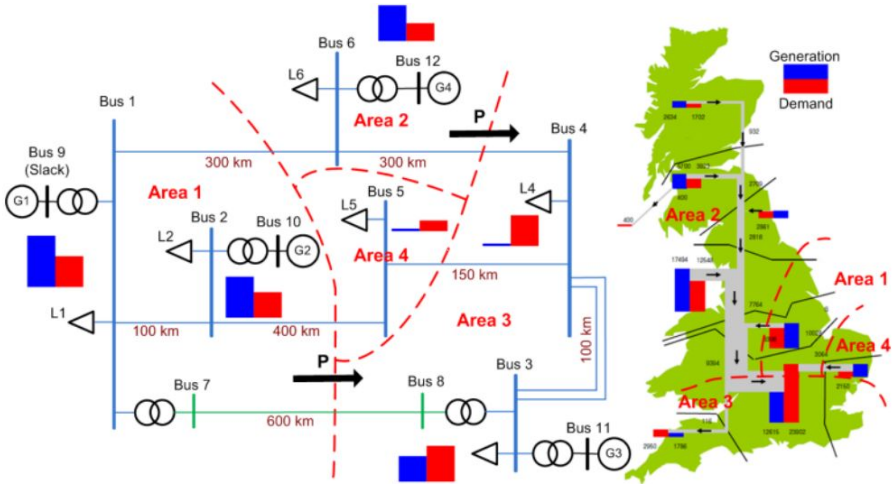

Figure 3.3: Topology of the analysed 12-bus system [66].

considered to have an homogeneous frequency.

3.3 Hybrid Power Plant's Topology

As aforementioned, several companies are interested in developing HyPP in order to increase the utilisation factor of the overall plant, as well as to be able to ensure certain production (reservoir) and provide ancillary services. However, to the knowledge of the author, there is no consensus or a rule of thumb in order to size such plants. Some factors to consider when addressing the plant design are: technical or code limitations in the PCC, business case associated to the grid service and, in the case of battery, targeted ancillary service (frequency control, trading, etc). Analysing all those possibilities could constitute another master thesis by itself, thus, in this work, a simplified approach is followed in order to estimate the plant's topology. The WF is considered to be pre-installed, then its production is estimated; the PV plant is sized afterwards in order to rise the utilisation factor and, finally, the BESS is included with the main task of providing FFR support and power smoothing. It should be stated that, even though this sizing is not optimised, it will provide a good approximation for the tasks at hand. Lastly, the Scottish WF called *Black Law Phase I* has been selected as a possible site to be turned into a HyPP since such WF has 97 MW of installed power, thus resembling the proposed system. Therefore, all the used meteorological data has been extracted from that site. Lastly, it should be stated how the utilities (transformer, transmission grid, etc) of the HyPP are sized according to the WF's pre-installed capacity.

3.3.1 Pre-existing plant - Wind Farm

The WF's size is considered to be of 100 MW whose individual WTs are 5 MW devices modelled as presented in [67], such size results quite relevant when analysing the current market of WTs. The 100 MW value has been chosen due to its relevance in modern installations and the simplicity to be scaled up or down when combined with the 5 MW WT. It should be noted how, the expected generation of the site is then obtained using 1 year of wind speed data, obtaining a 54,5 % capacity factor. Then, Figures 3.4 and 3.5 present the yearly estimated generation as a line diagram and histogram respectively. Such plots clearly present how the vast majority of the year the plant is producing

close to 100 %, however, there are still a significant proportion of hours under 50 % production.

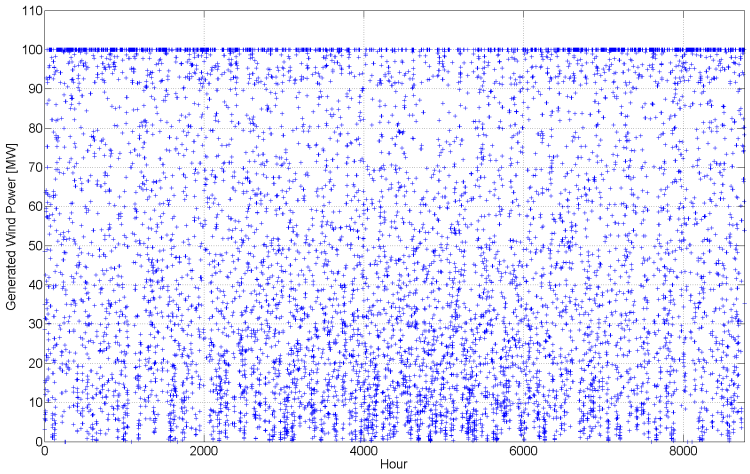

Figure 3.4: Yearly estimated WF production.

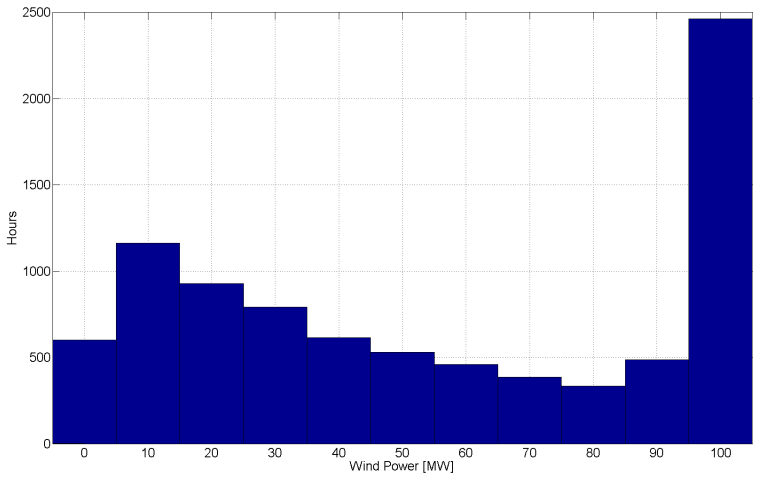

Figure 3.5: Histogram of the annual estimated WF production.

3.3.2 PV plant

Subsequently, the PV plant is approached as follows; first one year of solar irradiance and temperature data is used in order to estimate the expected production for one panel and then scaled up until a satisfactory utilisation factor is achieved. Also, it must be stated how the reference model of the PV is [68]. The obtained capacity factor is 9,1 %, which results quite close to the expected since the average in the UK is 9,7 % for utility size PVPs [69]. The selected installed power is 31,5 MW which corresponds to 150 panels. Finally, Figures 3.6 and 3.7 present the yearly production again as a line diagram and histogram respectively. Such plots clearly state how the production is less than 10 % during the vast majority of the year, however this is deeply influenced by the number of night hours.

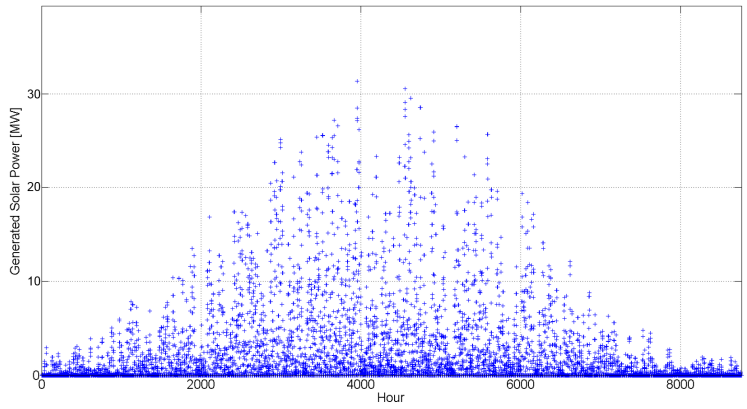

Figure 3.6: Yearly estimated PVP production.

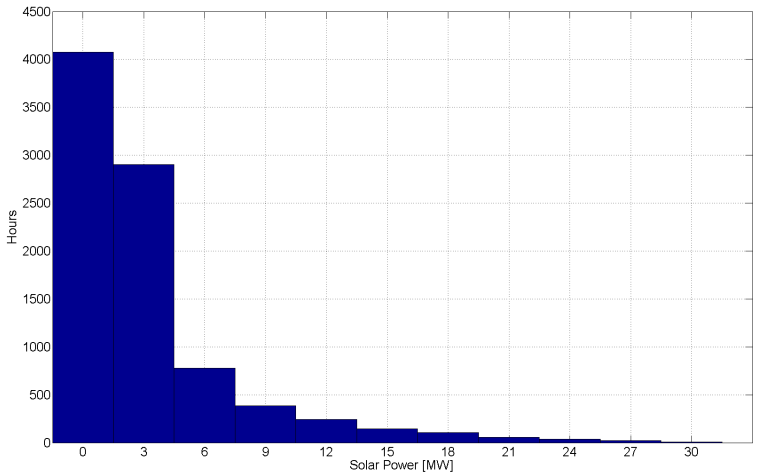

Figure 3.7: Histogram of the annual estimated PVP production.

3.3.3 Combined WF and PV sub-plants

The overall capacity factor of the plant considering both WF and PVP is 57,34 %. Figures 3.8 and 3.9 present the production as a cloud of points and histogram respectively. Such graphs illustrate how the production of the plant is close to 100 % the vast majority of the year, and how the PV addition reduces the amount of unproductive hours, but also creates a reduced amount of overproduction hours. Also, it should be stated that the full production hours (optimal) are 2140 during the year, representing a 24,43 % of the time, while the over production is 506 hours, thus 5,8 %.

3.3.4 Battery Storage System

Finally, due to the lack of scientific literature covering the storage sizing for FFR applications, the BESS is assumed to have a size of the 21 % of the combined plant (WF and PVP). This is due to the fact that, FFR theoretically, does not need an immense energy source and the high price of the BESS. Therefore, its rated power is 28 MW which, according to [70], should be able to provide 7 MWh in discharge mode without affecting its lifetime. It should be stated that, the selected BESS is a lithium-ion battery modelled as in [71].

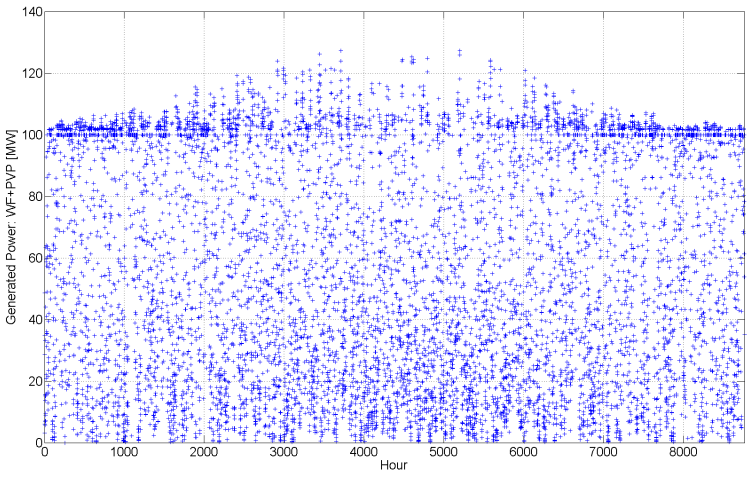

Figure 3.8: Yearly estimated production combining WF and PVP.

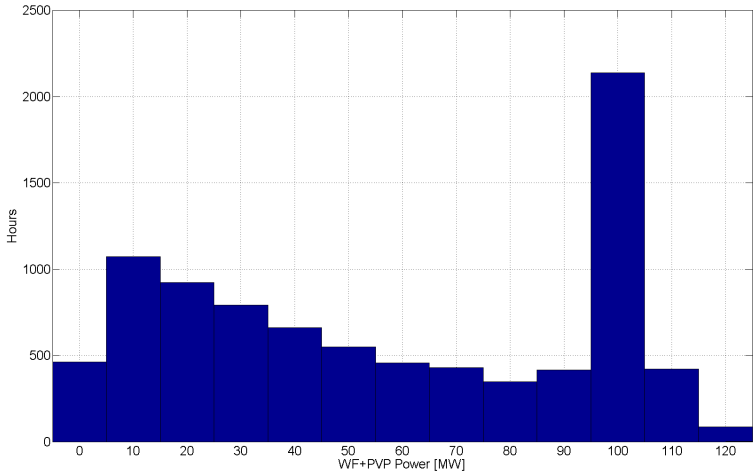

Figure 3.9: Histogram of the annual estimated production combining WF and PVP.

3.3.5 Hybrid Plant's Final Configuration

The balance of plant is presented in Figure 3.10, where the POCs and PCC are highlighted. Regarding the layout, the 20 WTs are considered to be installed in two rows of 10 while the PVs and the BESS as single point elements; such distribution is only used to account for power losses and communication delays, thus, it is not related to the actual electrical connection of the elements, which falls beyond the scope of this project. However, it should be stated how the POC of the BESS is inside the substation, while for the WF and the PVP there is still a relatively long transmission line until the PCC. Regarding measurement points, the PCC and the POCs have smart meters as specified in Section 3.4, however, it should be noticed how the intra-plant transmission lines will cause differences in the parameters from the measurement point. In fact, Section 4.2 presents the procedure followed in order to estimate the losses. Finally, it should be stated how, during the testing stage, the actual necessity of those and additional measurement points has been evaluated, reaching the conclusion that it is enough to know the power injection in the POC of every sub-plant and the PCC, in order to estimate the

overall behaviour.

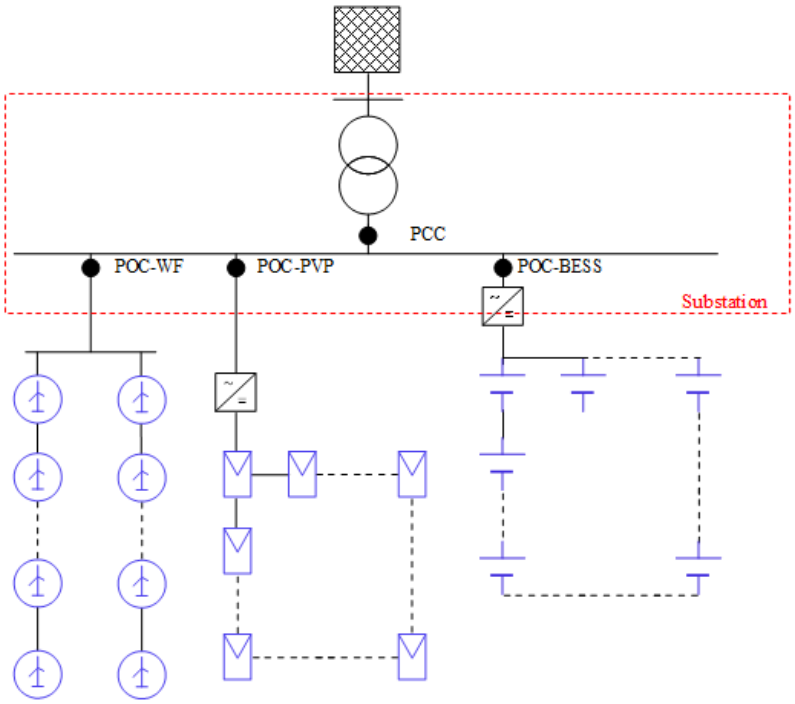

Figure 3.10: Simplified layout of the Hybrid Power Plant.

3.4 General Requirements and Specifications

Since 2009, European SO are working together trying to bring the different grid codes to a common ground, such task is being enforced by ENTSO-E. In fact, ENTSO-E is creating regulations and recommendations for SO considering future technologies and scenarios that have not been implemented yet such as FFR. Therefore, in this thesis, the ENTSO-E regulations are considered whenever possible [10]. However, as presented in Section 3.2, the 12-bus is based on the UK grid, thus, whenever a topic not cover by ENTSO-E regulations is found, the UK grid code provided by National Grid is used [72].

3.5 Hybrid Plant's Control Architecture

The fundamentals of the designed control scheme are presented in Figure 3.11, where the grid's power requirements and the meteorological data are used to estimate and control the power provided at the PCC of the overall plant. Therefore, the system has two different classes of inputs, on the one hand, Active Power requirements, which are established by the SO, the frequency control and the FFR supervisor, respectively. While, on the other hand, meteorological data (wind speed, temperature, irradiance) and initial SOC determine the availability of each asset, from which sub-plant and overall ones can be easily obtained.

It should be noted how the system obtains the overall performance of the plant by individually addressing the availability of every asset. Also, the first DISPATCH block obtains the reference for every sub-plant which then, after a second dispatch function, obtains the production of every asset; reconstructing the overall performance

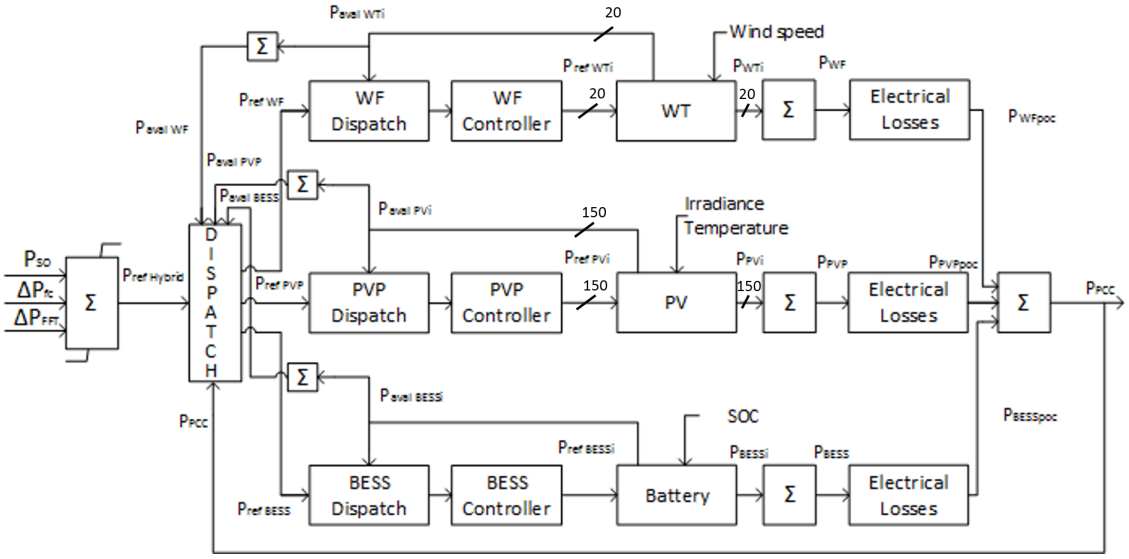

Figure 3.11: General Block Diagram of the Hybrid Power Plant.

afterwards. Finally, the actual generation of the HyPP is used to estimate the electric losses inside the plant, resulting in the production found in the PCC, which is then used as feedback for the overall Power Plant Controller (PPC).

3.6 Definition of Scenarios

Since the focus of this project is on FFR, the defined scenarios should allow to capture relevant issues in the system, while being relevant to reality. Thus, all the scenarios start in steady state operation for reference, then a N-1 contingency occurs, the variable part of the scenarios is the penetration rate of the HyPP on the overall system and the size of the fault.

3.7 Evaluation Criteria

Provided the nonexistence of grid codes regulating FFR, few constraints, as well as an evaluation criteria are introduced in this section in order to establish what is considered acceptable by the author.

Constraints:

- Nadir: The nadir point is not allowed to fall beyond the original value with traditional generators instead of renewable based.
- National Grid codes limits frequency deviations below 49.5 Hz for no more than 60 seconds.
- Load shedding is not allowed, therefore the frequency mustn't fall below 49,2 Hz.
- Second Dip: As it was aforementioned, European SO do not allow a second frequency dip after the IR under any circumstance. However, this is an issue for the FCR, not FFR.

Regarding the evaluation criteria, the results are considered to be successful if, after an N-1 contingency, the nadir point is kept over the 49,2 Hz limit and the reaction occurs in less than 1 second.

3.8 Summary

In this chapter, the system's operational essence has been presented, as well as the analysed system and plant; but also the general requirements and specifications. Subsequently, the functional description of the control system to be implemented was introduced a long with the considered scenarios and the evaluation criteria.

Briefly, the 100 MW HyPP, compound by a 100 MW WF, 31,5 MW PVP and 28 MW BESS, is connected in bus 5 of the 12-bus system. The control strategy computes the power needs of the grid and the availability in order to establish the operational set-points of, both, sub-plants and individual assets. Such control strategy relays on the idea of computing the power needs while considering the availability at the same time. Finally, the objective is primarily to avoid a frequency reduction capable of triggering load shedding stages or even blackouts; and, secondarily, improve the Nadir point and recovery time comparatively with a traditional IR lead by synchronous generators.

The next chapter is focused in the control architecture, the type of control, the followed tuning procedure and preliminary testing; but also, intra-plant losses estimation.

Chapter 4

Control System Design

In this chapter, the methodology used to derive the plants' transfer function is presented, along with the estimation and impact of the electrical losses. Finally, several controllers are designed to regulate the normal operation of the HyPP.

4.1 Characterisation of Transfer Functions

Transfer Functions can be used to study and alter a system's behaviour by including a controller. Therefore, first order transfer functions have been used to represent the response of the three sub-plants compounding the HyPP system, whose expression is presented by equation 4.1. In such equation, the gain k has been considered to be unitary, while the settling time T_s has been determined by studying each specific model's response to step inputs.

$$G(S) = \frac{k}{T_s S + 1} \tag{4.1}$$

According to [73], the time constant a of a system represents, the initial slope of the response, or the period of time elapsed until the 63 % of the steady state value is reached, and it is expressed by equation 4.2. On the other hand, Ts is defined as the time required for the response curve to reach and stay within a 2 % range of the final value and, as presented by equation 4.3, it is related to the largest time constant of the system.

$$Initial\ slope = \frac{1}{Time\ constant} = a \tag{4.2}$$

$$T_s = \frac{4}{a} \tag{4.3}$$

Table 4.1 presents the estimated T_s for every sub-plant along with the implemented ones. They have been computed by considering power reference inputs of 0.7, 0.2 and 0.6 p.u. respectively for the WT, PV and BESS models described in Chapter 3. It should be stated that the used values have been extracted from industry insights, since, as aforementioned, several companies are investigating the potential of HyPP. Also, the T_s of the power converter used as link between the sub-plant and the grid has been included, since the control system should account also for its delay, which limits the speed of the BESS.

Table 4.1: Settling Times of the Transfer Functions.

Ts [s]	WF	PVP	BESS	Converter
Computed	0,8	0,4	0,0025	
Implemented	1	0,3	0,005	0,05

4.2 Losses Estimation

The internal losses of the HyPP must be accounted for in order to ensure a precise power injection at the PCC. The losses are derived from the electric transmission from the POC of the sub-plants to the substation where the PCC is placed as defined in Figure 3.10. It should be noted how, since the BESS is connected directly to the PCC, there are no losses to consider.

Distances between WTs are usually quite remarkable, in the range of 5 to 7 rotor diameters, therefore, a distance of 900 meters was considered. Also, 300 additional meters from the first WT to the WF's POC and then a 1 km line from there to the PCC. On the other hand, in the case of the PVP, only a 1 km line has been considered from the POC to the PCC. Data related to cable selection and parameters can be found in Appendix A. Lastly, it should be stated that such losses where computed by using the software DIgSILENT PowerFactory.

The impact of the various electrical parameters, such as the voltage at the PCC (Vg), the short circuit ratio (SCR), X/R ratio, and the injected power in the intra-plant losses were investigated in [74]. Therefore, in this thesis a similar approach has been followed. The power delivered to the PCC can be computed as expressed in equation 4.4. Also, The diagram of the plant is presented in Figure 4.1.

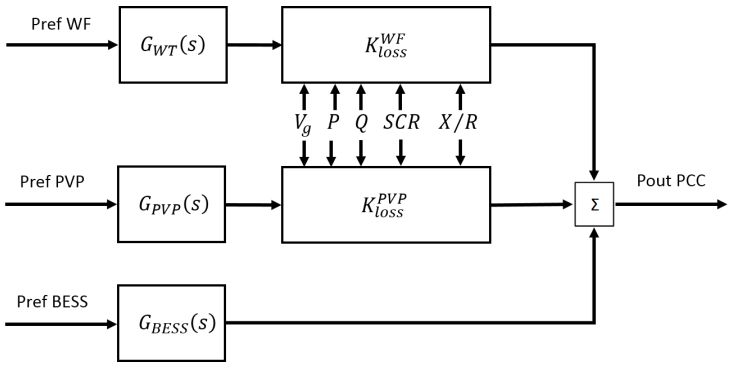

Figure 4.1: Transfer Function Diagram.

$$P_{PCC} = P_{POC}^{WF} + P_{POC}^{PVP} + P_{POC}^{BESS} - P_{loss}^{WF} - P_{loss}^{PVP} \tag{4.4}$$

Where P_{PCC}, P_{POC}^{WF}, P_{POC}^{PVP}, P_{POC}^{BESS}, P_{loss}^{WF}, and P_{loss}^{PVP} stand for the power injected in the PCC by the HyPP, power injected by the WF, PVP and BESS in their particular POCs and the losses of the WF and the PVP respectively. As it was aforementioned, such losses are a function of several parameters that can be expressed as:

$$P_{loss} = f\,(Vg,\, P,\, Q,\, SCR,\, R/X) \tag{4.5}$$

An analytic solution for the losses is not viable due to the large number of busses and the complexity of the system. In addition, different wind speeds, temperatures and irradiances lead to different operational points, causing different loading and losses. Therefore, simplifications are to be made in order to obtain a transfer function suitable for classical single input single output control theory. The plants are described as first order transfer function as it was already mentioned and a K_{loss} which will depend on Vg, X/R, etc. Such simplification is solid if the same output power is assumed for every asset in the sub-plant. Furthermore, since [74] proved the low effect of SCR, Q and X/R variations on the overall active losses, by considering them fixed, the final equation for the losses is:

$$P_{loss} = f\,(Vg,\, P) \tag{4.6}$$

Therefore, the losses of the WF and the PVP have been computed for different generation rates and Vg ranging from 0 to 1 p.u. in 0,1 steps for the power and from 0.9 til 1,1 p.u. in 0,05 steps for the voltage. Such limits for the voltages have been selected according to the TSO requirements in the UK. It should be stated that a SCR and X/R ratio of 10 has been considered. The resultant losses are presented in Figure 4.2 for the WF and the PVP respectively.

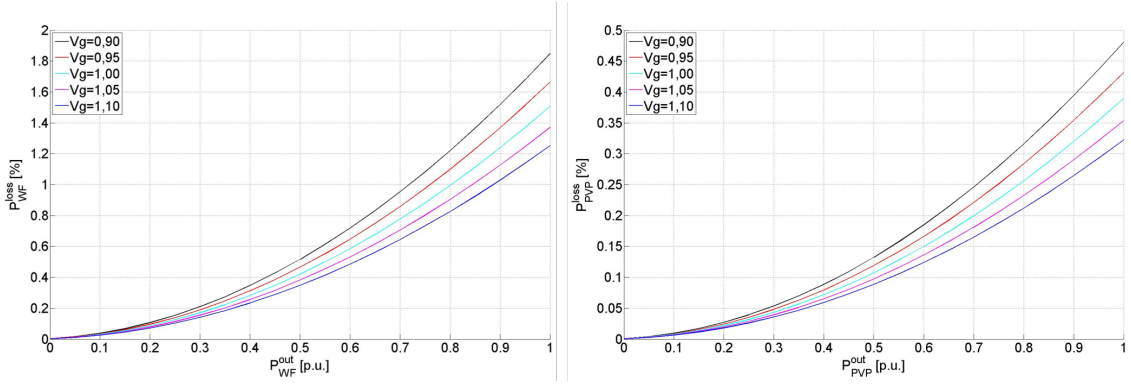

Figure 4.2: Losses for different P and Vg ratios for the WF (left) and the PVP (right).

Matlab's Curve Fitting Toolbox has been utilised to obtain the expression of the function described by equation 4.6. The fitting has been performed using 2nd, 3rd, 4th and 5th order polynomials, whose errors were then compared. Finally, 4th order polynomial was selected due to the fact that was the one with lowest error. The equation describing the curves is 4.7 while the final K_{loss} responds to equation 4.8. The values of the 4th order polynomial are presented in Table 4.2 while the errors for both the WF and the PVP are presented in Figure 4.3 respectively. It should be noted how the errors reduce quite fast as P increases, also, how the biggest error corresponds to areas where the operational point will not be commonly placed during long periods of time.

$$\begin{aligned} P_{loss} = {} & p00 + p10\,V_g + p01\,P + p20\,V_g^2 + p11\,V_g\,P + p02\,P^2 + p30\,V_g^3 + p21\,V_g^2\,P + \\ & + p12\,V_g\,P^2 + p03\,P^3 + p40\,V_g^4 + p31\,V_g^3\,P + p22\,V_g^2\,P^2 + p13\,V_g\,P^3 + p04\,P^4 \end{aligned} \tag{4.7}$$

$$\begin{aligned} K_{loss} = {} & 1 - (\, p00 + p10\,V_g + p01\,P + p20\,V_g^2 + p11\,V_g\,P + p02\,P^2 + p30\,V_g^3 + p21\,V_g^2\,P + \\ & + p12\,V_g\,P^2 + p03\,P^3 + p40\,V_g^4 + p31\,V_g^3\,P + p22\,V_g^2\,P^2 + p13\,V_g\,P^3 + p04\,P^4\,)/100 \end{aligned} \tag{4.8}$$

Table 4.2: Coefficients of the 4th order fitted polynomial

Coefficient	WF	PVP
p00	1,612	0,1449
p10	-7,167	-0,6467
p01	6,472	0,556
p20	11,86	1,074
p11	-17,82	-1,557
p02	7,835	0,6695
p30	-8,639	-0,7802
p21	16,9	1,5
p12	-10,04	-0,8905
p03	-0,1873	0,0007221
p40	2,337	0,2133
p31	-5,41	-0,4867
p22	3,609	0,33
p13	0,1633	0,004966
p04	-0,01342	-0,003787

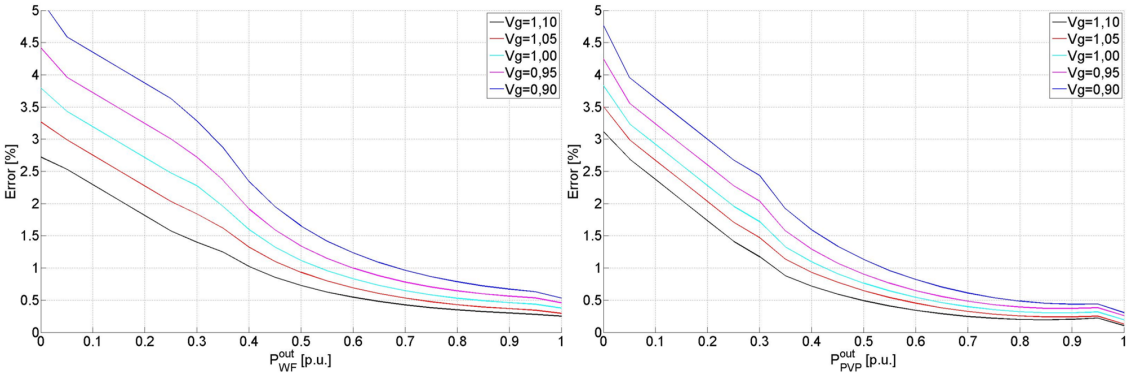

Figure 4.3: 4th order polynomial error for the WF (left) and the PVP (right).

4.3 Controller Design and Tunning

In this section, several different active power controllers are designed and evaluated. Even though the final objective of the thesis is to develop a FFR controller, it is a prior requirement to have a functional P controller in which a FFR stage will be added. The section starts by defining the minimum requirements of the controller based on grid codes, continues by designing and testing first a proportional controller and then an integral.

4.3.1 Performance Requirements

The minimum performance requirements established by the different considered grid codes are a settling time of less than 10 seconds for a 0,1 p.u. power reference variation, steady-state error less than 2 %. In addition to those, no overshoot has been allowed.

The basic diagram of any controlled system is presented in Figure 4.4, where the error signal between the power reference and the measured values (in the PCC) serve as the input. According to this, the controller generates an appropriate reference for the plant.

Table 4.3: Summary of the plant's operational point.

Parameter	Vg	P	Q	SCR	X/R	K_{loss}
WF	1	0,7	0	10	10	0,9922
PVP	1	0,5	0	10	10	0,9658
BESS	1	0,8	0	10	10	1

It should be noted that, every sub-plant has its individual controller, apart from one for the overall HyPP.

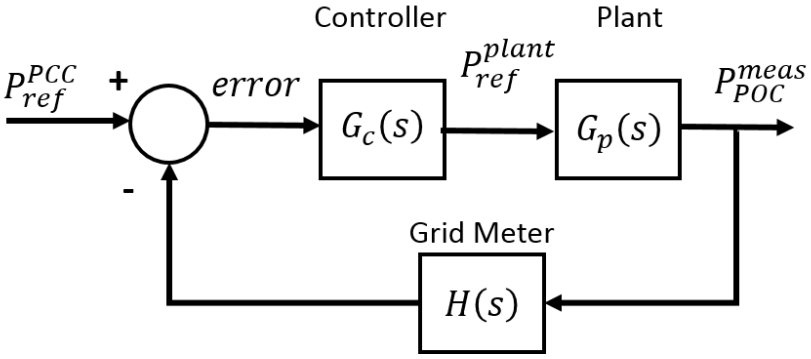

Figure 4.4: Closed loop control scheme.

Based on the closed loop scheme, the overall transfer function can be expressed as:

$$G_{cl}(s) = \frac{G_c(s)\, G_p(s)}{1 + G_c(s) G_p(s) H(s)} \tag{4.9}$$

Particularly, the plant's transfer function depends on K_{loss}, however, it should be noted how its value is 1 when applied to the BESS since the POC and the PCC coincide. Then, any of the sub-plants can be defined as:

$$G_p(s) = \frac{K_{plant} K_{loss}}{T_s S + 1} \tag{4.10}$$

Since K_{loss} does not have a fixed value, but can be expressed as a 4th grade polynomial as presented in Section 4.2, particular operational points are to be defined in order to design a controller. The summary of such operational points is presented in Table 4.3.

The active power measured in the PCC is not sent instantaneously to the controller. According to [75] the typical value of the delay is 15 ms, which can be modelled as a first order system with the following transfer function:

$$H(s) = \frac{1}{T_m S + 1} \tag{4.11}$$

Now that all the involved transfer functions have been presented, the suitability of different controllers is evaluated for each of the plants.

4.3.2 Proportional Controller Design

In this subsection, the procedure followed to design a suitable proportional controller and its evaluation is presented. First, the transfer function of any P controller is:

$$G_c(s) = K_p \tag{4.12}$$

Therefore, the closed loop transfer function of the a system with a P controller can be expressed as:

$$G_{cl}(s) = \frac{K_p K_{loss}\left(T_m S + 1\right)}{T_m T_{plant} S + \left(T_{plant} + T_m\right) S + 2 + K_p K_{loss}} \tag{4.13}$$

Then, the steady-state value of the closed loop with a P controller is expressed by:

$$P_{PCC}^{meas} = \lim_{s \to 0} G_{cl}(s) P_{PCC}^{ref} = \frac{K_p K_{loss}}{K_p K_{loss} + 1} P_{PCC}^{ref} \tag{4.14}$$

Therefore, by applying the final value theorem, the expression for the steady-state error can be computed for an step input as presented in equation 4.15, which, rearranging, leads to the expression of K_p dependent of the error as presented by equation 4.16.

$$error = \frac{1}{K_p K_{loss} + 1} \tag{4.15}$$

$$K_p = \frac{\frac{1}{error} - 1}{K_{loss}} \tag{4.16}$$

As it was aforementioned, the error should be less than 2 % according to the grid codes. In order to provide a reasonable safety margin, the desired error has been set to 1, 1,5 and 2 %; then, the behaviour of such K_p has been studied. The different values of K_p are presented in Table 4.4 for each sub-plant.

Table 4.4: K_p values for each sub-plant and allowed error.

Error [%]	K_p^{WF}	K_p^{PVP}	K_p^{BESS}
1	99,77	102,51	99
1,5	66,18	67,99	65,67
2	49,38	50,73	49

The Root locus of the closed loop of every plant after the addition of a controller was analysed in order to study the gain range within stable operation. In order to keep the report short, here only the root loci including the WF's Proportional controller is presented in Figure 4.5, were it can be seen how the system is stable for any K value. However, the rest of the graphs and analysis are presented in Annex Annex B.

Additionally, Bode plots were used in order evaluate the stability, but also the Gain Margin (GM) and Phase Margin (PM) of the system. Again, only the Bode plot of the WF is included in order to avoid over-repeating, however, the rest of the graphs and analysis can be found in Annex B. Thus, Figure 4.6 presents the bode plot of the P controller, open- and closed-loops. The systems GM is infinite since the phase never crosses 180^o and the PM corresponds to $53,2^o$; resulting in a stable system as it was expected form the root locus.

In order to verify the performance of these controllers, a series of simulations have been carried out for the upper and lower values of K_p. In such simulations the reference

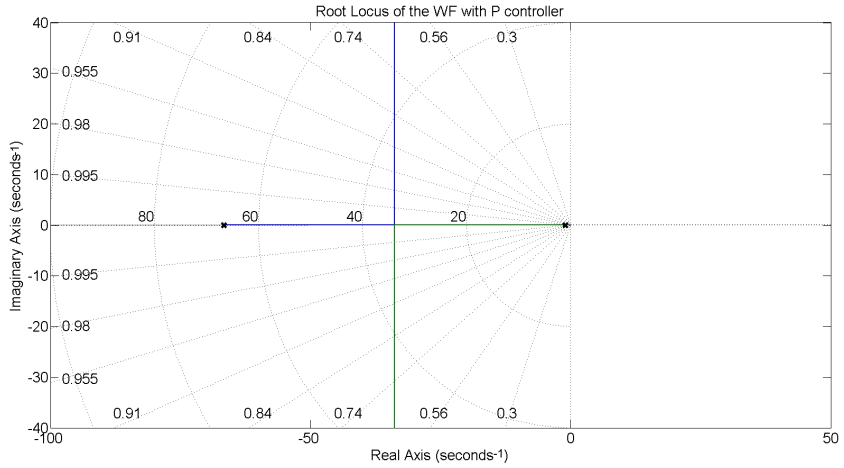

Figure 4.5: Root locus of the closed loop WF with P controller.

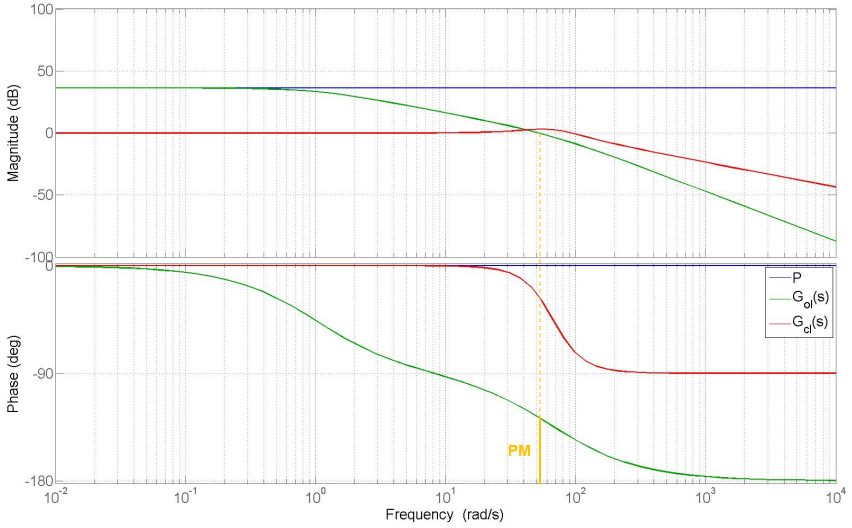

Figure 4.6: Bode Plot of the closed loop WF with P controller.

has been varied 0,1 p.u. and since the results present a steady-state error of 1,5 %, it has been concluded that a proportional controller is not enough for the system. Therefore, a Integral stage is considered.

4.3.3 Integral Controller Design

The PI-controller is designed by replacing the slowest pole of the sub-plant's transfer function with a pole in the origin. Ultimately yielding a closed loop transfer function with a response similar to the sub-plant. Equation 4.17 presents the transfer function of such controller.

$$G_{PI} = K_{PI}\frac{T_{PI}\,s + 1}{T_{PI}\,s} \tag{4.17}$$

Where K_{PI} and T_{PI} are the proportional and time constants of the PI controller respectively. In fact, T_{PI} has the same value as the sub-plant's time constant. On the

other hand, K_{PI} is obtained as:

$$K_{PI} = \frac{T_{PI}}{K_{loss}} \tag{4.18}$$

Table 4.5 presents the results of the PI design for the three sub-plants.

Table 4.5: PI-controller parameters for each sub-plant.

K_p^{WF}	T_{PI}^{WF}	K_p^{PVP}	T_{PI}^{PVP}	K_p^{BESS}	T_{PI}^{BESS}
1,008	1	0,3106	0,3	0,005	0,005

Again, the Root locus of the closed loop of every plant after the addition of a PI controller was analysed in order to study the gain range within stable operation. In order to keep the report short, here only the root loci including the WF's PI controller is presented in Figure 4.7, were it can be seen how the system is stable for any K value. However, the rest of the graphs and analysis are presented in Annex B.

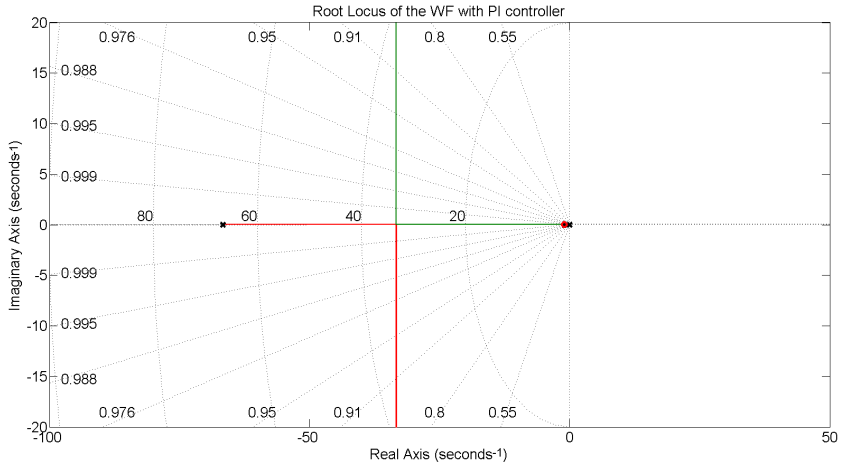

Figure 4.7: Root locus of the closed loop WF with PI controller.

Additionally, Bode plots were used in order evaluate the stability, but also the Gain Margin (GM) and Phase Margin (PM) of the system. Again, only the Bode plot of the WF is included in order to avoid over-repeating, however, the rest of the graphs and analysis can be found in Annex B. Thus, Figure 4.8 presents the bode plot of the P controller, open- and closed-loops. The systems GM is infinite since the phase never crosses 180^o and the PM corresponds to $89,1^o$; resulting in a stable system as it was expected form the root locus.

Finally, the behaviour of the different power plants is studied; Figures 4.9 to 4.12 present the responses of the WF, PVP, BESS and overall HyPP respectively. It should be noted how the responses comply with the requirements stated in section 4.3.1. Also, it should be noted how the different sub-plants present different actuation times, which might not be currently an issue but it can be problematic, once the FFR functionality is added on top of this basic control layer.

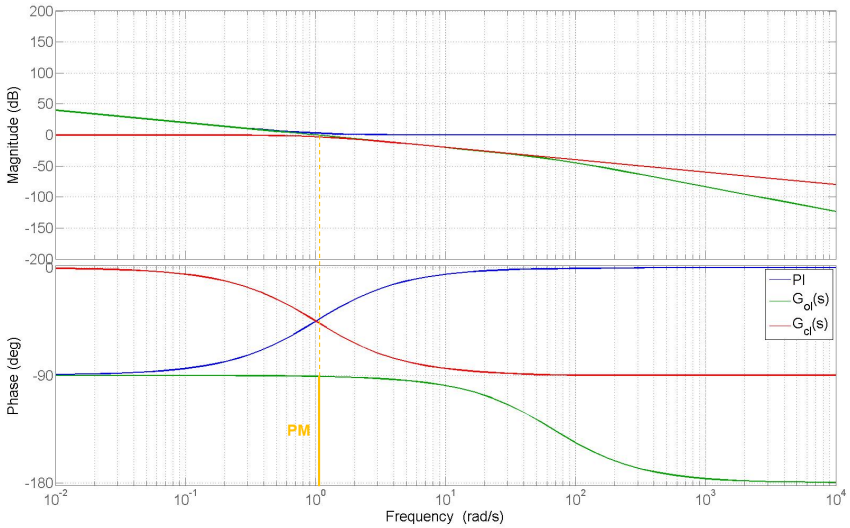

Figure 4.8: Bode Plot of the closed loop WF with PI controller.

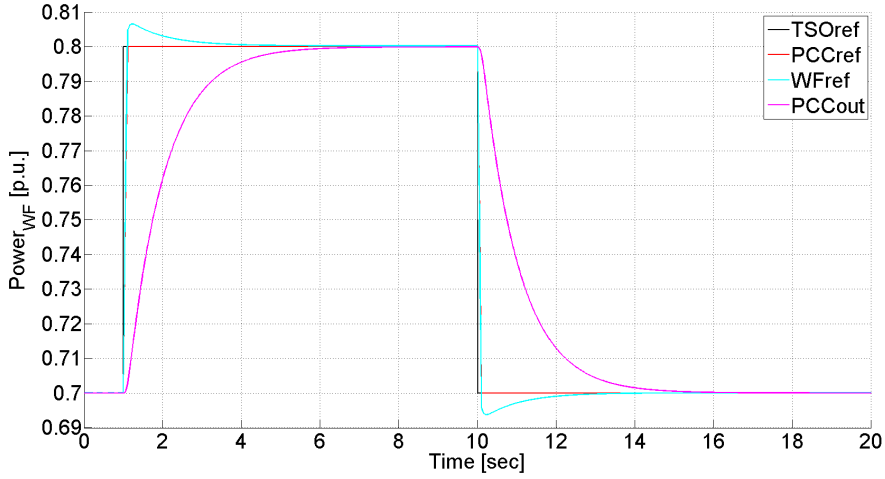

Figure 4.9: WF response for a 0,1 p.u. variation.

4.4 Dispatch

In this section, the considered approach for the HyPP's dispatch is presented. During the initialisation, the demand is allocated prioritising WF and PVP generation over BESS discharge. Also, if there is enough availability, the dispatch distributes the generation leaving curtailed power in both sub-plants, since that potential is interesting for controlling purposes. Then during the normal operation of the HyPP, the external reference (TSO's signal) will vary in steps according to the expected load at any time, but also, the automatic frequency control strategies will modify such reference, however more frequently and in predictably smaller proportion. Therefore, considering such operation, the main considerations of the implemented dispatch function are:

- Desirable power allocation with a maximum step size of 0.1 p.u.
- The priority when allocating is minimising the stresses while responding fast.

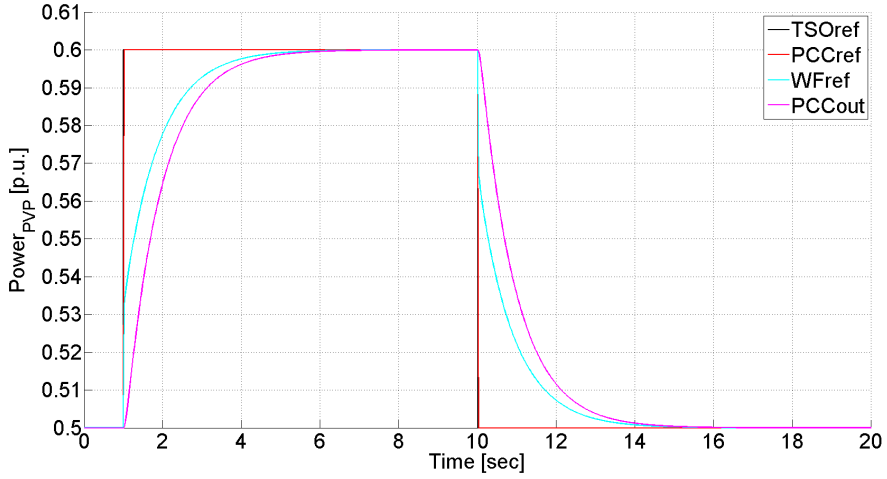

Figure 4.10: PVP response for a 0,1 p.u. variation.

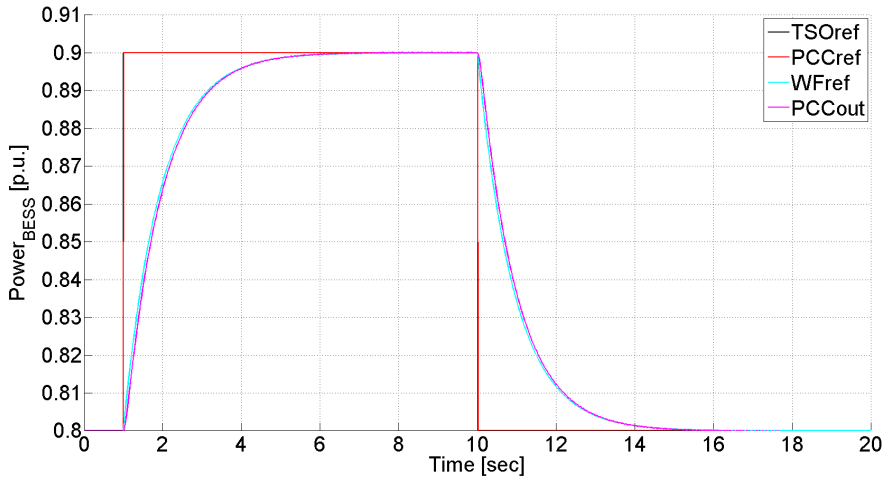

Figure 4.11: BESS response for a 0,1 p.u. variation.

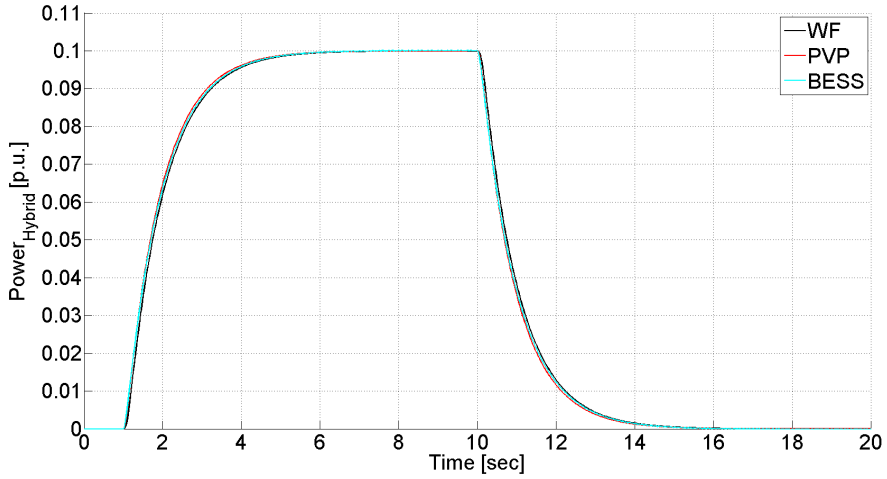

Figure 4.12: Hybrid response for a 0,1 p.u. variation.

- Avoid unnecessary life-expectancy reduction.

The allocation limit responds to the objective of sharing the demand among the sub-plants as evenly as possible. The second requirement is meant to reduce mechanical stresses in the WTs on the one hand and to avoid losing stored energy in the BESS, since its targeted ancillary service is more likely to be power smoothing and up-ward frequency regulation. Finally, the third objective considers the physical behaviour of every system (stress, inertia, operational limits, etc) in order to avoid operational points or settings that might damage the assets, i.e. the charge limit of the BESS is limited to 0.5 p.u. while the discharge is allowed up to 1 p.u. (4-C rate).

The scope of the project should be kept in mind when analysing the designed dispatch function. Since the objective is to analyse frequency response strategies and not regular steady state operation, there is no economical optimisation or the like. Thus, once the frequency response is triggered, the priority is set in the speed of the reaction; subsequently, the priority when assigning power changes is BESS, PVP and WF.

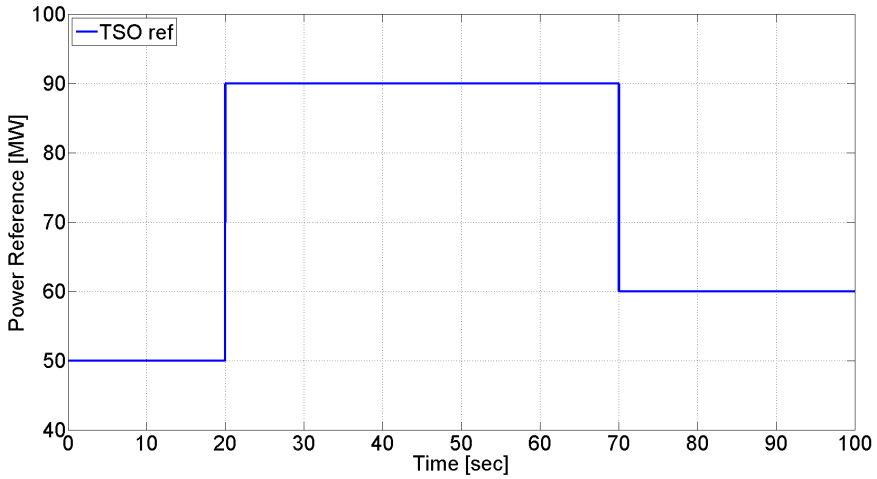

Figure 4.13: Power Set-point Characteristic.

In a preliminary set of simulations, the system's response to changes in the TSO reference was studied. Figure 4.13 presents the considered TSO reference, it should be noted how it starts with a value of 50 MW, in second 20 changes to 90 MW; finally being modified to 60 MW in second 70. The first step is meant to represent a sudden lost of generation or load increase in the power system, while the second the opposite. Particularly, Figures 4.14 to 4.17 presents the output of the Dispatch function; the reference signals of every sub-plant, and the output of every sub-plant and the HyPP in the PCC respectively. Thus, the reaction of the sub-plants to the different references is shown. Finally, Figure 4.18, which presents the evolution of the deviation from the reference during the operation, proves how the designed system chases the reference as a first order system without overshoot and no steady-state error.

Provided the satisfactory results obtained at this point, the model is ready to include a frequency response stage, whose design is covered in the next section.

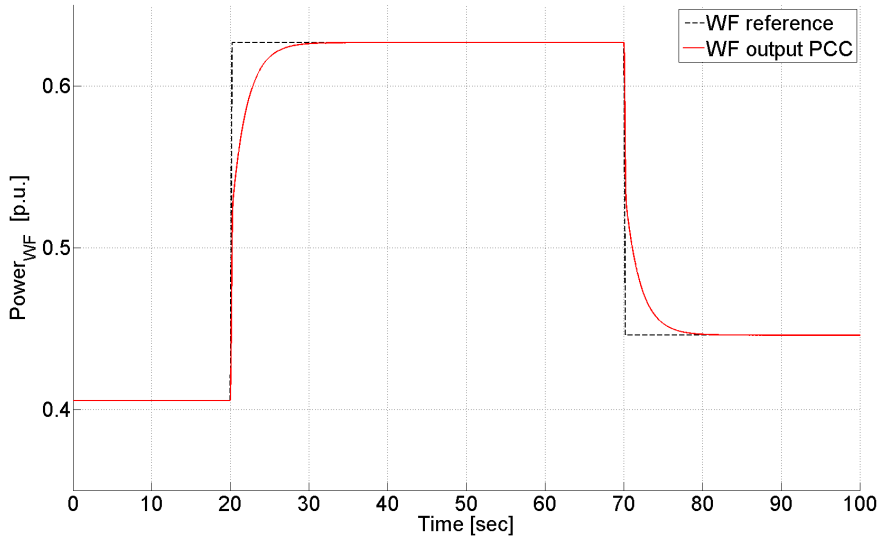

Figure 4.14: Reference and response of the WF sub-plant.

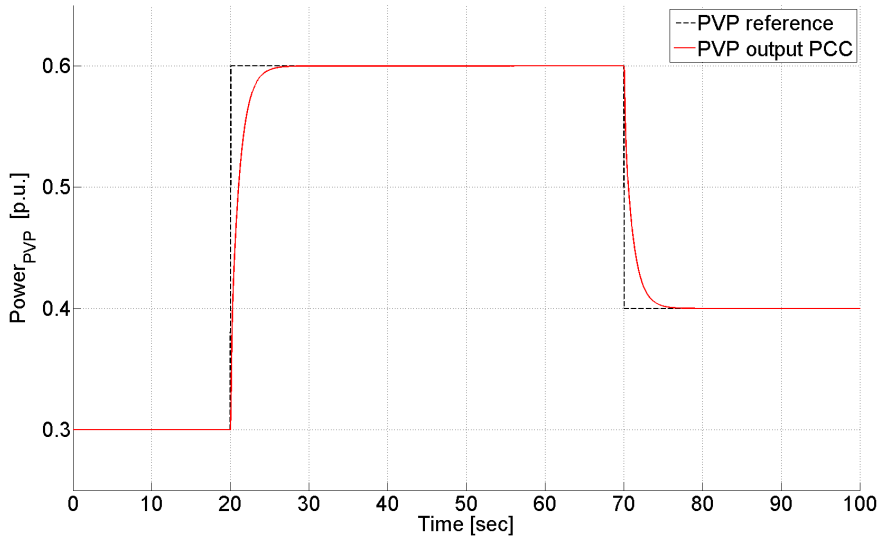

Figure 4.15: Reference and response of the PVP sub-plant.

4.5 Fast Frequency Response Implementation

To the knowledge of the author there is currently no consensus in how to approach FFR. However, authors like [76, 77, 78] coincide in the idea of combining a classical droop control with a df/dt, since both system have been in use in automatic frequency control for years.

Briefly, droop control consist on a straight-line function, that establishes a linear actuation based on the input (the slope) defined by equation 4.19. Where R, f_{meas}, f_n, P_0, P_{Gen} and P_n stand for the droop constant or slope, measured frequency at the PCC, nominal frequency of the system (50 or 60 Hz), active power production before the frequency variation, instantaneous active power generated and nominal active power of

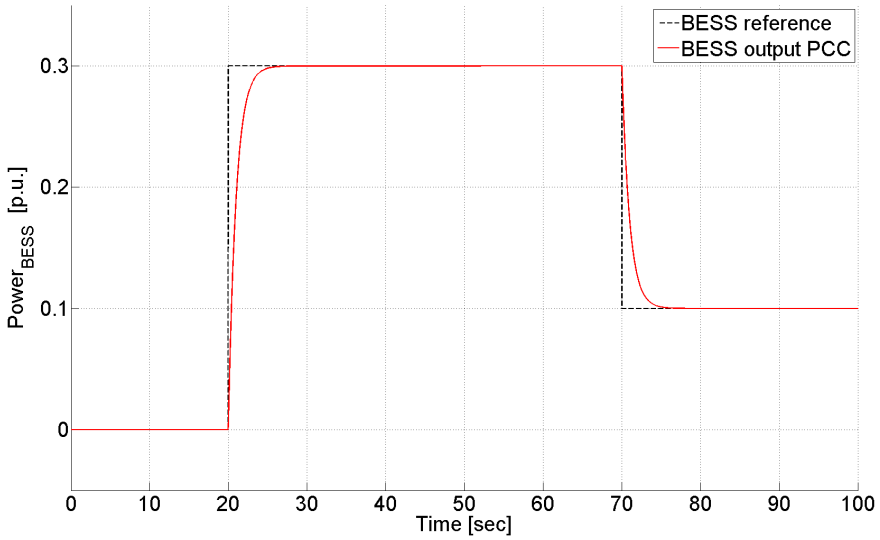

Figure 4.16: Reference and response of the BESS sub-plant.

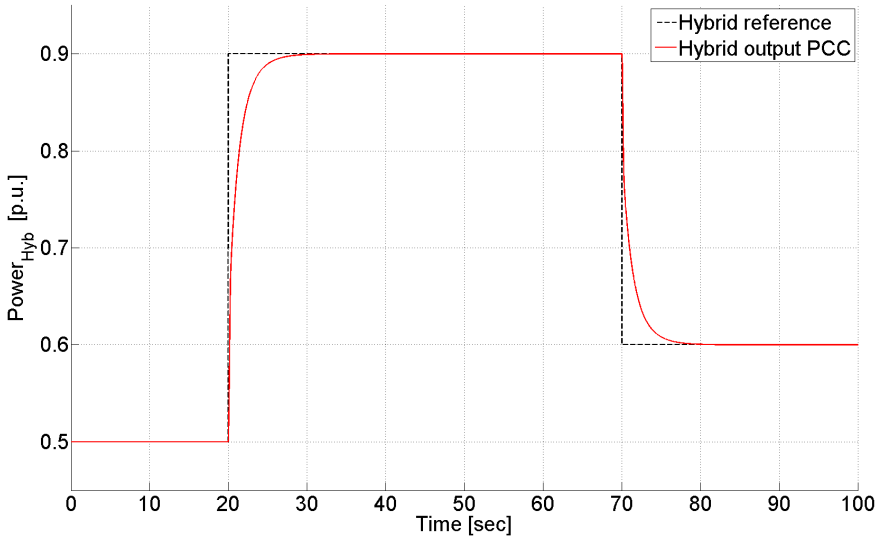

Figure 4.17: Reference and response of the Hybrid plant.

the plant. In this case, the input is f_{meas} and the output P_{Gen}. Again, there is no consensus about the value of such slope, however, ENTSO-E recommends values between 2 and 12 %; nevertheless, rates between 3 and 5 % are implemented in practice [79]. Figure 4.19 presents the droop actuation for an R of 5%, it should be noticed how the response is positive for frequency values under 50 Hz and vice versa.

$$R = -\frac{\frac{f_{meas}-f_n}{f_n}}{\frac{P_0-P_{Gen}}{P_n}} \tag{4.19}$$

On the other hand, the derivative control, or df/dt control, modifies the active power reference by means of the ROCOF value and a gain. As aforementioned in Section 2.4.5, current frequency detection techniques include a fair amount of noise in the measure-

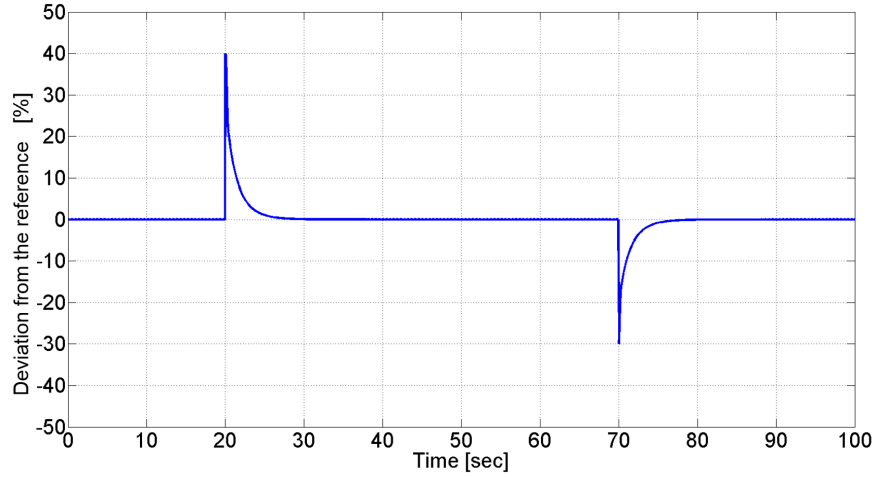

Figure 4.18: Deviation from the reference of the Hybrid plant.

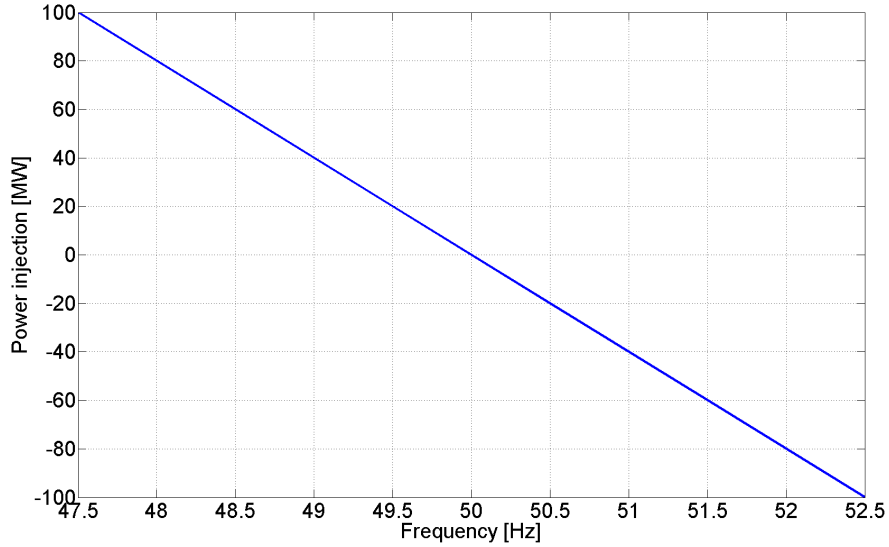

Figure 4.19: Block Diagram of the Frequency Control.

ments and, since derivative control is sensitive to it, a low-pass filter is added. It is worth mentioning how Figure 4.20 presents the block diagram of both control approaches. Suitable dead bands have been included in order to avoid undesired actuation in the vicinity of the nominal frequency value. Finally, A summary of important parameters can be found in Table 4.6. Finally, it should be stated how Figure 4.21 presents an example of the FFR control actuation, where the green line marks the nadir point. The df/dt control actuates only during high ROCOF variations, while the droop control does it during the whole fault.

The values presented in Table 4.6 are based on experimental obtainment given the nonexistence of a better approach. However, the selected values are supported by the thorough sensitivity analysis presented in [77] and the ENTSO-E recommendations. This frequency control stage is added to the already existing model and tested in the next chapter.

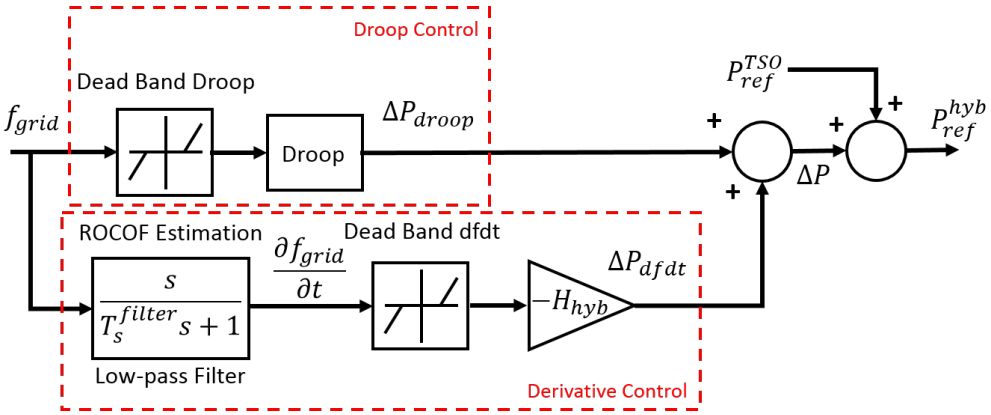

Figure 4.20: Block Diagram of the Frequency Control.

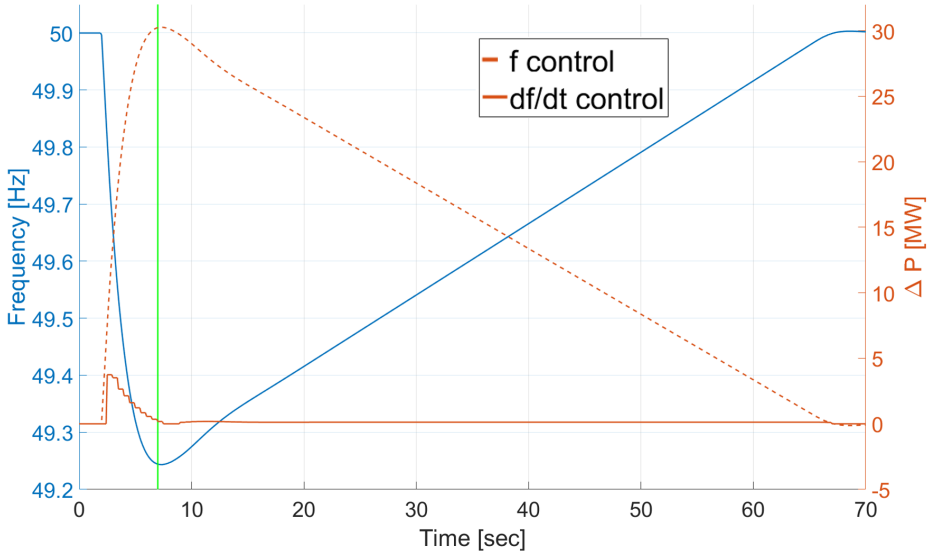

Figure 4.21: Block Diagram of the Frequency Control.

Table 4.6: Summary of the implemented frequency control parameters.

Parameter	Unit	Value	Notes
Dead band - Droop	Hz	0,02	Reduce activity of the control
R	%	5	Slope of the Droop control
Dead band - df/dt	Hz/s	0,5	Reduce activity of the control
T_{LPF}	s	0,025	Time constant of the low-pass filter
H_{hyb}	s	5	Inertia Constant of the plant

4.6 Summary

In this chapter, the characterisation of transfer functions has been presented, as well as the intra-plant losses estimation; performed as a polynomial approximation of the plant's simulated behaviour in Power Factory. Subsequently, the design and tunning of the active power controllers was addressed; firstly by establishing their performance

requirements. Then, root locus and bode plots of the designed P and PI-controllers were analysed in order to select the most suitable. Afterwards, the considerations taken into account while programming the Dispatch function of the HyPP were presented along with a preliminary testing of the model. Finally, FFR stage was designed and implemented as a two stage control: droop and ROCOF (df/dt).

The next chapter is focused in model testing, first in the continuous time (S-domain) and then in the discrete time (Z-domain). Also, few relevant scenarios are defined and tested in a similar approach.

Chapter 5

Tests and Evaluation

In this chapter, the developed model is tested along with the different control systems. Such tests are undertaken first in continuous time and then, after converting the the model from S to Z-domain, in discrete time. In the particular case of the discrete model, several scenarios are defined and evaluated. Lastly, conclusions are dragged from the analysed scenarios.

5.1 Continuous Time Model Testing

In order to evaluate the performance of the model with the additional frequency control, a frequency signal is needed. However, since the model does not include and external grid yet, the analysis is in open loop, using artificially generated frequency values. The generated values are random numbers between 48 and 52 Hz with a resolution of 100 values per second, Figure 5.1 presents 1,5 seconds of such signal, along with the cumulative power injection calculated by the additional frequency control.

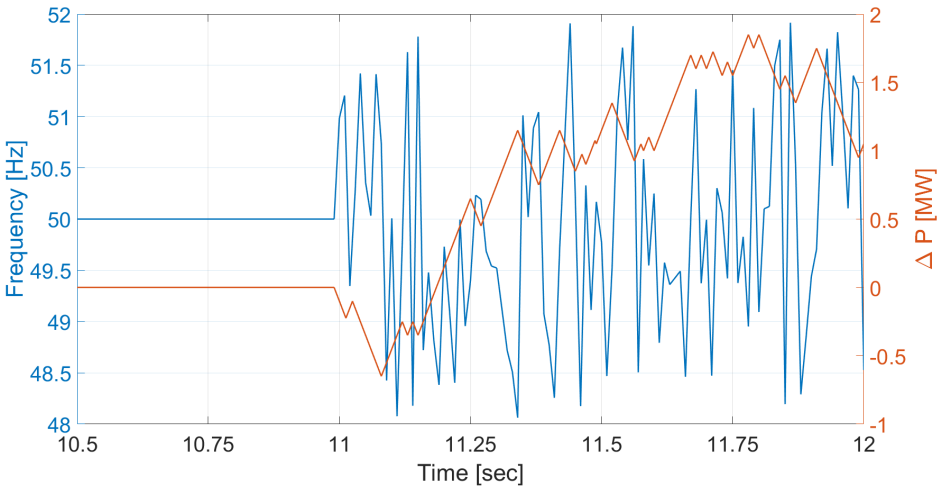

Figure 5.1: Frequency Signal and Requested Power Injection.

Subsequently, the system's response to changes in the TSO reference together with the frequency control was analysed. Figure 5.2 presents the considered reference, it should be noted how, the TSO reference starts again with a value of 50 MW, in second 20 changes to 60 MW; finally being modified to 40 MW in second 70. Particularly, Figure 5.3 presents the output of the Dispatch function; the reference signals of every sub-plant, and the output of every sub-plant and the HyPP in the PCC. Thus, the re-

action of the sub-plants to the different references is shown, it should be noted how the BESS response is enough to compensate for the frequency control, while the WF and the PVP get activated only when the TSO reference is changed, thus the HyPP is able to support the grid's frequency without affecting their lifetime. Finally, Figure 5.4 presents the evolution of the active power deviation between reference and output during the operation, it is worth mentioning how it remains within ± 2 % except right after the TSO reference is changed; thus following the requirements stated in Chapter 4. Also, provided the artificial frequency values in use, it is expected how, in a real system, the deviation will be significantly smaller than in this simulations, since the variations won't be random, but casual.

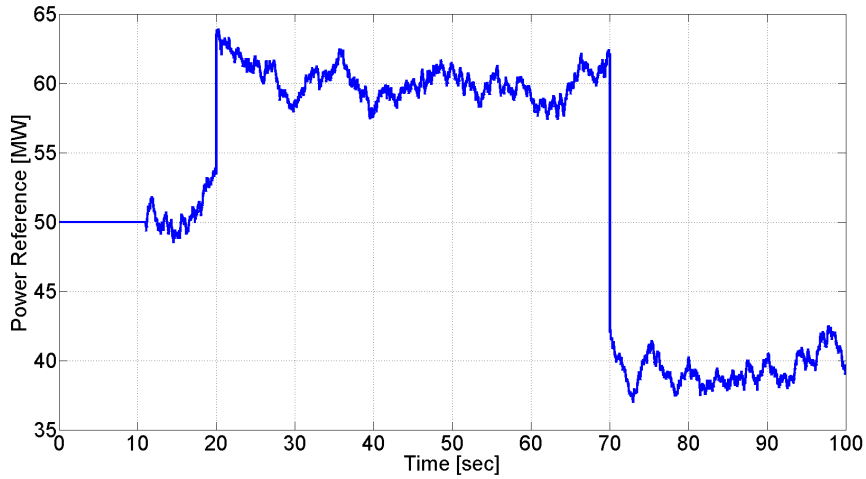

Figure 5.2: Power Set-point Characteristic.

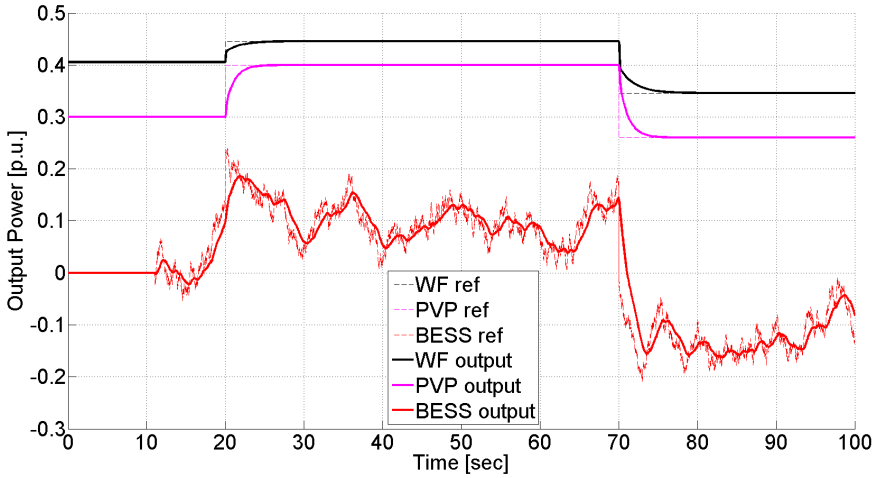

Figure 5.3: Reference and response of the sub-plants.

In conclusion, despite of the fact that at this point it is not possible to analyse the effect of the HyPP behaviour in a power system, the developed model responds as expected, thus resulting in promising results. However, so far the model was studied in the continuous time, in the next section, its discretization is addressed and re-evaluated.

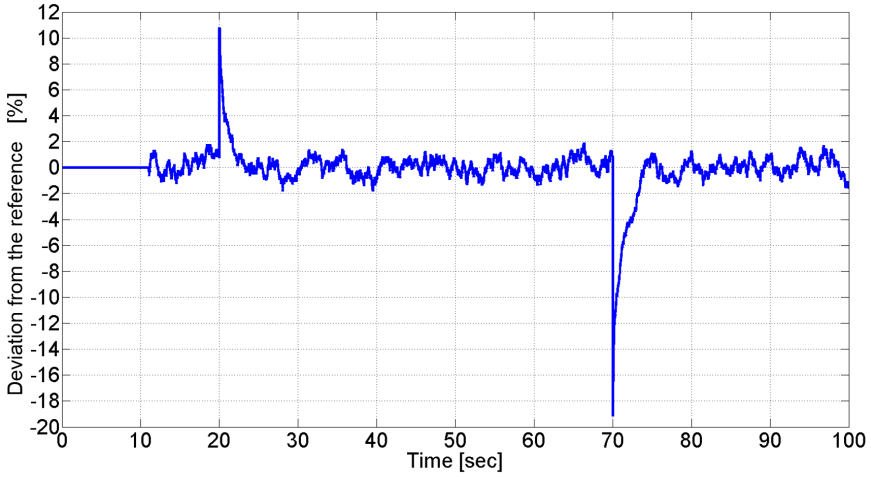

Figure 5.4: Active power deviation between the reference and the output.

5.2 Model Discretization

The model has been discretized by using the Backward Euler Method, since it is easy to implement and unconditionally stable, whereas in the Forward Euler method is limited by the step size. On the other hand, the Trapezoidal method (Tustin) was not selected despite having the best theoretical accuracy due to its higher computational demands and since in real applications such additional precision is lost as according to [80].

A deeper explanation of the followed discretization process is presented in Annex C. Also, the selected sampling times are summarised in Table 5.1, such values have been chosen according to real industrial applications and the limitations of comercial controllers.

Table 5.1: Summary of the Sampling Times.

System	Measurements	Sub-plant	Control
Sampling time [ms]	10	1	100

The Discrete model was validated following the same approach as for the continuous, obtaining similar results, thus, in order to avoid over-repeating, such analysis can be found also in Annex C.

5.3 Discrete Time Model Testing

Provided the accurate performance of the open loop (in terms of active power) discrete model, a block representing the electric grid is added in order to evaluate the frequency behaviour. Equation 1.1, which was presented in Chapter 1, explains the dependency of the frequency, by rearranging such expression, equation 5.1 is obtained.

$$ROCOF = \frac{\Delta f}{\Delta t} = \frac{(P_G - P_L)\ f_n}{2\,H\,S} \tag{5.1}$$

In the emulated system, H is considered to be 3 seconds, since it is the typical value of grids with high rates of renewable energy like Denmark, while S is 1000 MW. Then, from the previous equation, the frequency is easily obtained by integrating the ROCOF; both signals are then appropriately connected to the frequency control stages of the FFR controller. Figure 5.5 presents the included block which performs such tasks, which internally implements equation 5.1. It should be noted how, despite using the electric system presented in Section 3.2, it was scaled down to 1000 MW of installed power, thus the HyPP size is relevant, representing a 10 % of the total system. However, in few of the scenarios, the plant's size is increased up to 500 MW in order to represent a 50 % system penetration. Also, the natural IR of the synchronous generators present in the 12-bus has not been included in the model; thus, only the implemented FFR prevents the frequency drop; configuring a worst case scenario.

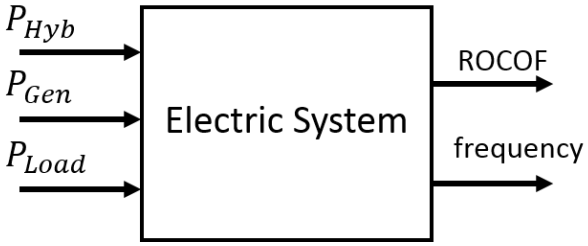

Figure 5.5: Frequency Estimation Block.

5.3.1 Definition of Scenarios

This section contains a brief description of few selected scenarios whose results and evaluation are presented in the following section. Table 5.2 summarises the different scenarios analysed in this chapter, however, two additional ones are presented in Annex D due to their reduced relevance.

Table 5.2: Summary of Scenarios

Scenario	Hybrid Plant Size [MW]	Penetration [%]	Event
A	100	10	Single -30 MW variation
B	500	50	Single -30 MW variation
C	500	50	Single -100 MW variation
D	500	50	1000±5 MW secondly variation

It is worth mentioning how, in Table 5.2, ΔP stands for the difference between the instantaneous generated and consumed power. While, particularly, penetration is calculated by following equation 5.2; where P_{Hyb} and P_{Syn} stand for the installed power of Hybrid and traditional Synchronous power plants respectively.

$$Penetration = \frac{P_{Hyb}}{P_{Hyb} + P_{Syn}} 100 \tag{5.2}$$

All the scenarios start with a balanced system where the production matches the demand. In this initialisation, the HyPP is providing 50 % of its maximum output. Then, the event is triggered, which in scenarios A, B and C consist on a generation loss (N-1

contingency); then the HyPP responds alone to the event until it is cleared. Particularly, in scenario D, the load is considered to have a changing value of $1000 \pm 5\,MW$, such value is modified randomly once every second. This scenario is meant to represent the normal behaviour of a normal power system in which load is permanently changing in the vicinity of the predicted value, creating small frequency disturbances that should be minimised by the power plant in charge of the regulation. Again, such regulation is performed only by the HyPP.

5.3.2 Test and Evaluation

In the following sections, the aforementioned scenarios are analysed. However, it should be stated how, in order to resemble a realistic frequency response, after the FFR stage (focus of this thesis) a simple PFR has been included. It consists of a 0.1 pu/s power ramp that starts 3 seconds after the event detection and stops once the 50 Hz pre-event frequency has been reached. If this compensation is not added, then the FFR stage will only be able to stop the frequency drop, but it won't compensate it. The time delay of 3 seconds has been chosen according to the ENTSO-E and British grid regulations which state that PFR should act with a delay of maximum 2 seconds in inertial plants. This simplistic PFR helps to evaluate the quality of the FFR stage. Finally, it should be stated how the power slope considered for the PFR complies with current technical limitations as Maximum Ramp Rates for External Control of WTs as according to [81].

5.3.3 Contingencies - FFR

Scenario A

In this scenario, a 30 MW generation loss is compensated by the HyPP. It should be noted how this variation represents 30 % variation of the plant's maximum production, and, since it starts by producing 50 %, the final production after the faults is around 60 % more than the initial.

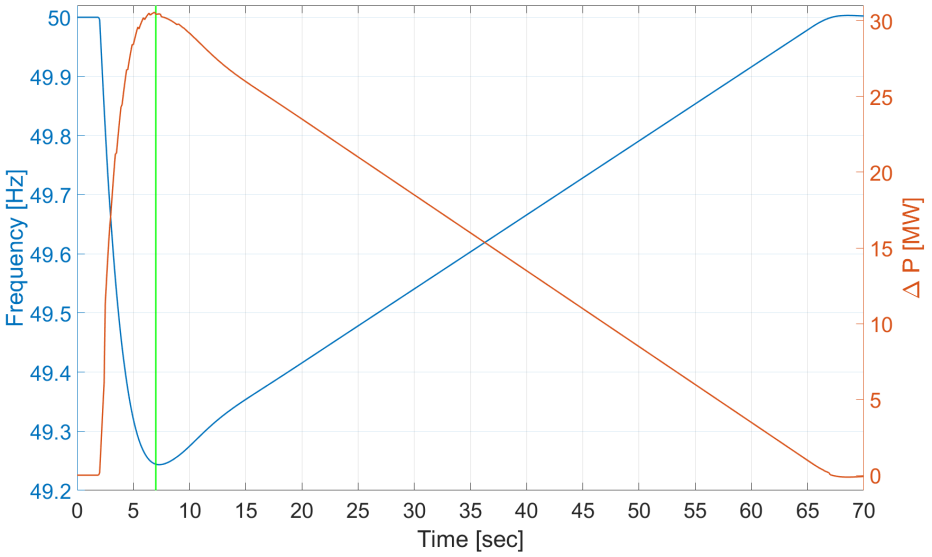

Figure 5.6: Frequency and ΔP_{FFR} variation.

Figure 5.6 presents the frequency variation along with the active power variation caused by the FFR controller. It should be stated that the PFR compensation is not recorded in this Figure. In this Scenario the Nadir point is reached 2.8 seconds after the fault (marked with the green line in the graph) with a value of 49,24 Hz. Then, the nominal frequency is smoothly regained after 50 seconds thanks to the simplistic PFR.

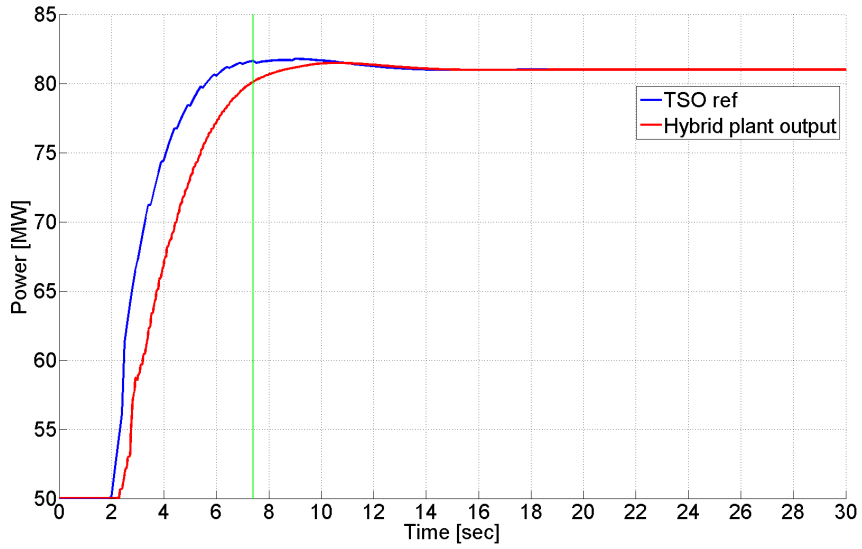

Figure 5.7: Hybrid plant reference and output.

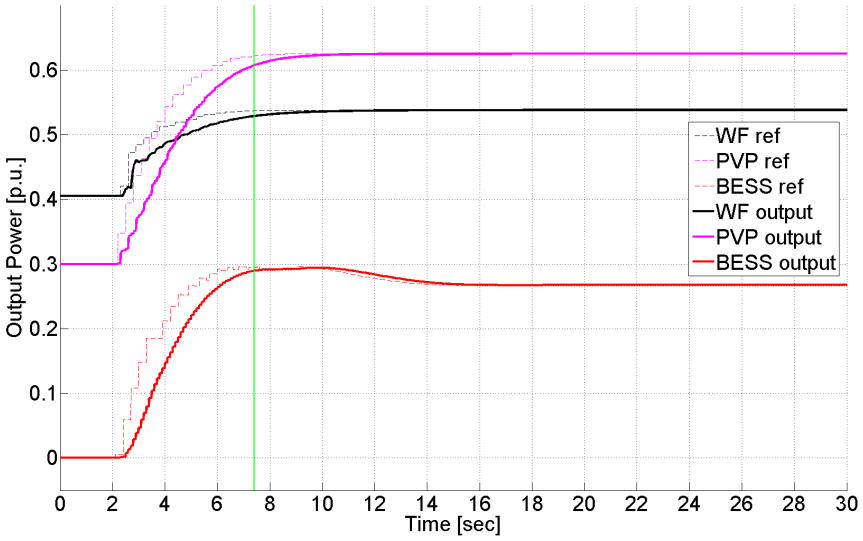

Figure 5.8: Sub-plants reference and output.

Figure 5.7 presents the reference of the whole HyPP, which is compound by, the TSO reference (constant at 50 MW), the FFR controller and, lastly, the simplistic PFR. In the same graph is also presented the output of the HyPP in the PCC. On the other hand, Figure 5.8 presents the references sent by the Dispatch function to every sub-plant and their subsequent response. It should be noted how the reference modifications are performed in the smallest steps possible and the reduction is optimised to affect only the

BESS discharge while maintaining steady the RE production. Again, the green lines signal the Nadir time. Finally, Figure 5.9 presents the overall active power deviation in the PCC computed as the difference between the HyPP's reference and output in %. It should be noted how the maximum deviation is found before the Nadir is reached, since that is the moment where the maximum ROCOF triggers the biggest response.

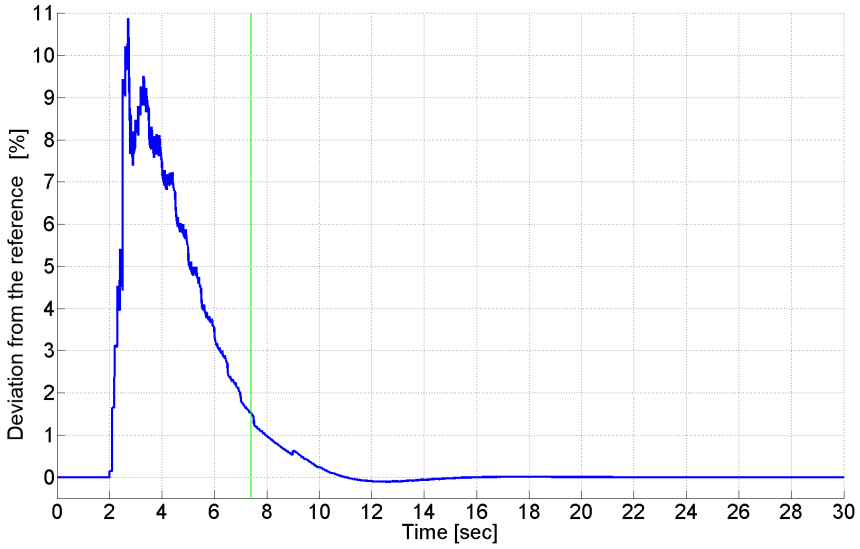

Figure 5.9: Active power deviation in the PCC.

The results obtained in this scenario are satisfactory, since the frequency is contained above 49,2 Hz point where frequency protections will be triggered, activating load shedding stages. Then, the power injection of the HyPP alone is capable of smoothly restoring the nominal operation of the system.

Scenario B

In this scenario, a 30 MW generation loss is compensated by the HyPP. It should be noted how this represents 6 % variation of the plant's maximum production, and, since it starts by producing 50 %, the final production after the faults is around 2,54 % more than the initial, thus the fault is comparatively smaller than the previous scenario.

Figure 5.10 presents the frequency variation along with the active power variation caused by the FFR controller. It should be stated that the PFR compensation is not recorded in this Figure. In this Scenario, the Nadir point is reached 0.8 seconds after the fault (marked with the green line in the graph) with a value of 49,77 Hz. Then, the nominal frequency is regained after 13 seconds thanks to the simplistic PFR. Particularly in this scenario, the recovery is not smooth, due to the amplitude of the FFR countermeasures and the long delay considered for the PFR, however, such undesired oscillations fall beyond the scope of this project.

Figure 5.11 presents the reference of the whole HyPP, which is compound by, the TSO reference (constant at 250 MW), the FFR controller and, lastly, the simplistic PFR. In the same graph is also presented the output of the HyPP in the PCC. On the other hand,

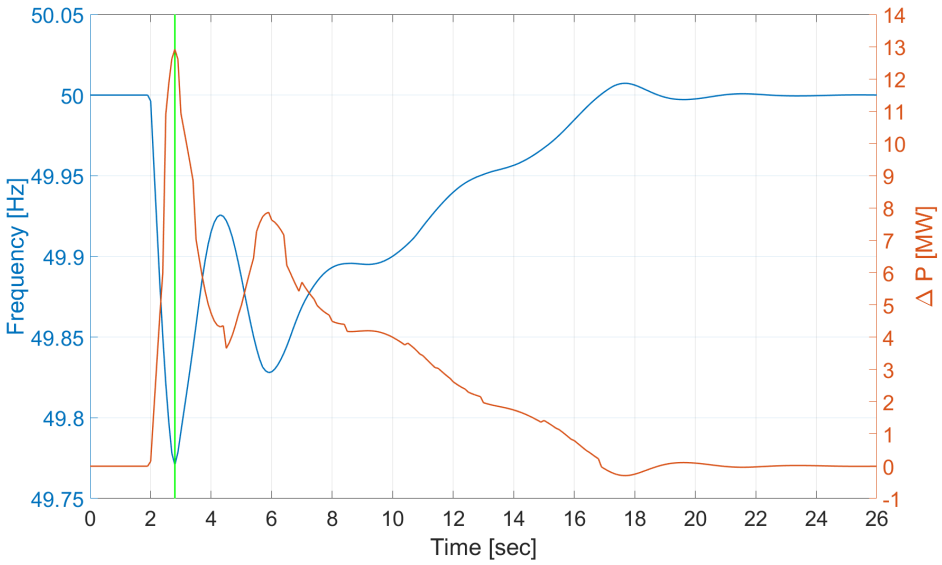

Figure 5.10: Frequency and ΔP_{FFR} variation.

Figure 5.12 presents the references sent by the Dispatch function to every sub-plant and their subsequent response. It should be noted how the reference modifications are performed in the smallest steps possible and the reduction is optimised to affect only the BESS operation while maintaining the RE production. Again, the green lines signal the Nadir time.

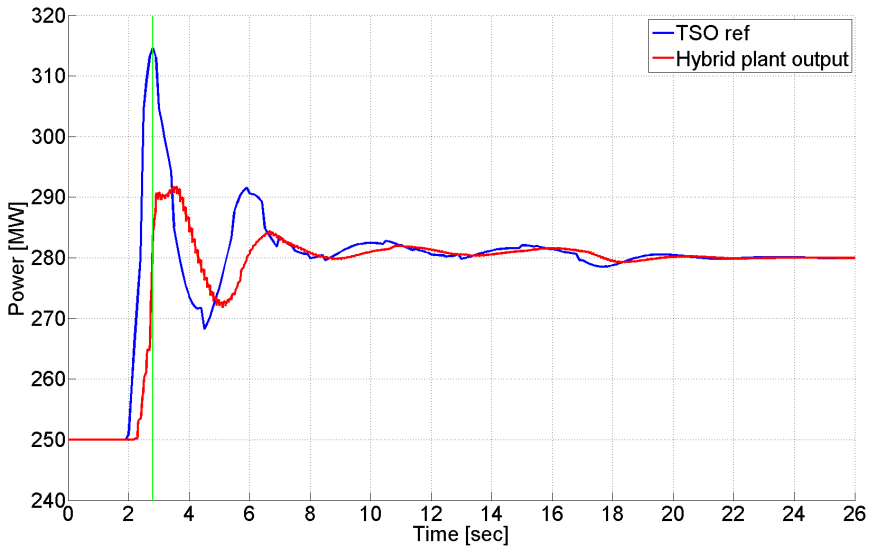

Figure 5.11: Hybrid plant reference and output.

Finally, Figure 5.13 presents the overall active power deviation in the PCC computed as the difference between the HyPP's reference and output in %. It should be noted how the maximum deviation is found before the Nadir is reached, since that is the moment where the maximum ROCOF triggers the biggest response. Then a considerably large deviation corresponding to the intermediate frequency oscillations is also found, proving the need for a refined PFR to work along with the designed FFR.

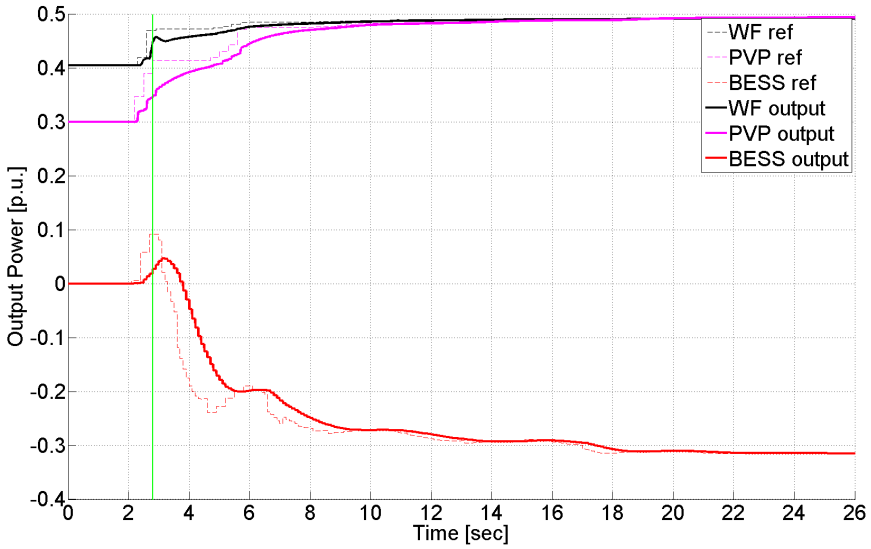

Figure 5.12: Sub-plants reference and output.

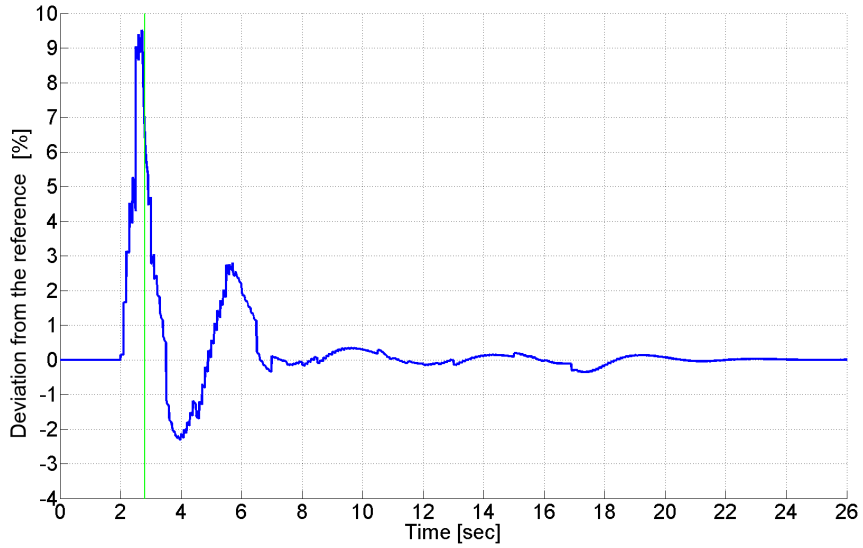

Figure 5.13: Active power deviation in the PCC.

The results obtained in this scenario are satisfactory, since the frequency is contained above 49,8 Hz threshold where both ENTSO-E and British regulations define under-frequency events. Thus, the sudden loss of 30 MW won't effectively affect the system's operation.

Scenario C

In this scenario, a 100 MW generation loss is compensated by the HyPP. It should be noted how this variation represents 20 % variation of the plant's maximum production, and, since it starts by producing 50 %, the final production after the faults is around 40 % more than the initial.

Figure 5.14 presents the frequency variation along with the active power variation caused by the FFR controller. Again, the PFR compensation is not recorded in this Figure. In this Scenario the Nadir point is reached 0.8 seconds after the fault (marked with the green line in the graph) with a value of 49,23 Hz. Then, the nominal frequency is regained after 12 seconds thanks to the simplistic PFR. In this scenario, the recovery is not smooth, due to the amplitude of the FFR countermeasures and the long delay considered for the PFR, however, such undesired oscillations fall beyond the scope of this project.

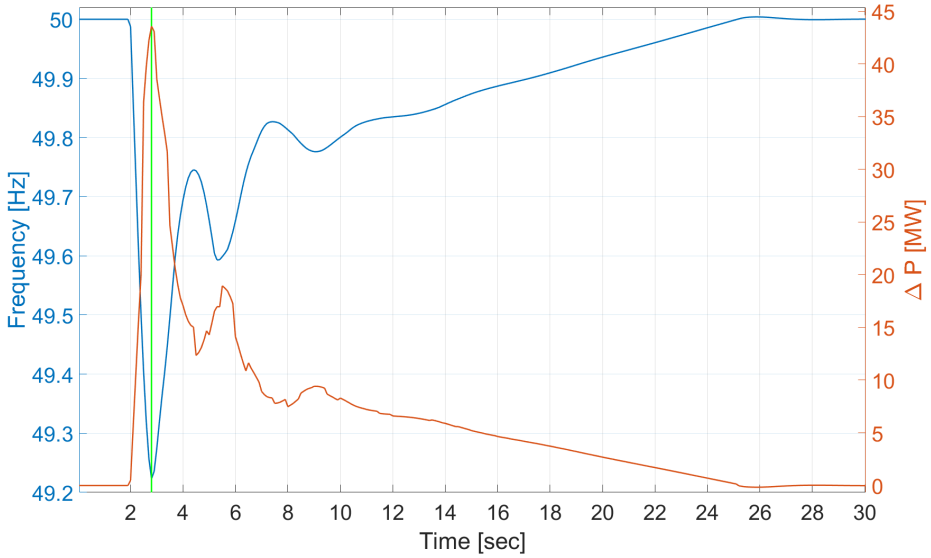

Figure 5.14: Frequency and ΔP_{FFR} variation.

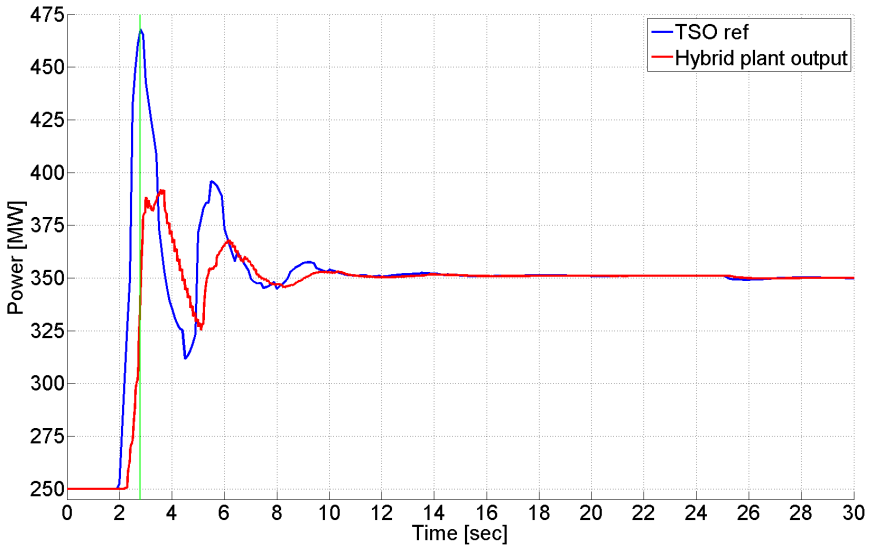

Figure 5.15: Hybrid plant reference and output.

Figure 5.15 presents the reference of the whole HyPP, which is compound by, the TSO reference (constant at 250 MW), the FFR controller and, lastly, the simplistic PFR. In

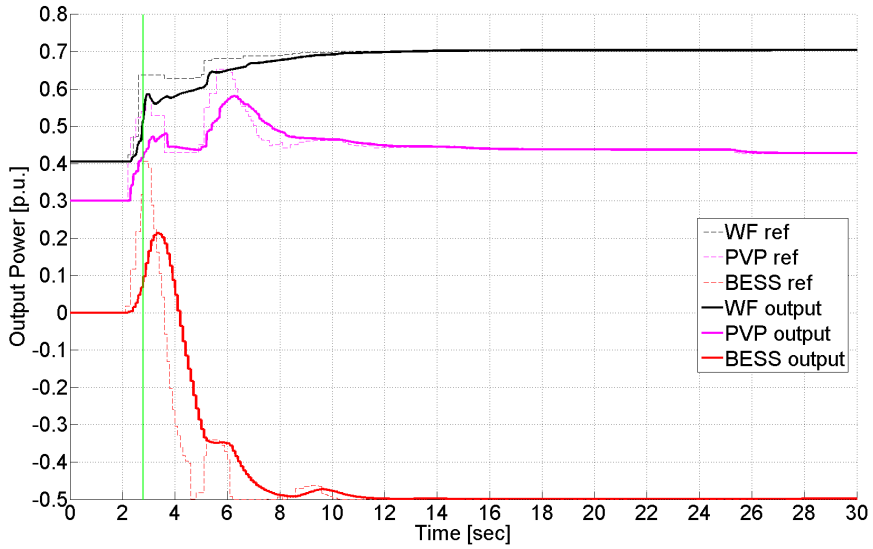

Figure 5.16: Sub-plants reference and output.

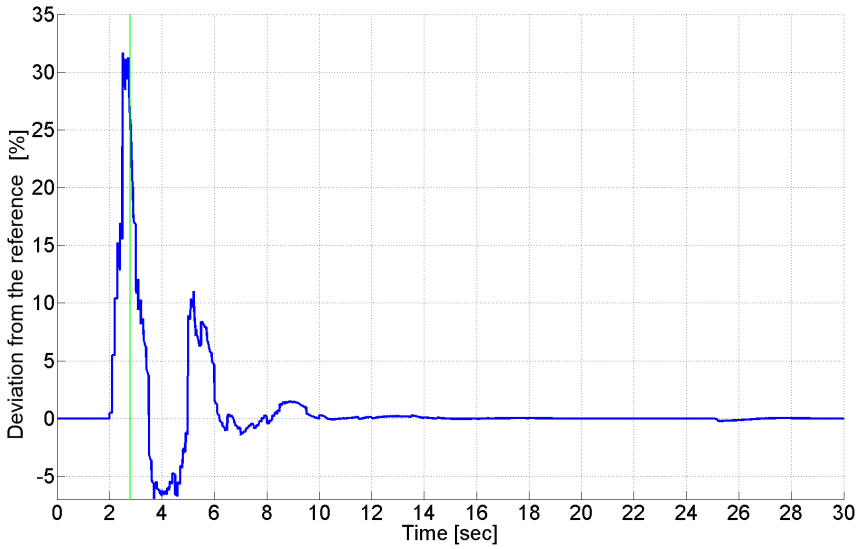

Figure 5.17: Active power deviation in the PCC.

the same graph is also presented the output of the HyPP in the PCC. On the other hand, Figure 5.16 presents the references sent by the Dispatch function to every sub-plant and their subsequent response. It should be noted how the reference modifications are performed in the smallest steps possible and the reduction is optimised to affect only the BESS operation while maintaining steady the RE production. Again, the green lines signal the Nadir time. Finally, Figure 5.17 presents the overall active power deviation in the PCC computed as the difference between the HyPP's reference and output in %. It should be noted how the maximum deviation is found before reaching the Nadir, since that is the moment where the maximum ROCOF triggers the biggest response. Then a considerably large deviation corresponding to the intermediate frequency oscillations is also found, proving the need for a refined PFR to work along with the designed FFR.

The results obtained in this scenario are satisfactory, since the frequency is contained above 49,2 Hz point where frequency protections are triggered, activating load shedding stages. Then, the power injection of the HyPP alone is capable of smoothly restoring the nominal operation of the system.

5.3.4 Regular Operation - Normal Frequency Response

Scenario D

The particularity of this scenario is to randomly modify the system's load in the vicinity of the nominal value in order to resemble the regular operation of any electric system. Then, the load's value is $1000 \pm 5\ MW$, which changes once every second. Figure 5.18 presents the load evolution trough the simulation.

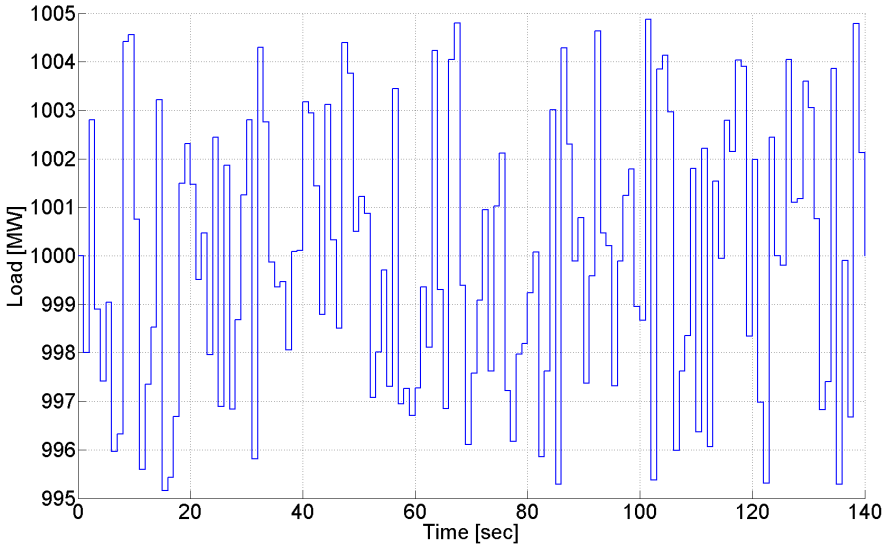

Figure 5.18: Active power demand profile.

Subsequently, Figure 5.19 represents the frequency profile along with the active power variation caused by the FFR controller. Again, the PFR compensation is not recorded in this Figure. In this Scenario the Nadir point is reached 0.8 seconds after the fault in the vicinity of 49,2 Hz. Then, the nominal frequency is regained approximately after 20 seconds even with the load variations that affect the system. Again, the initial recovery is not smooth, since second and third dips are present. However, such undesired oscillations fall beyond the scope of this project. Additionally, Figure 5.20 shows a detailed view of the initial frequency oscillation and subsequent power injection.

Figure 5.21 presents the reference of the whole HyPP, which is compound by, the TSO reference (constant at 250 MW), the FFR controller and, lastly, the simplistic PFR. In the same graph is also presented the output of the HyPP in the PCC. On the other hand, Figure 5.22 presents the references sent by the Dispatch function to every sub-plant and their subsequent response. It should be noted how the reference modifications are performed in the smallest steps possible and the reduction is optimised to affect only the BESS and PV operation while maintaining unaffected the WF production. This is meant to minimise the mechanical stresses in the WTs, since the expected life of the other two sub-plants are less influenced by such modifications. Again, the green lines signal the

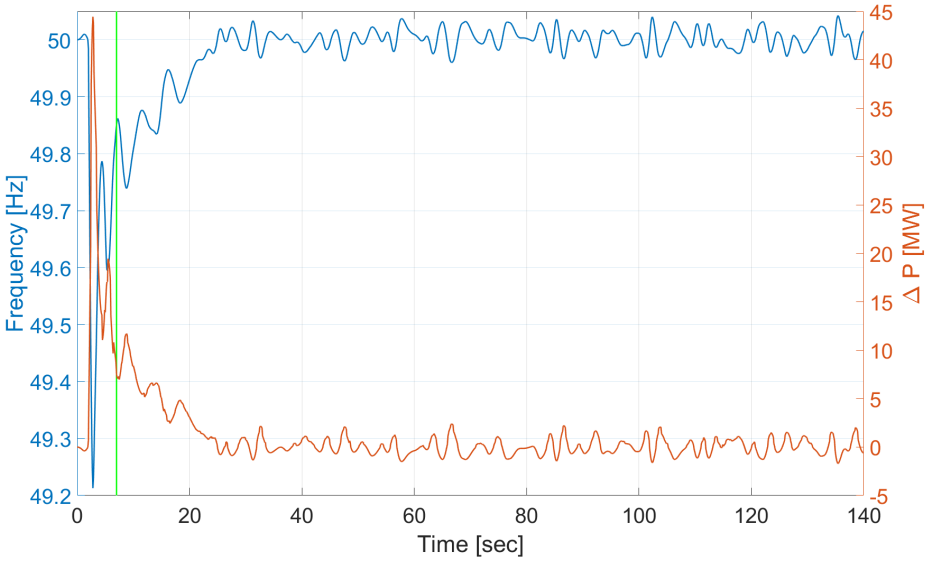

Figure 5.19: Frequency and ΔP_{FFR} variation.

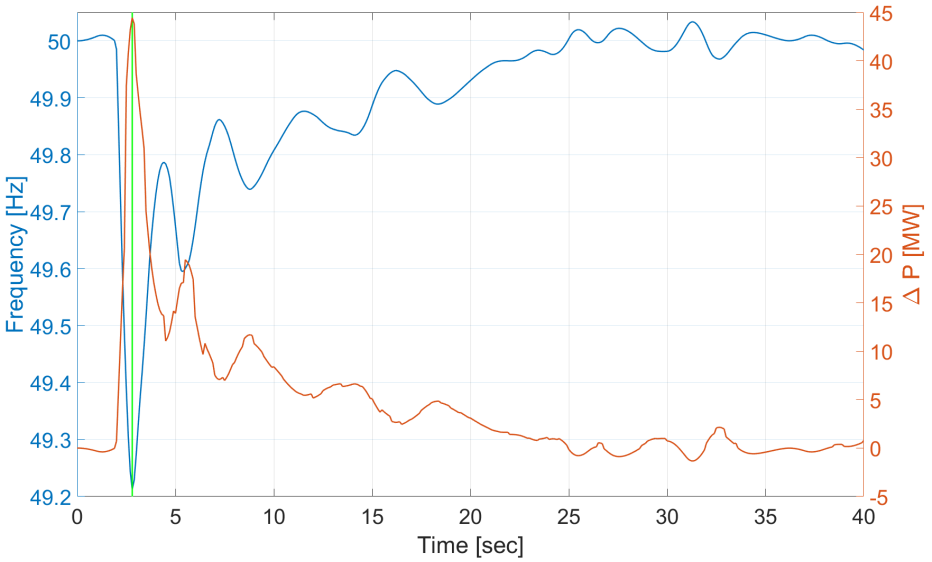

Figure 5.20: Detailed Frequency and ΔP_{FFR} variation.

Nadir time.

Finally, Figure 5.23 presents the overall active power deviation in the PCC computed as the difference between the HyPP's reference and output in %. It should be noted how the maximum deviation is found before the Nadir is reached, since that is the moment where the maximum ROCOF triggers the biggest response. Then a considerably big deviation corresponding to the intermediate frequency oscillations is also found, proving the need for a refined PFR to work along with the designed FFR.

The promising results obtained in this scenario prove how FFR strategies combined with a simplistic PFR are able to keep the frequency in values notoriously close to 50 Hz. However, in order to evaluate the frequency behaviour in scenario D, 24 hours

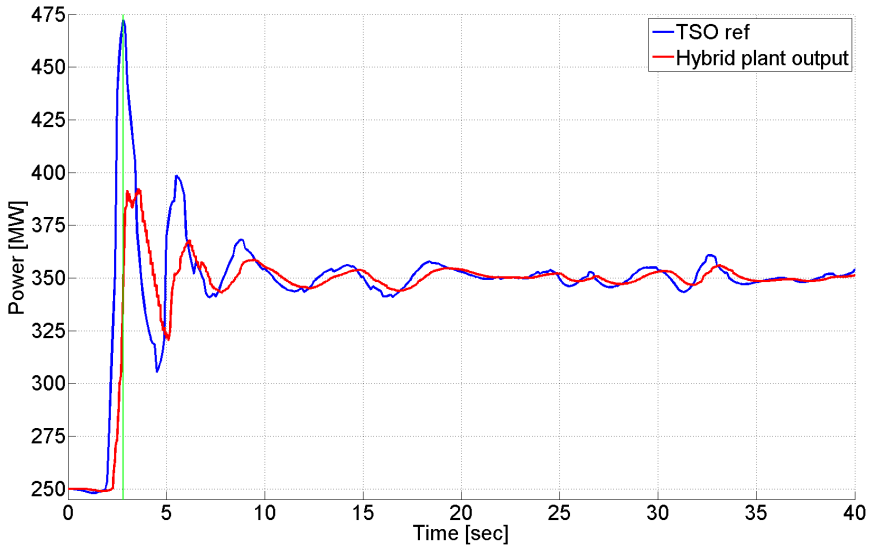

Figure 5.21: Hybrid plant reference and output.

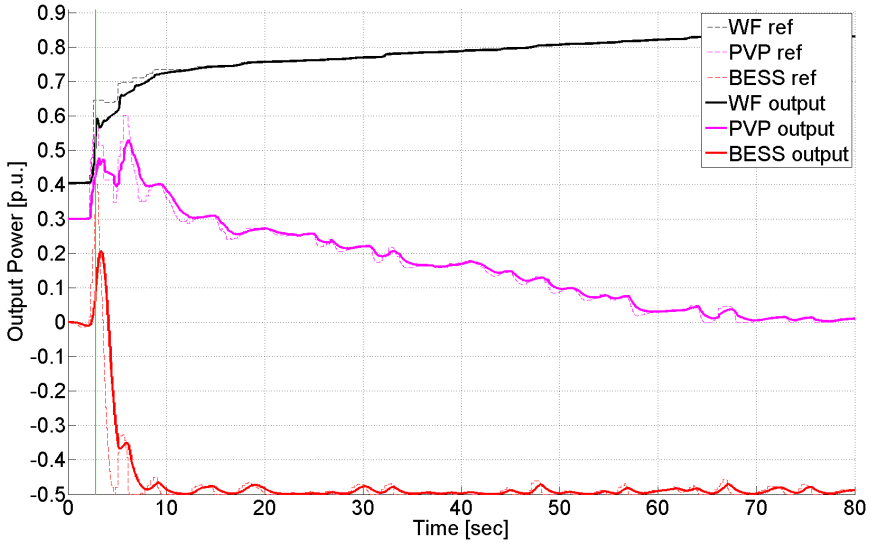

Figure 5.22: Sub-plants reference and output.

of frequency data recorded in 100 ms intervals from Denmark has been used [82]. Figures 5.24 and 5.25 present the histograms of the different frequency values recorder in Denmark during a typical day and in the simulation respectively. The length of the analysis is based on current evaluations of power quality standards; 10 minutes. In the Danish case, the frequencies are concentrated at 50 Hz because a long period of time (24 hours) is considered, while in the simulation is only 600 seconds. Finally, it can be stated that the frequency behaviour of the system results satisfactory and close to the normal operation of a real system, even though only the first stage of frequency control has been properly designed and implemented.

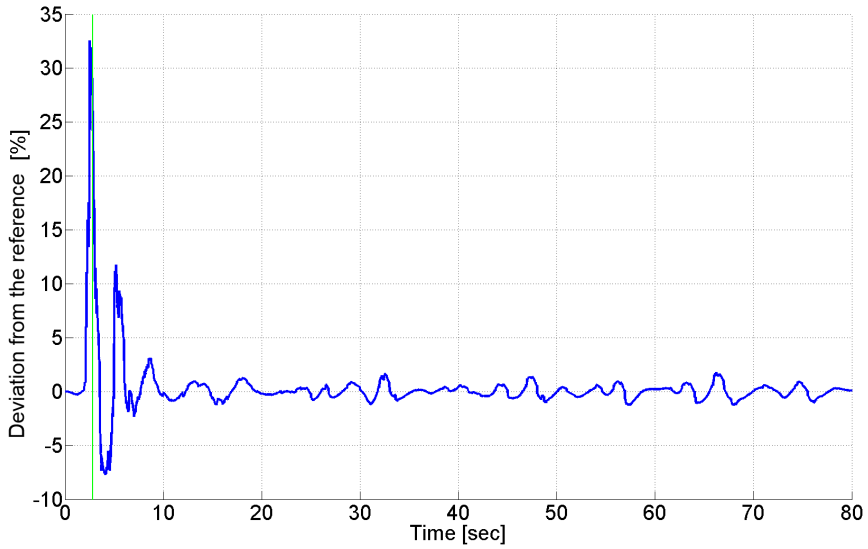

Figure 5.23: Active power deviation in the PCC.

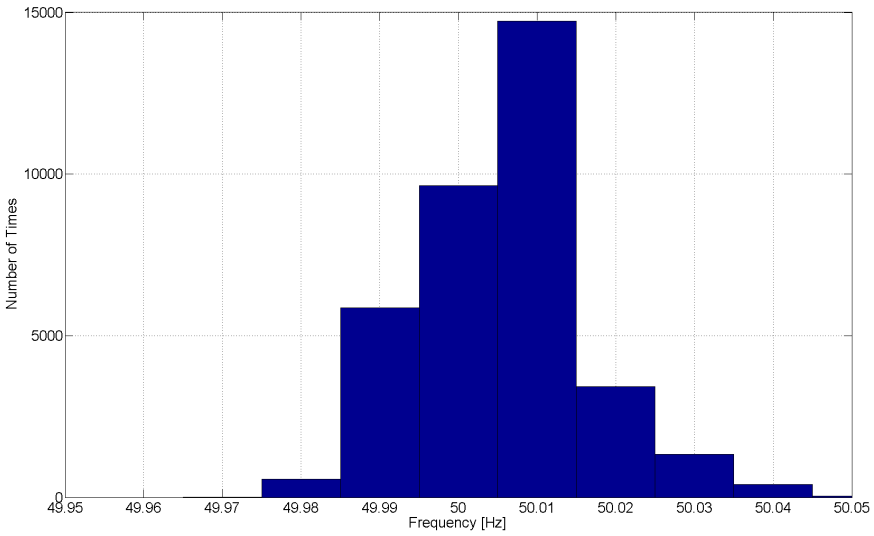

Figure 5.24: Histogram of frequencies in DK.

5.4 Summary

In this chapter, the model development is finished in S-domain and, then, transformed into Z-domain. Subsequently, four different scenarios are defined in order to test the frequency regulation capacity of the control system.

The results show how, in a low penetration scenario (10 %), the plant is able to perform a FFR capable of slowing down the ROCOF enough to apply a simplistic PFR which ultimately smoothly restores the nominal frequency without second dips. On the other hand, in a high penetration scenario (50 %), the same faults analysed in the low penetration scenario do not disturb the frequency behaviour of the system due to the fact that the FFR corrects then before causing any harm. When, larger active power

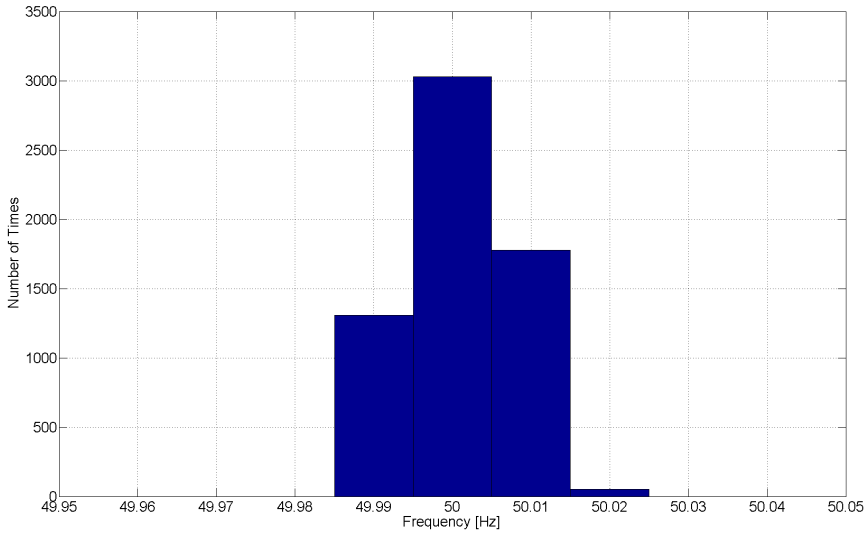

Figure 5.25: Obtained post-fault histogram of frequencies.

variations are studied (10 % of the whole system and 20% of the plant's size), the results show that the designed FFR is able to keep the frequency over 49,2 Hz, avoiding load shedding activation and blackout risk. However, despite the simplistic PFR being able to restore the nominal frequency, it is not accurate enough to avoid second dips. In such case a refined PFR, or FCR, should be implemented, nevertheless such tasks fall beyond the scope of this project.

Lastly, it should be mentioned how the simplistic PFR consists of a active power slope respecting the limitations of modern WTs; and that it was included only for the sake of obtaining a realistic frequency response from the system. Also, the selected sampling times are the same as for current control and monitoring systems in the industry, therefore, it could be easily implemented in already installed plants.

Chapter 6

Conclusions and Future Work

This chapter summarises the report, discusses its findings and contributions, points out limitations of the current work, and also outlines directions for future research

6.1 Conclusions

This thesis has presented problems related to frequency caused by the inertia loss in power grids worldwide due, mostly, to the inclusion of RES, while reviewing also the future trends in frequency detection, surveillance and control. The main objective was to develop a FFR strategy that could be implemented in a HyPP compound by a WF, a PVP and a BESS.

The first chapter presented, on the one hand, the current background and future situation of the European power grid along with examples of blackouts caused by frequency disturbances; while the problem statement, objectives, methodology and limitations for the developed research on the other. Subsequently, Chapter 2 presented an overview on the inertia loss trends found in modern grids and highlighted the importance of the HyPPs in such context. Subsequently, different options to provide inertia to the system without using synchronous generators were explored. In addition, the frequency response and control needs of electric power systems were discussed; highlighting the differences between traditional grids (with high inertia) and future ones (with little to no inertia). In such section, concepts like FFR, FCR, FRR, and ROCOF were presented, while also pointing out the difficulties found in frequency measurement. Finally, the chapter presented an overview of current literature dealing with power plant control, coordination and the influence of the ICTs in the system architecture.

Particularly, Chapter 3 is focused on the operational conditions of a power grid containing a HyPP and the topology of the last one including the balance of plant. Lastly, the used criteria when evaluating the response of a frequency controller was included. Afterwards, the design of the analysed model was covered in Chapter 4, which builds up the model complexity starting from the transfer function definition and inner plant losses estimation. Addressing then, the sub-plant controllers design and tunning. Subsequently, the implemented Dispatch function is explained and, finally, the FFR stage of the control is presented.

The performed tests, their results and subsequent evaluation are included in Chapter 5, which starts with a brief validation of the model in S-Domain, converting it then

to Z-domain. Such discretization is performed with the Backward Euler method. Thereafter, several relevant scenarios are defined and assessed. The results of scenarios A, B and C proved how the designed FFR accurately responds to the N-1 contingency, being capable of stopping frequency drops even after faults representing 20 % of the total power system with a low inertia and no IR from synchronous generators. However, FFR alone is, by definition, incapable of restoring the frequency, thus, a simplistic PFR was included in order to illustrate a realistic frequency response; the obtained response resulted really promising. On the other hand, scenario D proved how the designed frequency controller is capable of reacting to regular load variations keeping the frequency within a narrow band ($< \pm 0,04$ Hz) of the nominal frequency. Lastly, it is worth mentioning how the model was implemented with sampling times that are currently being used in the industry for plant control and grid surveillance.

In conclusion, the designed FFR controller, combined with the implemented Dispatch and sub-plant controllers, responds accurately to frequency variations, being capable of satisfactorily react and eliminate ROCOF. Also, the selected sampling times makes it suitable for implementation in modern renewable plants, fulfilling all the objectives stated in the first chapter. On the other hand, FFR is only capable of eliminating ROCOF, being necessary to include additional control stages to ensure complete frequency restoration. In fact, ENTSO-E recommends two extra stages (namely FCR and FRR) in addition to FFR. Nevertheless, after the results presented in this work, it falls within reason to obtain satisfactory frequency restoration results only with two control stages (FFR and FCR, or FFR and FRR). Finally, the obtained results show how the Nadir is approximately reached after 1 second, thus, the second stage should start acting in that moment, continuing the power injection of the FFR while reducing it gradually, keeping the frequency variation smooth and stable until is restored. Therefore, a critical point is easily identified in the instant when FFR ends and the second stage picks up the pace. A power reference discontinuity in that moment will cause the biggest frequency instability of the frequency recovery, producing second and subsequent dips.

6.2 Future Work

This project has succeeded in developing a FFR controller for a HyPP, that could be easily adapted for the most common renewable plants. The considered architecture set the frame for the designed dispatch function and plant controllers. There are however complementary research paths to be followed in order to finalise the future frequency controller in a real system. Some aspects to be covered in future work are as follows:

- Real-time evaluation of the model in a Hardware-in-the-loop test-bench like OPAL-RT.
- Addition of a FCR and a FRR stages to the already developed model.
- Optimal sizing of the additional PVP and BESS sub-plants to be added on the WF.
- Development of an techno-economically optimised Dispatch function, considering at least four different operational modes: steady-state, FFR, FCR and FRR.
- Include more sources of Virtual Inertia, both mechanical and electrical.
- Lifespan assessment of HyPP supporting frequency control. The continuous change in operational set points causes stresses that need to be assessed.

- In scenarios without curtailment, study the recuperation time of the WF after providing mechanical inertia.
- Study the influence of ICT's (delays, loss of information, malicious attacks, etc) in the coordination of the power system.
- Study local and regional frequency variations, as well as frequency and ROCOF estimation techniques.
- Develop energy models for the RE generators, since those are more suitable to analyse virtual inertia support.

Bibliography

[1] eurostat. *Europe 2020 in a nutshell @MISC*. 2017. URL: http://ec.europa.eu/eurostat/web/europe-2020-indicators/europe-2020-strategy.

[2] Jo Dirix et al. "Strengthening bottom-up and top-down climate governance". In: *Climate Policy* 13.3 (2013), pp. 363–383.

[3] Danish Wind Industry Association. *The Danish Market @MISC*. 2018. URL: http://www.windpower.org/en/knowledge/statistics/the_danish_market.html.

[4] P Sorknæs et al. *Overview of the Danish power system and RES integration*. Tech. rep. Technical report, Jul, 2013.

[5] Erik Ørum et al. "Future system inertia". In: *ENTSOE, Brussels, Tech. Rep.* (2015).

[6] Danish Energy Association et al. "Smart Grid in Denmark 2.0". In: *Energinet. dk: Erritsø, Denmark* (2013).

[7] Danish Ministry of Climate. "The intelligent energy system of the future." In: *Energy and Building, May* (2013).

[8] L. Haitao et al. "Research on the conceptual model of smart energy system". In: *2017 IEEE Conference on Energy Internet and Energy System Integration (EI2)*. 2017, pp. 1–6. DOI: 10.1109/EI2.2017.8245690.

[9] *European Power System 2040 - Completing the map. System dynamics and operational challenges*. Tech. rep. ENTSO-E, May, 2018.

[10] ENTSO-E ENTSO-E Network Code. "Requirements for Grid Connection Applicable to All Generators". In: *ENTSO-E: Brussels, Belgium* (2013).

[11] F Vandenberghe et al. "FINAL REPORT of the Investigation Committee on the 28 September 2003 Blackout in Italy". In: *UCTE, Tech. Rep* (2004).

[12] Günther Beck et al. "Global blackouts–Lessons learned". In: *Power-Gen Europe*. Vol. 28. 2005, p. 30.

[13] Ekraft System. *Power failure in Eastern Denmark and Southern Sweden on 23 September 2003 Final report on the course of events*. Tech. rep. Ekraft System, 2003.

[14] Enquiry Committee et al. *Report of the enquiry committee on grid disturbance in northern region on 30th July 2012 and in northern, eastern & north-eastern region on 31st July, 2012*. 2012.

[15] Australian Energy Market Operator. "Black System, South Australia, 28 September 2016". In: *Report of the Australian Energy Market Operator Limited (AEMO)* (2017).

[16] General Electric Renewable Energy. *Hybrid Power @MISC*. 2018. URL: https://www.gerenewableenergy.com/hybrid.

[17] Siemens Global Website. *Hybrid Power Solutions @MISC*. 2018. URL: https://www.energy.siemens.com/us/en/renewable-energy/distributed-and-hybrid-power/hybrid-power-solutions.htm.

[18] ENTSO-E ENTSO-E Network Code. "Network Code on Load-Frequency Control and Reserves". In: *ENTSO-E: Brussels, Belgium* (2013).

[19] Xiaoyu Wang, Meng Yue, and Eduard Muljadi. "PV generation enhancement with a virtual inertia emulator to provide inertial response to the grid". In: *Energy Conversion Congress and Exposition (ECCE), 2014 IEEE*. IEEE. 2014, pp. 17–23.

[20] Xiao Zhaoxia et al. "Frequency participation by using virtual inertia in wind turbines including energy storage". In: *Industrial Electronics Society, IECON 2017-43rd Annual Conference of the IEEE*. IEEE. 2017, pp. 2492–2497.

[21] European Environment Agency. *Renewable energy in Europe 2017; Recent growth and knock-on effects*. Tech. rep. European Union, Mar, 2017.

[22] Lata Gidwani. "A Comparative Power Quality Study of DFIG and PMSG Based Wind Energy Conversion System". In: *WSEAS Transactions on Systems and Control, Rajasthan Technical University, Kota, India* (2015).

[23] Seifeddine Benelghali, MEH Benbouzid, and Jean Frédéric Charpentier. "Comparison of PMSG and DFIG for marine current turbine applications". In: *Electrical Machines (ICEM), 2010 XIX International Conference on*. IEEE. 2010, pp. 1–6.

[24] Hemant Ahuja, G Bhuvaneswari, and R Balasubramanian. "Performance comparison of DFIG and PMSG based WECS". In: (2011).

[25] Hemant Ahuja, Rahul Virmani, and Arika Ahuja. "Performance comparison of most prevalent wind energy conversion systems". In: *Power Electronics (IICPE), 2016 7th India International Conference on*. IEEE. 2016, pp. 1–6.

[26] Bernard Chabot. "Onshore and Offshore Wind Power Capacity Factors: How Much they Differ Now and in the Future: A Case Study for Denmark". In: (2013).

[27] Jianhui Meng et al. "Adaptive virtual inertia control of distributed generator for dynamic frequency support in microgrid". In: *Energy Conversion Congress and Exposition (ECCE), 2016 IEEE*. IEEE. 2016, pp. 1–5.

[28] A. B. T. Attya and J. L. Dominguez-García. "Insights on the provision of frequency support by wind power and the impact on energy systems". In: *IEEE Transactions on Sustainable Energy* PP.99 (2017), pp. 1–1. ISSN: 1949-3029. DOI: 10.1109/TSTE.2017.2759503.

[29] Yujun Li, Zhao Xu, and Kit Po Wong. "Advanced control strategies of PMSG-based wind turbines for system inertia support". In: *IEEE Transactions on Power Systems* 32.4 (2017), pp. 3027–3037.

[30] Eberhard Waffenschmidt and Ron SY Hui. "Virtual inertia with PV inverters using DC-link capacitors". In: *Power Electronics and Applications (EPE'16 ECCE Europe), 2016 18th European Conference on*. IEEE. 2016, pp. 1–10.

[31] C. M. Deepak, A. Vijayakumari, and S. R. Mohanrajan. "Virtual inertia control for transient active power support from DFIG based wind electric system". In: *2017 2nd IEEE International Conference on Recent Trends in Electronics, Information Communication Technology (RTEICT)*. 2017, pp. 809–814. DOI: 10.1109/RTEICT.2017.8256710.

[32] Y. Wang et al. "Control of PMSG-Based Wind Turbines for System Inertial Response and Power Oscillation Damping". In: *IEEE Transactions on Sustainable Energy* 6.2 (2015), pp. 565–574. ISSN: 1949-3029. DOI: 10.1109/TSTE.2015.2394363.

[33] E. Waffenschmidt and R. S. Y. Hui. "Virtual inertia with PV inverters using DC-link capacitors". In: *2016 18th European Conference on Power Electronics and Applications (EPE'16 ECCE Europe)*. 2016, pp. 1–10. DOI: 10.1109/EPE.2016.7695607.

[34] A. Anzalchi, M. M. Pour, and A. Sarwat. "A combinatorial approach for addressing intermittency and providing inertial response in a grid-connected photovoltaic system". In: *2016 IEEE Power and Energy Society General Meeting (PESGM)*. 2016, pp. 1–5. DOI: 10.1109/PESGM.2016.7742056.

[35] X. Hao et al. "A hybrid adaptive fuzzy control strategy for DFIG-based wind turbines with super-capacitor energy storage to realize short-term grid frequency support". In: *2015 IEEE Energy Conversion Congress and Exposition (ECCE)*. 2015, pp. 1914–1918. DOI: 10.1109/ECCE.2015.7309930.

[36] D. Munteanu, I. Serban, and C. Marinescu. "Improving the dynamic response of PV systems in microgrids by using supercapacitors". In: *2017 International Conference on Optimization of Electrical and Electronic Equipment (OPTIM) 2017 Intl Aegean Conference on Electrical Machines and Power Electronics (ACEMP)*. 2017, pp. 636–641. DOI: 10.1109/OPTIM.2017.7975040.

[37] Shahid Olsen-Iov Hansen Xue Petersen Altin. *Deliverable D1.1 - Specifications for ReGen plant model and control architecture*. Tech. rep. Technical report, AAu, DTU Vestas, 2015-2018.

[38] Claudia Rahmann and Alfredo Castillo. "Fast frequency response capability of photovoltaic power plants: The necessity of new grid requirements and definitions". In: *Energies* 7.10 (2014), pp. 6306–6322.

[39] Fei Teng et al. "Benefits of demand-side response in providing frequency response service in the future GB power system". In: *Frontiers in Energy Research* 3 (2015), p. 36.

[40] ENTSO-E guidance document for national implementation for network codes on grid connection. *Rate of Change of Frequency (ROCOF) withstand capability*. Tech. rep. ENTSO-E, 2017.

[41] E. Quitmann S. Engelken C. Strafiel. *Frequency Measurement for Inverter-based Frequency Control*. Tech. rep. in Wind Integration Workshop, Vienna, 2016.

[42] K. Creighton S. Temtem. *Summary of Studies on Rate of Change of Frequency events on the All-Island System*. Tech. rep. EIRGRID, Soni, 2012.

[43] Omkar N Buwa and Ganesh N Jadhav. "Primary frequency support by virtual synchronous generator with precise frequency detection techniques". In: *Power India International Conference (PIICON), 2016 IEEE 7th*. IEEE. 2016, pp. 1–6.

[44] RG-CE System Protection & Dynamics Sub Group ENTSO-E. *Frequency Stability Evaluation Criteria for the Synchronous Zone of Continental Europe*. Tech. rep. ENTSO-E, 2016.

[45] RG-CE System Protection & Dynamics Sub Group ENTSO-E. *Frequency Measurement Requirements and Usage*. Tech. rep. ENTSO-E, 2018.

[46] Yong Liu, Shutang You, and Yilu Liu. "Study of Wind and PV Frequency Control in US Power Grids—EI and TI Case Studies". In: *IEEE Power and Energy Technology Systems Journal* 4.3 (2017), pp. 65–73.

[47] Danny Ochoa and Sergio Martinez. "Fast-Frequency Response provided by DFIG-Wind Turbines and its impact on the grid". In: *IEEE Transactions on Power Systems* 32.5 (2017), pp. 4002–4011.

[48] Anderson F Hoke et al. "Rapid active power control of photovoltaic systems for grid frequency support". In: *IEEE Journal of Emerging and Selected Topics in Power Electronics* 5.3 (2017), pp. 1154–1163.

[49] Nikolay Nikolaev et al. "Optimal tuning and contribution of wind turbines and PV plants to the power system frequency control". In: *Environment and Electrical Engineering (EEEIC), 2014 14th International Conference on*. IEEE. 2014, pp. 102–107.

[50] Wei Zhang and Kailun Fang. "Controlling active power of wind farms to participate in load frequency control of power systems". In: *IET Generation, Transmission & Distribution* 11.9 (2017), pp. 2194–2203.

[51] Zhongguan Wang and Wenchuan Wu. "Coordinated Control Method for DFIG-Based Wind Farm to Provide Primary Frequency Regulation Service". In: *IEEE Transactions on Power Systems* (2017).

[52] Chengming He and Hongtao Wang. "Coordination frequency control strategy design of wind farm base on time sequence control". In: *Power and Energy Engineering Conference (APPEEC), 2013 IEEE PES Asia-Pacific*. IEEE. 2013, pp. 1–6.

[53] Anupam A Thatte, Fan Zhang, and Le Xie. "Coordination of wind farms and flywheels for energy balancing and frequency regulation". In: *Power and Energy Society General Meeting, 2011 IEEE*. IEEE. 2011, pp. 1–7.

[54] Francisco Díaz-González et al. "Coordinated operation of wind turbines and flywheel storage for primary frequency control support". In: *International Journal of Electrical Power & Energy Systems* 68 (2015), pp. 313–326.

[55] Ziping Wu et al. "Coordinated Control Strategy of Battery Energy Storage System and PMSG-WTG to Enhance System Frequency Regulation Capability". In: *IEEE Transactions on Sustainable Energy* 8.3 (2017), pp. 1330–1343.

[56] Saeed Sepasi et al. "A coordinated approach for frequency control of zero emission based smart PV-wind-battery power system". In: *Electrical and Computer Engineering (ICECE), 2016 9th International Conference on*. IEEE. 2016, pp. 166–169.

[57] KV Vidyanandan and Nilanjan Senroy. "Improved frequency regulation in wind-PV-DG hybrid microgrid using wind turbines". In: *Power Systems (ICPS), 2016 IEEE 6th International Conference on*. IEEE. 2016, pp. 1–6.

[58] Ricardo Enrique Pérez-Guzmán, Yamisleydi Salgueiro-Sicilia, and Marco Rivera. "Communications in smart grids". In: *Electrical, Electronics Engineering, Information and Communication Technologies (CHILECON), 2017 CHILEAN Conference on*. IEEE. 2017, pp. 1–7.

[59] Hongxu Zhu et al. "Review of state-of-the-art wireless technologies and applications in smart cities". In: (2017).

[60] Dheena Moongilan. "5G wireless communications (60 GHz band) for smart grid—An EMC perspective". In: *Electromagnetic Compatibility (EMC), 2016 IEEE International Symposium on*. IEEE. 2016, pp. 689–694.

[61] Michele Garau et al. "A 5G cellular technology for distributed monitoring and control in smart grid". In: *Broadband Multimedia Systems and Broadcasting (BMSB), 2017 IEEE International Symposium on*. IEEE. 2017, pp. 1–6.

[62] Z. Honglin et al. "Control of parallel-connected grid-side converters of a wind turbine with real-time ethernet". In: *IECON 2017 - 43rd Annual Conference of the IEEE Industrial Electronics Society*. 2017, pp. 2413–2418. DOI: 10.1109/IECON.2017.8216406.

[63] Wenye Wang, Yi Xu, and Mohit Khanna. "A survey on the communication architectures in smart grid". In: *Computer networks* 55.15 (2011), pp. 3604–3629.

[64] Kamal Shahid et al. "ICT based Performance Evaluation of Primary Frequency Control Support from Renewable Power Plants in Smart Grids". In: *Energies* (2018).

[65] Murat Kuzlu, Manisa Pipattanasomporn, and Saifur Rahman. "Communication network requirements for major smart grid applications in HAN, NAN and WAN". In: *Computer Networks* 67 (2014), pp. 74–88.

[66] Andrzej Adamczyk et al. "Generic 12-bus test system for wind power integration studies". In: *Power Electronics and Applications (EPE), 2013 15th European Conference on*. IEEE. 2013, pp. 1–6.

[67] Jason Jonkman et al. *Definition of a 5-MW reference wind turbine for offshore system development*. Tech. rep. National Renewable Energy Lab.(NREL), Golden, CO (United States), 2009.

[68] F. Iov DV. Pombo L. Petersen. *Solar PV System Performance Model*. Tech. rep. Smart Energy Systems Laboratory, Aalborg University, Denmark, 2017.

[69] James Hemingway. *Estimating generation from Feed in Tariff installations*. Tech. rep. Department of Energy and Climate Change (DECC), 2013.

[70] Maciej Świerczyński et al. "Field experience from Li-ion BESS delivering primary frequency regulation in the Danish energy market". In: *Ecs Transactions* 61.37 (2014), pp. 1–14.

[71] DI. Stroe DV. Pombo. *Lithium-Ion Battery Model*. Tech. rep. Smart Energy Systems Laboratory, Aalborg University, Denmark, 2017.

[72] National Grid. "THE GRID CODE, ISSUE 5, REVISION 21". In: *United Kingdom* (2017).

[73] Katsuhiko Ogata. *Modern control engineering*. Vol. 4. Prentice hall India, 2002.

[74] Iov Florin Ionita Claudiu. "Advanced Active Power and Frequency Control of Wind Power Plants". In: *Aalborg University; MSc Thesis* (2017).

[75] Jorge Martinez Garcia. *Voltage control in wind power plants with doubly fed generators*. Department of Energy Technology, Aalborg University, 2010.

[76] S.A. Baltac L. Toma M. Sanduleac. "RESERVE Project D2.2 - Review of relevance of current techniques to advanced frequency control". In: ().

[77] Müfit Altin. "Dynamic Frequency Response of Wind Power Plants". PhD thesis. PhD thesis, Aalborg University, Department of Energy Technology Aalborg, Denmark, 2012.

[78] Germán Claudio Tarnowski. "Coordinated frequency control of wind turbines in power systems with high wind power penetration". In: *Industrial PhD* (2011), pp. 07–026815.

[79] Commission Regulation (EU). *Establishing a network code on requirements for grid connection of generators*. Tech. rep. European Commission, Apr, 2016.

[80] M. Comanescu. "Influence of the discretization method on the integration accuracy of observers with continuous feedback". In: *2011 IEEE International Symposium on Industrial Electronics*. 2011, pp. 625–630. DOI: 10.1109/ISIE.2011.5984230.

[81] Vestas Wind Systems A/S. *General Specification - V112–3.0 MW 50/60 Hz*. Tech. rep. Vestas, Jan, 2011.

[82] Energinet. *Data Hub @MISC*. 2018. URL: https://www.energidataservice.dk/da_DK/.

[83] Prysmian. *Medium Voltage Cables*. Tech. rep. Prysmian Group, Australia, 2015.

Appendix A

Considered Cable Data

In this section, a summary of the considered data for the HyPP is presented. As it was already mentioned in Section 3.3, the POC of the WF and PVP were considered to be placed after a 1 km conductor from the main substation. Then the internal losses of the PVP were dismissed since the internal control of the inverter will already compensate for those; while for the WF the transmission losses were accounted for. The considered distances where 300 meters for the first WT while a distance of 7 rotor diameter between consecutive WTs, thus 882 m. A summary of this distances is presented if Figure A.1.

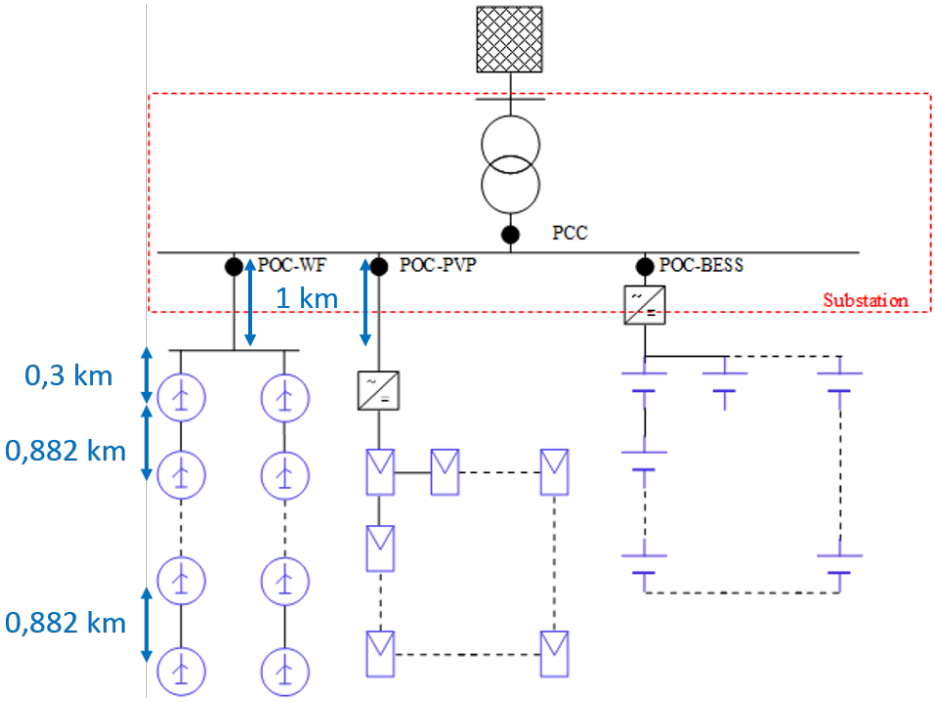

Figure A.1: Layout and cable distances of the Hybrid plant.

Regarding the selected conductors, all of them were considered copper, underground cable, with a maximum temperature of 90^oC. Three different sections were considered as it is the typical scheme in any modern WF. However, in few parts, additional parallel conductors were placed in order to be able to transmit full power. A summary of such cables is presented in Table A.1, however due to the simetry of the system, WT_i is equal to WT_{i+10}; while the parameters considered for the power flow analysis are presented in A.2.

Table A.1: Summary of Cable lengths and type of conductor.

From-To	Cable Type	Parallel Conductors	Length [km]
PCC-POC_{WF}	3x300 mm^2	3	1
PCC-POC_{WF}	2x95 mm^2	2	1
POC_{WF}**-WT1**	3x185 mm^2	3	0,3
WT1-WT2	3x240 mm^2	2	0,882
WT2-WT3	3x240 mm^2	2	0,882
WT3-WT4	3x240 mm^2	2	0,882
WT4-WT5	3x240 mm^2	2	0,882
WT5-WT6	3x240 mm^2	2	0,882
WT6-WT7	3x240 mm^2	1	0,882
WT7-WT8	3x240 mm^2	1	0,882
WT8-WT9	3x95 mm^2	1	0,882
WT9-WT10	3x95 mm^2	1	0,882

Table A.2: Summary of the cable data. [83]

Section	R [Ω /km]	X_L [Ω /km]	X_C [Ω /km]
95 mm^2	0,247	0,0964	0,171
185 mm^2	0,128	0,0874	0,113
240 mm^2	0,0987	0,0847	0,131
300 mm^2	0,08	0,0824	0,210

Appendix B

Root Locus And Bode Analysis

In this Annex, the behaviour of the different open-loop systems after the addition of P and PI controllers is analysed. The employed tools are Root Locus and Bode plots. While the root locus can only provide information related to the stability range of the system for different gains, and whether the system is under-, over- or critically-damped; the Bode approach provides useful information such as the GM and PM.

The GM is the reciprocal magnitude of $|G(\omega j)|$ at the frequency where the phase angle is 180^o. It is usually expressed in dB as:

$$GM = -20\, log\left(|G(\omega_1 j)|\right) \tag{B.1}$$

where ω_1 is the crossover frequency at which the phase angle of the open-loop transfer function equals -180^o. A positive value for the GM implies that the system is stable and how much the system gain can be increased before the system becomes unstable; further, a negative value implies the opposite, instability and how much gain reduction is needed for the system to become stable.

On the other hand, PM is the amount of additional phase lag at the gain crossover frequency required to bring the system to the verge of instability. The gain crossover frequency is the frequency where $|G(\omega j)| = 1$. The PM is then computed as:

$$PM = 180^o + \phi \tag{B.2}$$

where ϕ stand for the phase angle of the open-loop transfer function at the gain crossover frequency. If the PM is positive, then the system is considered to be stable; however, in Bode plots, the critical point in the complex plane corresponds to the $0dB$ and -180^o. Finally, it should be stated that it is necessary to employ both GM and PM in order to analyse the relative stability of any system; either of them alone does not provide all the information.

This Annex is structured as follows, Section B.1 presents the Root Locus and Bode plots after the inclusion of P controller, while Section B.2 applies a similar approach to the PI.

B.1 P Controller

In this section, the root locus and Bode diagrams of the PVP and BESS systems including a P controller are presented, since those were omitted in the report. As it is presented in Figures B.1 and B.2, both systems result stable for any gain value.

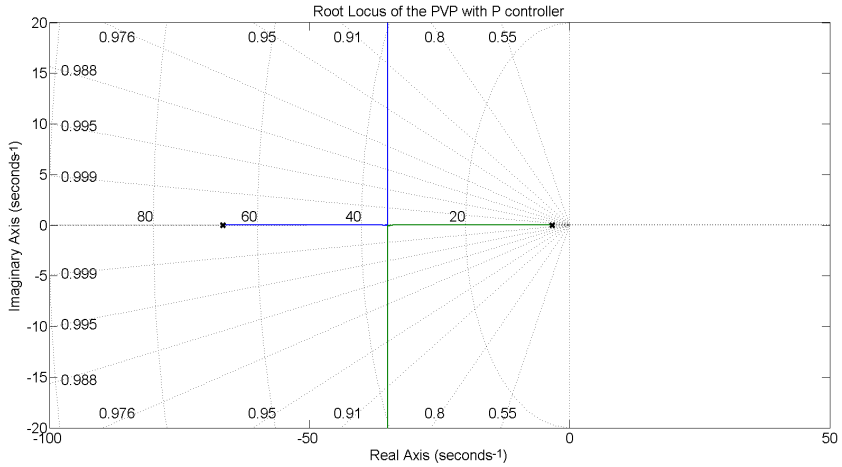

Figure B.1: Root locus of the closed loop PVP with P controller.

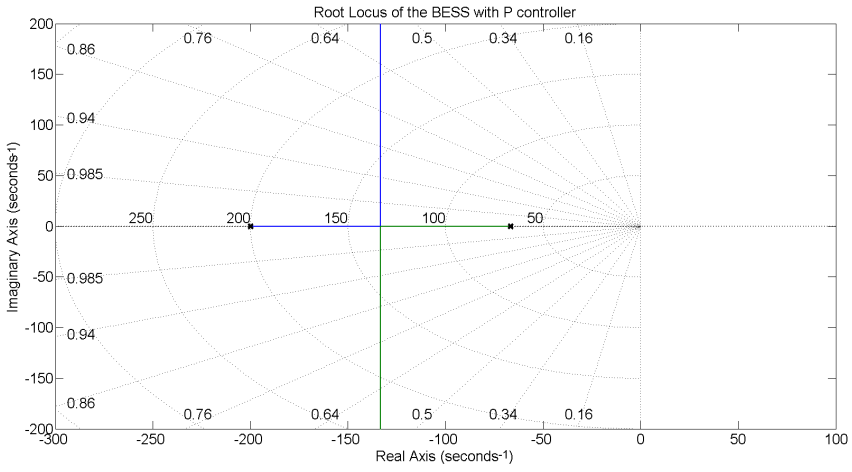

Figure B.2: Root locus of the closed loop BESS with P controller.

On the other hand, Figures B.3 and B.4 present the Bode plots of the PVP and the BESS respectively, while Table B.1 presents a summary of the GM and PM. Similar conclusions as for the root locus approach are obtained, since the system is stable for any gain value.

Table B.1: Summary of GM and PM of the system with P controller

System	GM	PM
PVP	Inf	$32,9^o$
BESS	Inf	$16,3^o$

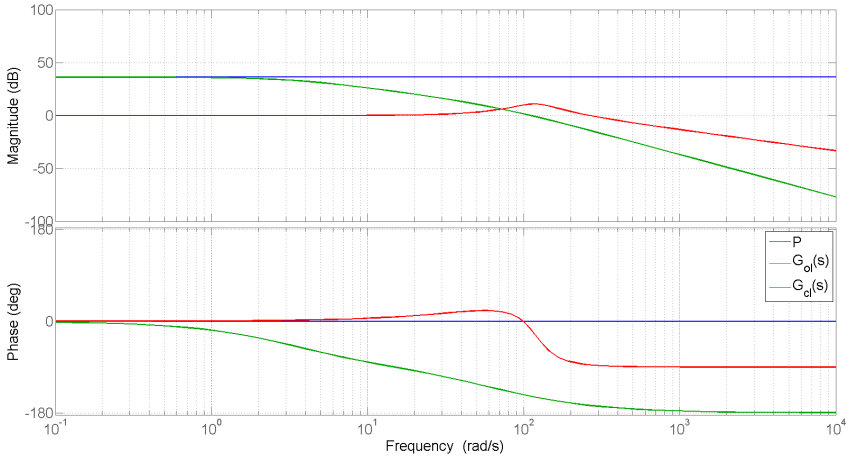

Figure B.3: Bode Plot of the closed loop PVP with P controller.

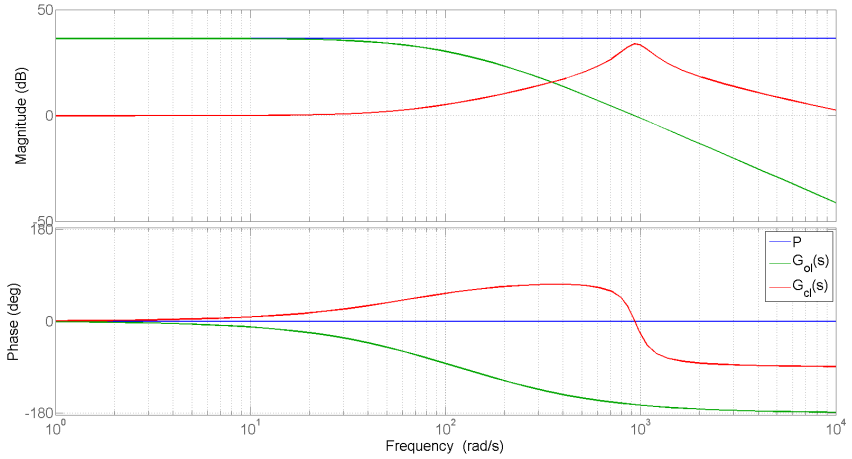

Figure B.4: Bode Plot of the closed loop BESS with P controller.

B.2 PI Controller

In this section, the root locus and Bode diagrams of the PVP and BESS systems including a PI controller are presented, since those were omitted in the report. As it is presented in Figures B.5 and B.6, both systems result stable for any gain value.

On the other hand, Figures B.7 and B.8 present the Bode plots of the PVP and the BESS respectively, while Table B.2 presents a summary of the GM and PM. Similar conclusions as for the root locus approach are obtained, since the system is stable for any gain value.

Table B.2: Summary of GM and PM of the system with PI controller

System	GM	PM
PVP	Inf	$87,1^o$
BESS	Inf	$32,1^o$

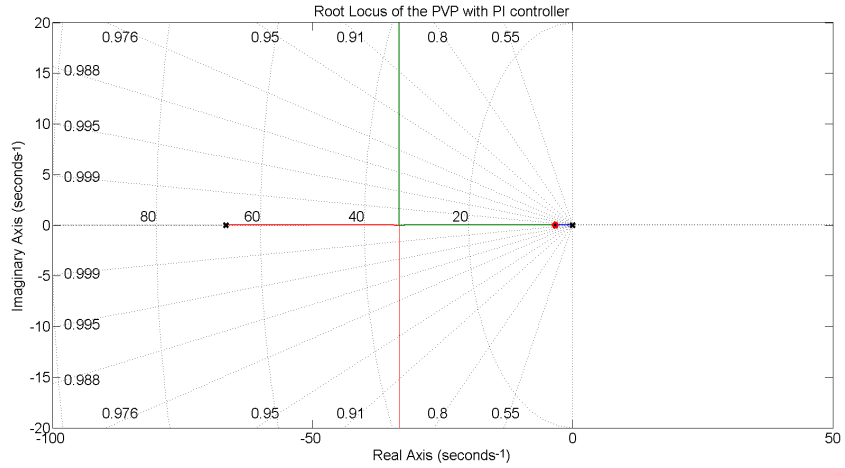

Figure B.5: Root locus of the closed loop PVP with PI controller.

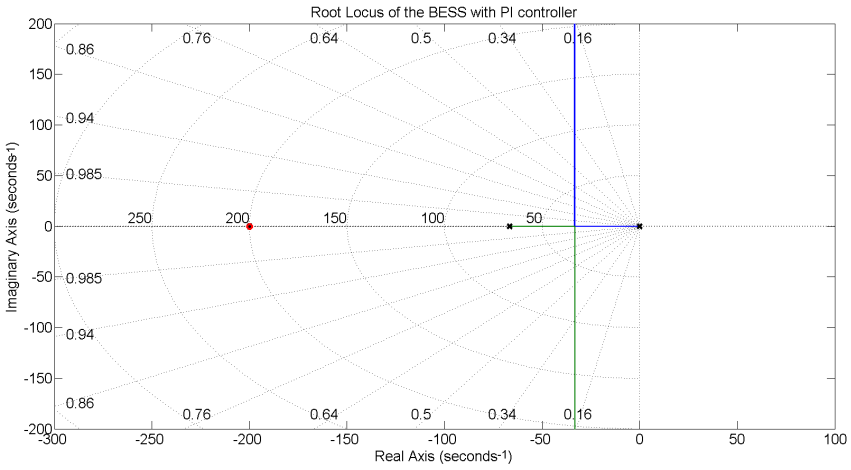

Figure B.6: Root locus of the closed loop BESS with PI controller.

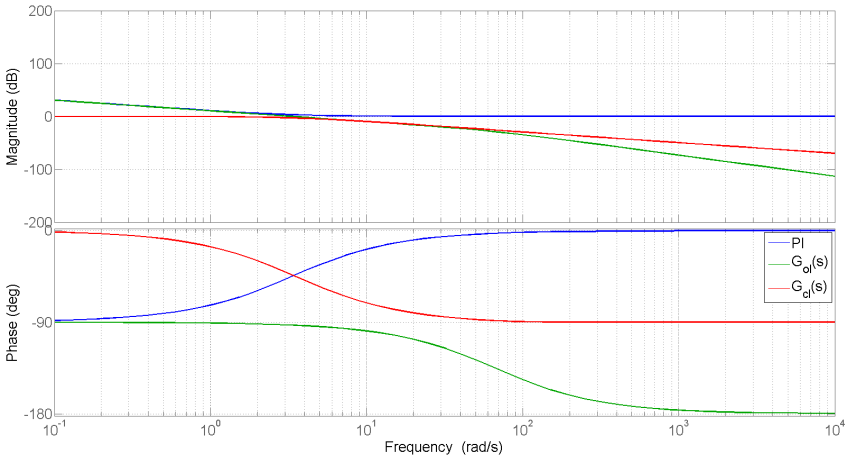

Figure B.7: Bode Plot of the closed loop PVP with PI controller.

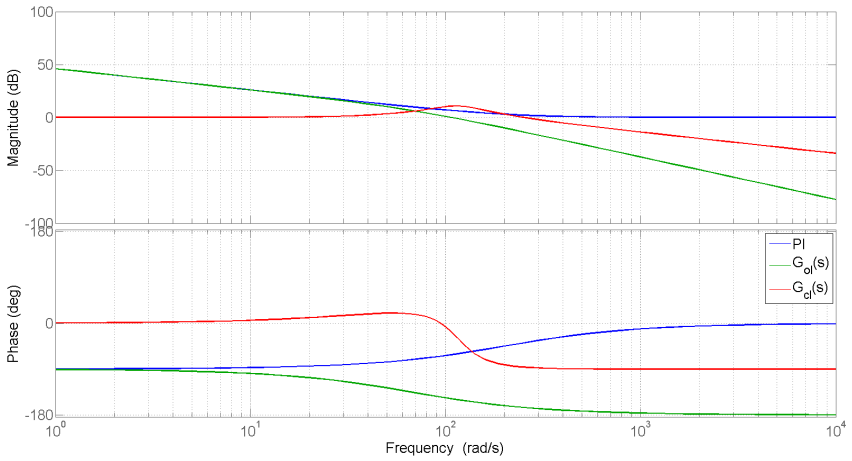

Figure B.8: Bode Plot of the closed loop BESS with PI controller.

Appendix C

Discretization Approach

In this Annex, a deeper explanation of the followed discretization procedure is presented, along with an analysis of the system's response.

Equation C.1 presents the transformation used from Laplace domain to Z-domain, where T_S stands for the selected sampling time. However, it should be noted that, in order to implement the transfer functions, the canonical form presented in Figure C.1 has been used; where the coefficients b0, b1 and a1 are given by equation C.2

$$\frac{1}{S} = \frac{T_S}{1 - Z^{-1}} \tag{C.1}$$

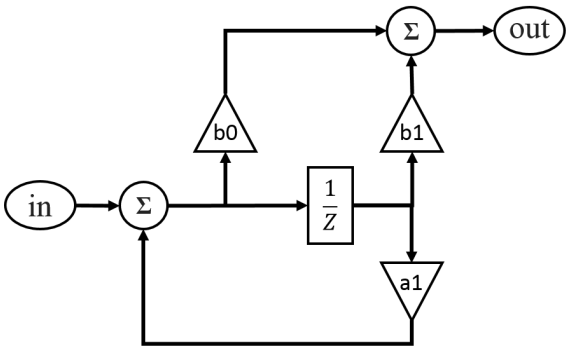

Figure C.1: Reference and response of the discrete sub-plants.

$$G_{(Z)} = \frac{b_0 + b_1\, Z^{-1}}{1 + a_1\, Z^{-1}} \tag{C.2}$$

After testing every individual system in standalone mode, all of them were joined into the Discrete Hybrid Plant Model. In order to evaluate its performance, the same frequency signal used in the continuous stage was used. Again, since the model does not include an external grid, the analysis is in open loop.

The system's response to changes in the TSO reference together with the frequency control was studied. It should be noted that, the reference signal is the same as for the continuous case, therefore, it can be checked in Figure 5.2. Then, Figure C.2 presents the output of the Dispatch function; the reference signals of every sub-plant, and the output of every sub-plant and the HyPP in the PCC. Thus, the reaction of the sub-plants

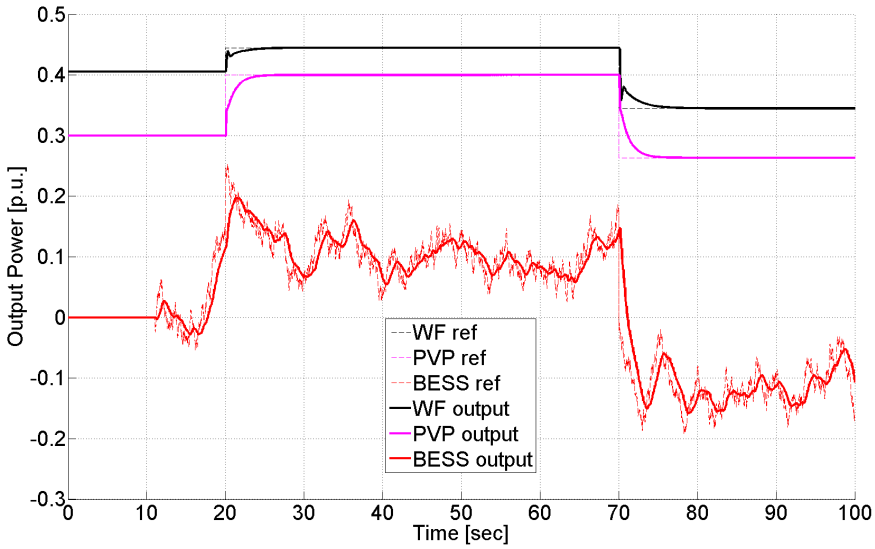

Figure C.2: Reference and response of the discrete sub-plants.

to the different references is shown, again, the BESS response is enough to compensate for the frequency control, while the WF and the PVP get activated only when the TSO reference is changed, thus the HyPP is able to support the grid's frequency without affecting their lifetime. However, it can be seen from the figure how the sub-plants, specially the WF oscillate before reaching steady state. Finally, Figure C.3 presents the evolution of the error during the operation, it is worth mentioning how, again, it remains within ± 2 % except right after the TSO reference is changed.

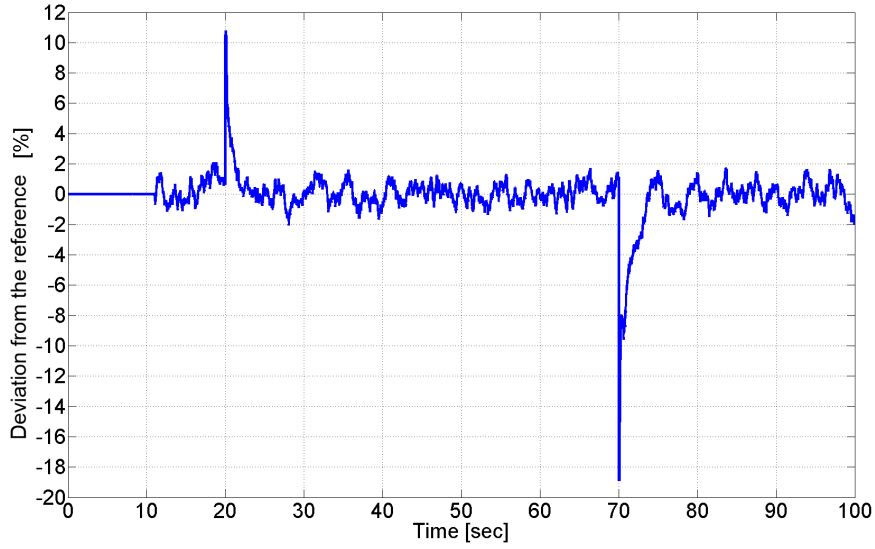

Figure C.3: Error signal between the reference and the output of the discrete model.